UNIVERSITÀ DEGLI STUDI DI TRIESTE

XXXI CICLO DEL DOTTORATO DI RICERCA IN

Scienze della Terra e meccanica dei fluidi

Low-frequency variability of the Pacific Subtropical Cells and their effect on tropical climate

Settore scientifico-disciplinare: **GEO/12**

DOTTORANDO
GIORGIO GRAFFINO

COORDINATORE
PROF. PIERPAOLO OMARI

SUPERVISORE DI TESI
DR. FRED KUCHARSKI

CO-SUPERVISORE DI TESI
DR. RICCARDO FARNETI

ANNO ACCADEMICO 2017/2018

Abstract

In the present dissertation we evaluate several properties of the Pacific Subtropical Cells (STCs), as modelled by ocean-only and ocean-atmosphere coupled models.

The importance of subtropical and extratropical zonal wind stress anomalies on STCs strength is assessed through several idealised and realistic numerical experiments, performed using a global ocean model. Different zonal wind stress anomalies are employed, and their intensity is strengthened or weakened with respect to the climatological value throughout a suite of simulations. Subtropical strengthened (weakened) zonal wind stress anomalies result in increased (decreased) STCs meridional mass and energy transport. Upwelling of subsurface water into the tropics is intensified (reduced), a distinct cold (warm) anomaly appears in the equatorial thermocline and up to the surface, resulting in significant tropical sea surface temperature anomalies. The remotely-driven response is compared with a set of simulations where an equatorial zonal wind stress anomaly is imposed.

A dynamically distinct response is achieved, whereby the equatorial thermocline adjusts to the wind stress anomaly resulting in significant equatorial sea surface temperature anomalies as in the remotely-forced simulations, but with no role for STCs. Significant anomalies in Indonesian Throughflow transport are generated only when equatorial wind stress anomalies are applied, leading to remarkable heat content anomalies in the Indian Ocean. Equatorial wind stress anomalies do not involve modifications of STCs transport, but could set up the appropriate initial conditions for a tropical-extratropical teleconnection involving Hadley cells, exciting a STCs anomalous transport which ultimately feeds back on the Tropics. Experiments performed with both time-constant and time-varying realistic wind stress anomalies also suggest a potential impact of midlatitude atmospheric modes of variability on tropical climate through STCs dynamics. Large temperature trends are found in the subsurface ocean at the Subtropics, as well as in the equatorial thermocline.

Results obtained from pre-industrial and future-scenario simulations, performed by a subset of state-of-the-art ocean-atmosphere coupled models, do not provide a coherent picture of natural STCs variability and future changes. Several mass transport diagnostics are compared for pre-industrial simulations, showing agreement among models about equatorward mass transport in the

Southern Hemisphere, but disagreement in the Northern Hemisphere. Also a general degradation of linear correlation coefficients between different STCs metrics is found when moving toward the Equator. According to future scenario simulations, STCs meridional energy transport is expected to decrease (increase) in the Northern (Southern) Hemisphere under warmer climate conditions.

Acknowledgements

After Bachelor and Master, this third round of my boxing match against academia is drawing close to an end. Thrilling round this one, exhausting at times, maybe the most important so far. Time to leave now, and find my place in the big hard world. Not before thanking some very important people I met during my exciting journey so far, going back in time from Trieste and Bologna, to Ospedaletti and beyond.

Let's start from the most recent friends: the dancing people. It all started as a game for me, ended up as a pretty serious thing, from Ljubljana nights to Bassano battle and Belgrade exchange, passing through birthday jams and vintage parties. Thanks to Elena and Nejc for having introducing me into this world, but special mentions to Paola, Gianni, Alessandra, Miryam, Andrea, Alessia, Adriano, and to all other "freaks" for this amazing experience.

VO.D.C.A. is (literally) more than a word. From that first meeting at Matilde's house to become a "serious association", who would have thought it! Many thanks to Pandi, Bianca, Pina, Dario, Laura, and all Sinapsi people for having made this happen.

Honourable mentions for other special friends in Trieste, with whom I spent some pleasant time and to whom I am grateful: Marta, Serena, Depa, Cata, Irene, Stefano, Presel, Laura, and all other PhDrinkers founders and members.

It has been not all dance and fun of course, but hard work as well. First of all, a big *bravo!* and good luck to my Ph.D. classmates Adriano, Simone, Matilde, Oliviero, Luca, Elena, and Francesca. I am also very grateful to my supervisors Riccardo and Fred, for their help and guidance during the last three years. Thanks to other current and former members of the ESP group, especially to Fabio, Rita, Graziano, Ramon, and Marco.

Back in Bologna, where the first rounds of this 10-years-long match have been fought. Thanks a lot to former classmates, flatmates and all people I met in seven long years, with whom I spent endless hours in classes, libraries, study rooms, and pubs and clubs as well. Thanks especially to Davide, Comma, Celeste, Federico, Raj, Anto, Guido, Caco, Marta, and Valentina.

Going farther back, I can not go further without remembering my oldest friends of all: Giulio, Vittorio, Giulia, and Nadine. Thanks for your presence, and for the time spent together in all possible places in Ospedaletti and nearby.

Last but not least, without my family all of this could never be happened. The most grateful thanks to my mother Giovanna, my father Claudio, my sister Donata, and my relatives, for the unbreakable love and support they gave me during this life-long journey.

Thanks a lot, for everything.

Contents

List of Figures

List of Tables

Chapter 1

Introduction

Ocean-atmosphere interactions shape both time-mean climate and its variability, as coupled ocean-atmosphere oscillation modes exist on many timescales (Neelin 1991; Delworth et al. 1993; Latif and Barnett 1994; Chang et al. 1997; Timmermann et al. 1998; Schneider 2000). Air-sea interactions massively contribute to the global ocean circulation (Fig. 1.1a) and to the renovation of water masses (Huang and Qiu 1994; Marshall and Schott 1999; Bacon et al. 2003; Baines and Condie 1999), with the wind stress forcing playing a leading role (Sverdrup 1947; Fofonoff 1981; Oort et al. 1994; Wunsch 1998; Watanabe and Hibiya 2002; Wang and Huang 2004). In fact, ocean simulations performed by Jayne and Marotzke (2001) show that the dominant physical processes of the meridional overturning circulation can be captured by a simple Ekman model, apart from the Equator where the flow is mainly driven by continuity and direct pressure force (Schopf 1980).

The interplay between air and sea is the leading character for many weather and climate processes. The most important example at the Tropics is El Niño-Southern Oscillation (ENSO; Walker 1928; Troup 1965), occurring in the Pacific Ocean; its evolution is based on an ocean-atmosphere feedback mechanism firstly described by Bjerknes (1969), which involves the interaction of ocean dynamics, atmospheric convection and surface winds in the Pacific Ocean. Ocean-atmosphere processes also maintain the climatological steady-state at the Tropics (Zebiak 1993; Neelin and Dijkstra 1995; Sun and Liu 1996; Cane et al. 1997) and the observed position of the Inter-Tropical Convergence Zone (ITCZ; Xie 2004; Schneider et al. 2014), but they are also crucial for the atmospheric variability at the midlatitudes (Lau 1997; Ma et al. 2016).

A remarkable effort has been spent during the last decades on the study of air-sea interactions and their impact on global climate (Weng and Neelin 1999;

Wu et al. 2005; Frankignoul and Sennéchael 2007; Alexander 2010; Medhaug et al. 2017). In particular, the seminal work of Bjerknes (1964) shows that the atmosphere forces the ocean on short timescales while the ocean drives the atmosphere on long timescales, with a compensation between oceanic and atmospheric heat transport (Shaffrey and Sutton 2006; Farneti and Vallis 2011; Yang et al. 2015). The slow response of the ocean to the highly-varying atmospheric forcing acts as a low-pass filtering of the signal, emphasising the long timescales (Trenberth and Hurrell 1994).

Meridional heat transport is also a major property of the ocean-atmosphere system. In fact, ocean and atmosphere act together on redistributing energy from the Tropics to the polar region (Peixoto and Oort 1992), but at very different temporal and spatial scales. Mesoscale eddies (100-200 km of size) dominate the kinetic energy spectrum in the ocean, whereas in the atmosphere the kinetic energy spectrum peaks at 2000-4000 km (Woods 1985a). Nevertheless, it has been shown that time-mean ocean heat transport is at the same order of magnitude of the atmospheric heat transport (Vonder Haar and Oort 1973; Carissimo et al. 1985; Trenberth and Caron 2001), despite large uncertainties affect these assessments and the partition of global heat transport as well (Keith 1995).

The present dissertation is structured as follows. The first Chapter includes an exhaustive literature review concerning the main subject of the present study, along with a description of motivations and objectives of the work. In Chapter 2 we describe the employed numerical models, computed metrics and diagnostics. Obtained results are shown in Chapters 3, 4, and 5. Conclusions and future outlook are given in Chapter 6.

1.1 The Subtropical Cells

Among all the air-sea interaction mechanisms relating equatorial ocean and (sub)tropical regions, the Subtropical Cells (STCs) are of paramount importance. STCs are shallow meridional overturning circulations, extending from 50 m to about 200 m depth (Cheng et al. 2007), and are observed in the Pacific and Atlantic Oceans with different characteristics due to different basin shapes and forcing (Fig. 1.1c,d). For the Indian Ocean case, a different kind of meridional circulation is observed (Fig. 1.1b) due to the lack of an equatorial upwelling zone (Schott et al. 2004).

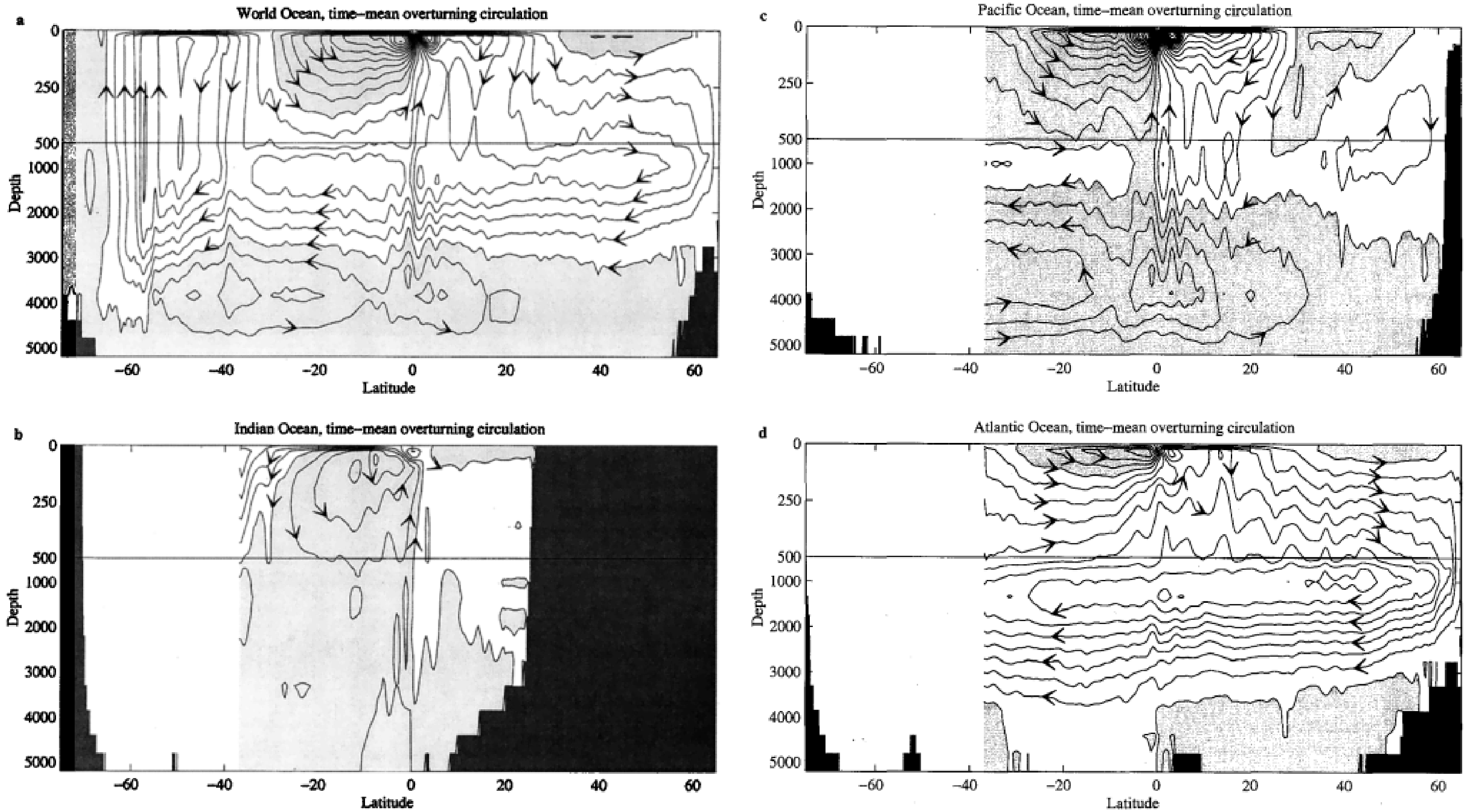

Figure 1.1: Time-mean overturning circulation for (a) the world ocean, (b) the Indian Ocean, (c) the Pacific Ocean, and (d) the Atlantic Ocean, obtained from an ocean model simulation. Negative values of the streamfunction are shaded and indicate counterclockwise overturning. Contour interval for the world ocean is 5 Sv (1 Sv = 10^6 m^3 s^{-1}), for the individual basins is 2.5 Sv. Taken from Jayne and Marotzke (2001).

The existence of such vertical circulations has been theorised by several works during the 1990s (McCreary and Lu 1994; Liu 1994; Lu et al. 1998). In fact, observational and modelling studies indicated the need of a shallow meridional overturning circulation in the Atlantic and Pacific Oceans connecting Tropics and Subtropics (Tsuchiya 1981; Fine et al. 1981a,b; McCreary and Yu 1992), with Luyten et al. (1983) theorising a ventilation process of the ocean thermocline by means of a layered system intersecting the sea surface, in which water is pumped down from the Ekman layer. Although simple ocean models were not able to reproduce this circulation (McCreary 1981; McPhaden and Fine 1981), McCreary and Lu (1994) could finally schematise shallow overturning structures by employing a 2 1/2-layer model forced by an idealised wind stress forcing. Furthermore, and contrary to previous speculations (Bryan 1991), McCreary and Lu (1994) demonstrate that STCs are not driven by equatorial dynamics but rather by the zonal wind stress pattern at the Subtropics. We will further explore the role of the wind stress on the STCs circulation in Chapters 3 and 4.

The amount of water subducted in the Subtropics does not directly define the strength of the cell, because part of it is recirculating inside the subtropical gyre. McCreary and Lu (1994) in fact identify the subtropical region affecting the STC circulation strength in their model (Fig. 1.2), located south of the cutoff latitude (conventionally set at 18°) and separated from the "shadow region", which instead gives no ventilation to the ocean thermocline (Luyten et al. 1983; Talley 1985; Huang and Russell 1994). On a realistic case, all the water moving toward the Equator would come from the northern and eastern part of the gyre, as previously suggested by Tsuchiya (1981). Analysing the propagation of particles in an ocean model, Liu et al. (1994) locate the separation between the recirculating and the mass exchange window at 12° of latitude. Liu (1994) compares instead an analytic solution with the results of a GCM model, still confirming that the subtropical gyre is formed by two parts: the recirculating window in the western part of the basin, and the mass exchange window in the eastern part. Furthermore, he shows that the size of the mass exchange window (that is, where the subducted water at the Subtropics is able to reach the Equator) depends on the wind stress at the southern boundary of the region, on the width of model domain, and on the Ekman pumping process within the subtropical gyre. However, the amount of water subducting at the Subtropics is larger than what provided by Ekman pumping only (Jenkins 1987, 1988), highlighting the fundamental role of ocean mixed layer intermediation (Stommel 1979; Woods 1985b; Pedlosky and Robbins 1991). Even tropical dynamical processes, through atmospheric teleconnections located over exchange windows (Lau and Nath 1994; Trenberth and Hurrell 1994), can affect subtropical subduction. The region of higher subduction rate in the Northern Hemisphere is located at 25°N, 130°W (Huang and Qiu 1994), whereas in the Southern Hemisphere it is found at 20°S, 120°W (Huang and Qiu 1998). On the other hand, assuming an Ekman-like transport driven by variable wind stress forcing as in Kraus and Levitus (1986), it is implied that the mass transport in the Ekman layer must be compensated by a return flow at depth. The return flow can be assumed as barotropic on short timescales (Willebrand et al. 1980; Böning and Herrmann 1994), although Anderson and Gill (1975) and Anderson et al. (1979) show that stratification and non-linear effects have a strong influence on the time-mean wind-driven circulation.

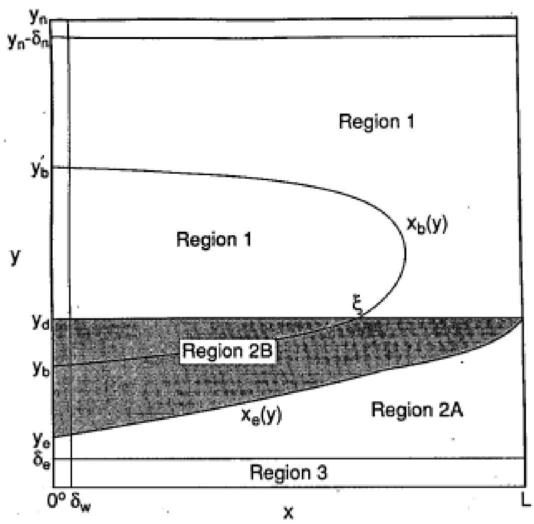

Figure 1.2: A schematic diagram illustrating the structure of the analytic solution of McCreary and Lu (1994).

Other than STCs, the shallow meridional overturning circulation of the tropical oceans is also defined by the Tropical Cells (TCs), schematised by both models (Lu et al. 1998; Kessler et al. 1998) and observations (Johnson 2001; Molinari et al. 1985). Despite their intensity, TCs are associated with a small heat transport (Hazeleger et al. 2001a; Held 2001), but force us to be cautious on the assessment of STCs properties.

Above all the influences of STCs on important climatic aspects, it has been proven that they can serve as ocean tunnels on decadal timescales (Yang and Liu 2005; Liu and Alexander 2007), contributing to the ventilation of the equatorial thermocline (Kleeman et al. 1999; Zhang et al. 2003), altering the ocean heat transport in the Subtropics (Klinger and Marotzke 2000; Held 2001), and driving equatorial temperature anomalies (Farneti et al. 2014a; Song et al. 2014). This is a fundamental aspect, since the oceanic meridional heat transport is larger in the Tropics than elsewhere, similar to the corresponding atmospheric transport at the same latitudes (Peixoto and Oort 1992; Wunsch 2005). Specifically, the mass transport involved in the STCs circulation is comparable to that of the Hadley cells, along with a large associated heat transport (Held 2001; Talley 2003). The relationship between Hadley cells and STCs is schematised in Fig. 1.3. Furthermore, STCs variability has been used to explain some features of the recent global warming slowdown by England et al. (2014) (see Fig. 1.4), related with an observed anomalously cool surface waters in the eastern Pacific Ocean (Kosaka and Xie 2013; Douville et al. 2015) and enhanced heat uptake by the subsurface Pacific Ocean (Meehl et al. 2011; Watanabe et al. 2013), eventually carried toward other ocean basins (Drijfhout et al. 2014; Lee et al. 2015).

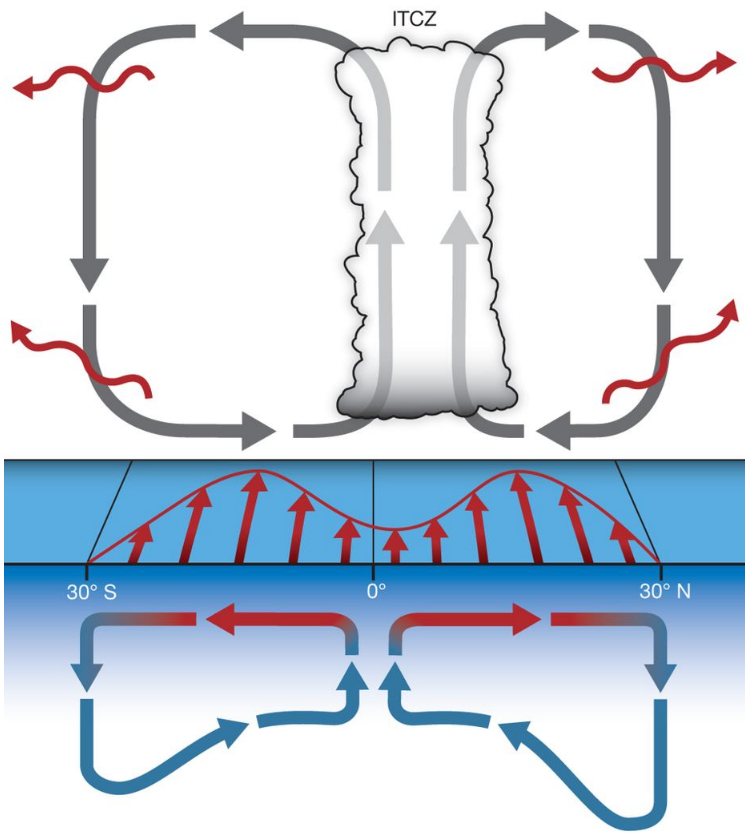

Figure 1.3: Schematic diagram showing the relationship between Hadley cells (grey arrows) and Subtropical cells (thick red and blue arrows). Also shown are the Intertropical Convergence Zone (ITCZ) at the convergence of the Hadley circulation, as well as the poleward eddies energy transport (red wavy arrows). Red arrows on the sea surface are the mean zonal wind stress associated with the Hadley cells, driving the STCs. Taken from Schneider et al. (2014).

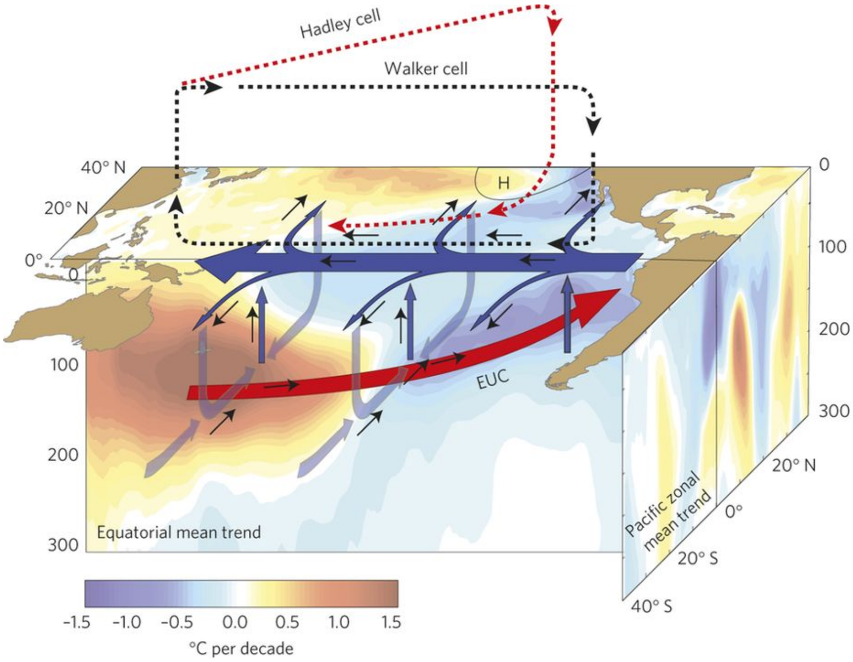

Figure 1.4: Schematics illustrating the basic structure of the STCs circulation in the tropical Pacific Ocean, with blue arrows indicating poleward/downward branches of the cells and a red arrow for the upward EUC branch. Also shown are the meridional Hadley cell in the Northern Hemisphere (red dashed arrow) and the zonal Walker circulation along the Equator (blue dashed arrow). Contours show observed temperature trends (°per decade) during 1992-2011 at the sea surface, in the zonal-depth plane, and in the meridional-depth plane. Taken from England et al. (2014).

1.1.1 Pacific Ocean

The basic properties of Pacific STCs have been extensively examined by observational (e.g., Huang and Qiu 1994; McPhaden and Zhang 2002, 2004; Zhang and McPhaden 2006) and modelling studies (e.g., Klinger et al. 2002; Nonaka et al. 2002; Solomon et al. 2003; Lohmann and Latif 2005). In the tropical Pacific we can observe a pair of fully-developed overturning structures connecting Tropics and Subtropics (Fig. 1.1c), consisting of: a subtropical subduction branch, an equatorward advection motion in the subsurface layers, a vertical rising of the water in equatorial and off-equatorial regions, and finally by a poleward return flow in the surface layers (Schott et al. 2004; Capotondi et al. 2005). However, Pacific STCs are not closed circulations (Lu et al. 1998) but they are connected to the Indonesian Throughflow (ITF; Butt and Lindstrom 1994; Johnson and McPhaden 1999; Sloyan et al. 2003; Zilberman et al. 2013), which contributes to enlarge the southern cell with respect to the northern one.

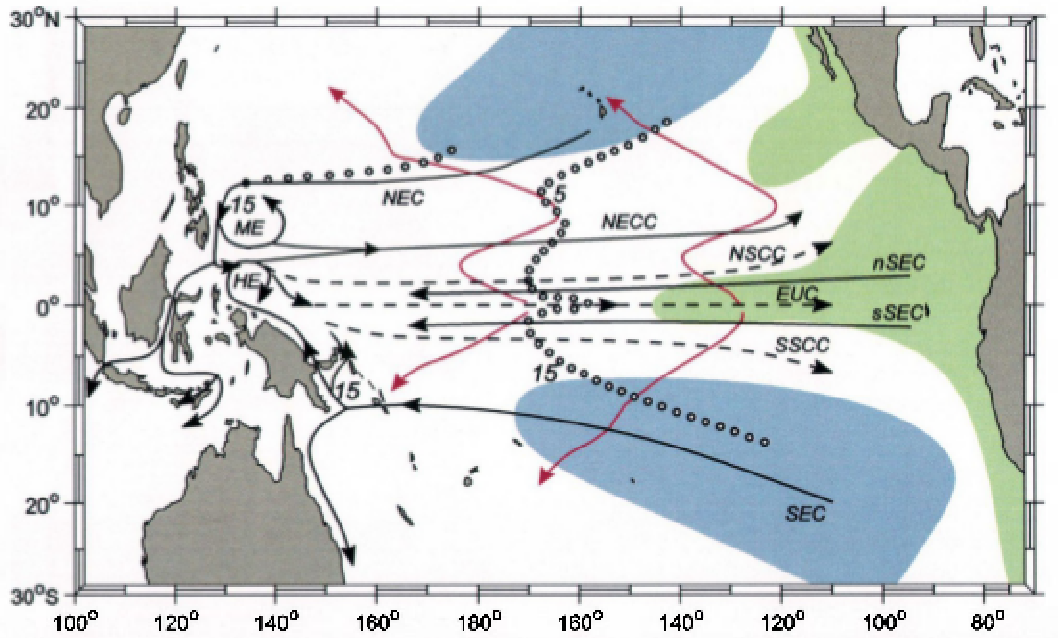

Figure 1.5: Schematics of the Pacific STCs branches and associated mass transport (Sv), with subduction (blue) and upwelling (green) zones. Ocean currents names are NEC = North Equatorial Current, nSEC/sSEC = north/south component of the South Equatorial Current, NECC = North Equatorial CounterCurrent, EUC = Equatorial UnderCurrent, NSCC/SSCC = North/South Subsurface CounterCurrent, ME = Mindanao Eddy, HE = Halmanera Eddy. Dotted lines are interior pathways, and magenta lines are surface poleward pathways for the central basin. Taken from Schott et al. (2004).

Pacific STCs Structure

As previously mentioned, the subduction of STCs waters occurs within the subtropical gyre, where the wind stress curl drives a downwelling motion and the resulting Ekman pumping feeds a Sverdrup flow within the thermocline, eventually propagating equatorward. A schematics of the complex ocean circulation associated with Pacific STCs is given in Fig. 1.5.

Lu et al. (1998) analyse the structure of the shallow overturning circulations in the Pacific Ocean by employing a 3 1/2-layer model on an idealised domain, computing the respective mass transport at three different levels. As seen in Fig. 1.6, TCs are very close to the Equator and basically recirculate tropical water, whereas STCs reach to the Subtropics. It is also shown a pair of Subpolar Cells at the midlatitudes, as well as an inter-ocean circulation connecting Pacific and Indian oceans.

By employing a corrected version of the Hellerman and Rosenstein (1983) wind stress climatology, Huang and Qiu (1994) find a downward Ekman pumping rate of 50 m/yr in the interior part of the northern Pacific subtropical gyre, which must be summed with a small contribution due to lateral induction to

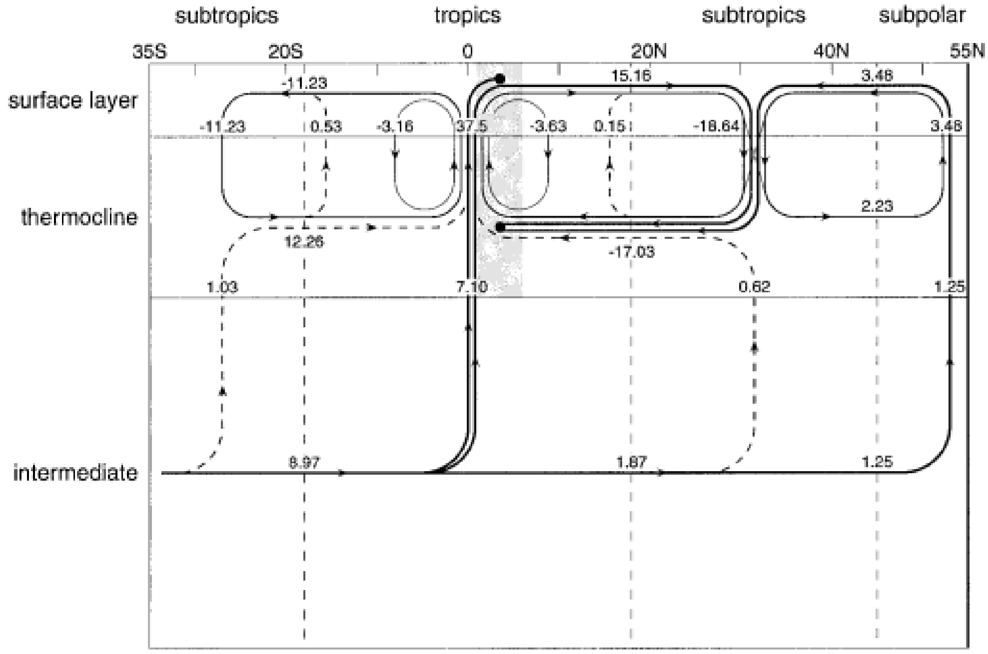

Figure 1.6: A schematic diagram illustrating the shallow overturning circulation in the Pacific Ocean, with associated mass transport (Sv). The meridional domain is divided into five regions: the northern (18°N < y < 45°N) and southern (y < 18°S) Subtropics, the northern (0 < y < 18°N) and southern (18°S < y < 0) Tropics, and the subpolar ocean (y > 45°N). Taken from Lu et al. (1998).

obtain the total vertical subduction. Overall, Huang and Qiu (1994) compute an Ekman-pumping mass transport of 28.8 Sv (1 Sv = 10^6 m^3 s^{-1}). Direct STCs mass transport observations estimate a Northern Hemisphere contribution to the equatorial Pacific upwelling of 35 Sv (Qiu and Huang 1995), while in the southern Subtropics the total water mass formation is 44 Sv, 27 Sv of which are available for equatorial upwelling (Karstensen and Quadfasel 2002).

The STC-generated flow occurs between the 1022 and 1026 kg m^{-3} isopycnals in the Northern Hemisphere and the 1022.5 and 1026.2 kg m^{-3} isopycnals in the Southern Hemisphere, since these layers reside in the subsurface equatorial ocean just below the Ekman layer (Quay et al. 1983; McPhaden and Zhang 2002; Sloyan et al. 2003). The pathway followed by subducted water parcels is different in the two hemispheres, because in the Northern Hemisphere the propagation is more tortuous than in the Southern Hemisphere (Wyrtki 1975; Fine et al. 1981a,b), as the observed equatorial convergence of water from the North Pacific ends abruptly near 5°N (Luther and Johnson 1990; Johnson and Luther 1994). As shown by Lu and McCreary (1995), this is due to the presence of a potential vorticity (PV) ridge close to 9°N, eventually caused by the atmospheric ITCZ. The PV ridge causes the water to take a longer route to reach the Equator, as shown by Johnson and McPhaden (1999) and Johnson

(2001). Therefore, the water flowing from the northern Pacific Ocean is made by two components: the western boundary (WB) part, and the interior (Int) part. Actually, the splitting of the equatorward flow into two components occurs in the Southern Hemisphere as well, but to a lesser extent (Liu and Philander 2001). Overall, the time a water parcel takes for travelling from the Subtropics to the Equator is ≈5-10 years for the Northern Hemisphere (McPhaden and Zhang 2002), and about 2 years for the Southern Hemisphere (Zilberman et al. 2013).

The observational study of Johnson and McPhaden (1999) assesses the properties of the pycnocline in the tropical Pacific Ocean, highlighting differences between the two hemispheres, while specifically addressing the problem of the interior convergence transport. Lu et al. (1998) and Johnson and McPhaden (1999) in fact show that the Northern Hemisphere mass transport contribution is about one third of the total equatorial mass transport, with the remaining part accounted by the Southern Hemisphere. Capotondi et al. (2005) model simulation shows that at 9°N the equatorward interior flow occurs between 180°W and 140°W, whereas at 9°S it extends from 160°W and 90°W; these estimates are also confirmed by Zhang and McPhaden (2006). According to Lee and Fukumori (2003) and Cheng et al. (2007) the interior pathway is more important for the interannual and decadal variability of the STCs, although the western boundary contribution is larger in a time-mean perspective. It has also been shown that the interannual variability of the interior pathway is particularly important for ENSO variability (Huang and Wang 2001). Furthermore, the mean meridional geostrophic transport in the interior part is shown to have an ENSO signature in the observational work of Zilberman et al. (2013).

The assessment of the water transports contributing via WB pathways is difficult using either model or observational datasets, mainly because of the presence of the Indonesian Straits (Rodgers et al. 1999). The interior contribution is not easy to evaluate as well, since the different models response to different physics and wind stress climatology employed. For example, Lee and Fukumori (2003) at 10°N estimate 15.7 and 5.6 Sv for the western boundary and interior contribution, respectively; at 10°S instead the computation gives 9.2 and 10.1 Sv, respectively. These assessments are similar with other estimates for the Northern Hemisphere (Lukas et al. 1991; Wijffels et al. 1995; Huang and Liu 1999; Capotondi et al. 2005), but slightly larger with respect to other Southern Hemisphere evaluations (Lindstrom et al. 1987; Butt and Lindstrom 1994; Huang and Liu 1999; Capotondi et al. 2005). This is a key point, since interannual and decadal variations of western boundary and interior components tend to compensate each other in both observations and ocean models (Zebiak 1989; Stacey et al. 1990; Lee and Fukumori 2003; Capotondi et al. 2005; Zhang and McPhaden 2006; Cheng et al. 2007; Schott et al. 2008), although with distinctions between Northern and Southern Hemisphere (Lübbecke et al. 2008), with STCs variations mainly locked to the interior component (McPhaden and Zhang 2002; Lee and Fukumori 2003; Hong et al. 2014). However, the relationship between western boundary and interior STCs transport in coupled models can vary significantly (Zhang and McPhaden 2006). The partial compensation of western boundary and interior contribution can be explained by modifications of the tropical gyre to changes in the wind stress curl (Lee and Fukumori 2003), or by baroclinic adjustment (Capotondi et al. 2005).

The main Pacific STCs upwelling zone is found in a narrow band along the Equator, from 2°N to 2°S and from 175°E to 90°W (Capotondi et al. 2005). Estimates of the thermocline water upwelled in the central Pacific are about 40-50 Sv (Wyrtki 1981; Quay et al. 1983), characterised by decadal-scale variations (Guilderson and Schrag 1998; McPhaden and Zhang 2002). The upwelling component of the STCs circulation involves the Equatorial Undercurrent (EUC; Pedlosky 1987, 1988), a jet-like, boundary-layer current particularly important for the tropical ocean state, feeding the thermocline at the Equator. EUC shoals from a depth of 220 m at 143°E to about 80 m at 110°W (Johnson et al. 2002). A significant part of the Pacific EUC transport can be traced back to the Extratropics (Tsuchiya et al. 1989; Butt and Lindstrom 1994), as it forms the equatorial branch for many meridional circulation structures. In fact, although some aspects of the EUC variability are driven by wind stress forcing at the Equator (Liu et al. 1994), the temperature of the EUC water is in the range of 15°-25°C, meaning that the main source region must be located between 20° and 40° of latitude (Wyrtki and Kilonsky 1984), even though local recirculation of tropical waters can contribute as well (Donguy et al. 1984; Johnson 2001). Pacific EUC mass transport ranges between 25 and 50 Sv at its maximum (Lukas and Firing 1984; Wilson and Leetmaa 1988), with western boundary sources supplying about 15 Sv and part of the EUC transport coming instead from the interior ocean through entrainment (McPhaden and Fine 1988).

The returning flow toward the Poles is mostly provided by Ekman drift at the Tropics and by western boundary currents at the midlatitudes, as highlighted by observational studies (Patzert and McNally 1981; Luther and Johnson 1990; Johnson 2001). Moreover, in the Northern Hemisphere the maximum poleward transport is found at the center of the basin, while in the Southern Hemisphere it is closer to the eastern boundary (Schott et al. 2004). Employing NCEP-NCAR wind stress data, Schott et al. (2004) evaluate 54 Sv of poleward Ekman transport divergence, computed as difference of the poleward mass transports at 10°N and 10°S. Particle analysis performed by Liu et al. (1994) shows that three preferred pathways exist for the EUC returning flow: two start flowing, more or less directly, along the western boundary of the basin toward the subtropical gyre, while the third involves a recirculation of the water close to the Equator. This means that Pacific STCs are not closed circulations. Employing drifter data, Johnson (2001) show a poleward and westward propagation for most of the observed streamlines at the surface, in which water parcels reach 22° of latitude after about 2 years. At the subsurface the response timescale is much longer (Fine et al. 1981b), although a large part of the water can recirculate inside the TCs. However, model simulations show that observed trends of the Pacific shallow overturning circulation (PSOC) are found between 50 and 200 m depth, suggesting the importance of subtropical subduction and equatorward transport involved in STCs, and a secondary role for TCs (Farneti et al. 2014a).

Pacific STCs Variability

Some aspects of the STCs variability have been matter of debate for a long time. First of all, many studies show how the time-mean meridional overturning circulation can differ from the seasonal pattern (Bryan 1982; Lee and Marotzke 1998; Nakano et al. 1999), and in the Pacific Ocean the amplitude of the seasonal cycle of the shallow meridional overturning circulation is about 25 Sv (Jayne and Marotzke 2001).

McPhaden and Zhang (2002, 2004) observe a decreasing STCs transport convergence at the Equator from the 1970s to the 1990s, and then an increasing convergence during the early 2000s. In particular, interior pycnocline convergent transport changed from 27 Sv in the period 1970-1977 to 13.4 Sv during 1990-1998, bouncing back to 24.1 Sv after 1998. A similar behaviour is reproduced in many studies (Nonaka et al. 2002; Lee and Fukumori 2003; Capotondi et al. 2005), and STCs decadal-scale variations are confirmed by ocean-only (Cheng et al. 2007; Farneti et al. 2014a) and coupled ocean-atmosphere simulations (Lohmann and Latif 2005; Zhang and McPhaden 2006). However, Schott et al. (2007) claim that observational data are not sufficient for an assessment of the STCs transport decadal variability. Using a 50-years-long assimilation run, Schott et al. (2007) in fact show that STC transports vary mainly from seasonal to interannual timescales, with a small low-frequency variability. Actually, this could be due to the employed wind stress forcing, known to have a large decadal trend in the Pacific equatorial zonal surface wind (Alory et al. 2005), as the same run performed by Schott et al. (2007) without data assimilation gives a more-than-doubled STCs variations at decadal scale. In fact, using a different atmospheric dataset, Schott et al. (2008) obtain similar STCs low-frequency variability as previously shown by McPhaden and Zhang (2002, 2004). On the other hand, Farneti et al. (2014b) show that an global ocean model forced with atmospheric reanalysis is able to reproduce most of the observed STCs and equatorial SST variability in the Pacific Ocean during the twentieth century.

Unlike uncoupled ocean models, coupled ocean-atmosphere models fail on reproducing many features of the observed Pacific STCs variability (Solomon and Zhang 2006; Zhang and McPhaden 2006; Yang et al. 2014; Farneti 2017). This can be due to many aspects, mostly related to the way models reproduce the tropical pycnocline structure (Zhang and McPhaden 2006) and the off-equatorial wind stress forcing variability (Solomon and Zhang 2006), both strongly linked to models resolutions and parametrizations. We shall focus on these important aspects in Chapter 5.

1.1.2 Atlantic Ocean

Subtropical-tropical overturning structures are observed in the Atlantic Ocean as well (Fratantoni et al. 2000; Lazar et al. 2002). Nevertheless, the narrowness of the basin and the presence of the Atlantic Meridional Overturning Circulation (AMOC; Kuhlbrodt et al. 2007) alter the expected shape of the cells (Malanotte-Rizzoli et al. 2000; Inui et al. 2002). In particular, the superimposition of AMOC and STCs complicates the interpretation of the tropical-subtropical pathways and the quantification of mass transports (Fig. 1.7; Zhang et al. 2003), although it is now clear that AMOC contributes to make the southern STC larger than the northern STC (Fratantoni et al. 2000; Harper 2000; Lazar et al. 2001).

In the past, modelling studies tried to understand where the water contributing to the Atlantic STCs came from. Malanotte-Rizzoli et al. (2000) and Hazeleger et al. (2003) argue that a contribution is given by both hemispheres, and Inui et al. (2002) show that water subduction occurs in the At-

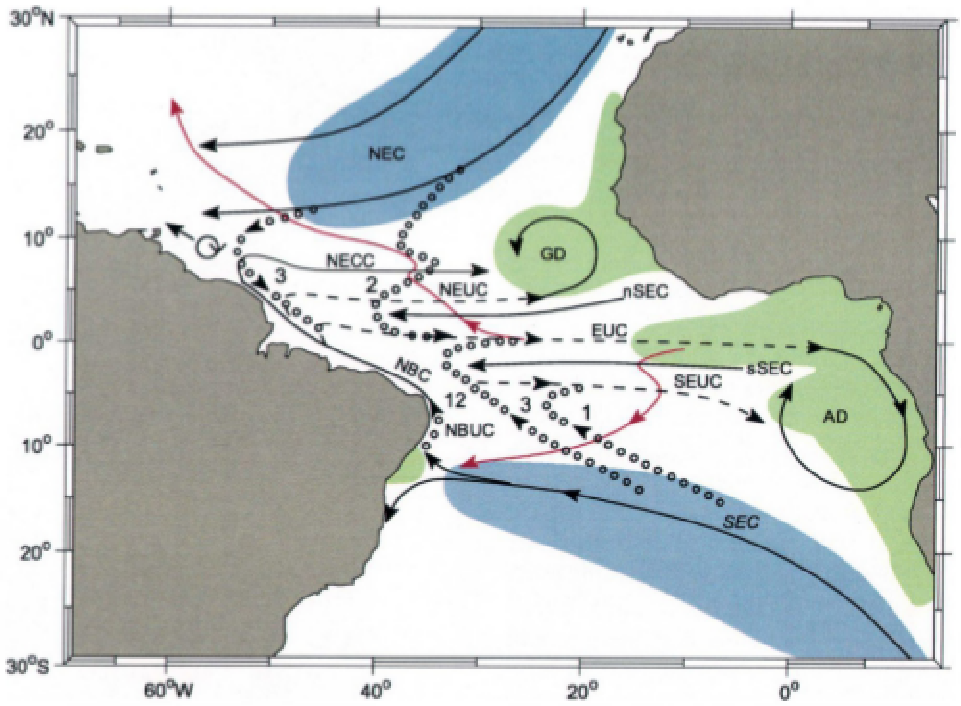

Figure 1.7: Schematics of the Atlantic STCs branches and associated mass transport (Sv), with subduction (blue) and upwelling (green) zones. Ocean currents names are NEC = North Equatorial Current, NECC = North Equatorial CounterCurrent, NEUQ/SEUQ = North/South Equatorial UnderCurrent, nSEC/sSEC = north/south component of the South Equatorial Current, SEC = South Equatorial Current, NBC/NBUC = North Brazil (Under)Current, GD/AD = Guinea/Angola Dome. Dotted lines are interior pathways, and magenta lines are surface poleward pathways for the central basin. Taken from Schott et al. (2004).

lantic subtropical gyre of both hemispheres. Moreover, the modelled northern STC supply is also very sensitive to the subtropical wind stress forcing (Inui et al. 2002). However, Harper (2000) claims that the subducted water found in the EUC comes from the Southern Hemisphere only, as already suggested by Tsuchiya (1986). Hüttl and Böning (2006) also confirm that the contribution of the northern STC to the equatorial upwelling is, if not zero, at least negligible compared to the southern STC and the AMOC parts.

Atlantic shallow overturning circulation show a pronounced interannual-to-decadal variability (Carton et al. 1996; Kröger et al. 2005), with the largest water velocity variance found near the western boundary (Hüttl and Böning 2006) and the bulk of the transport variability mostly related with the wind stress forcing (Kröger et al. 2005). Instead, it is very difficult to assess annual variations of the Atlantic STCs transport (Schott et al. 2003), since the joint influence of zonal wind stress and baroclinic waves (Philander and Pacanowski 1986). During the last decades, Atlantic STCs shown a weaker-than-average transport until the mid-1970s, followed by 20 years of enhanced transport and again a decline appeared during the mid-1990s (Hüttl and Böning 2006). Besides the influence of subtropical wind stress variations (Kröger et al. 2005), STCs variability is also forced by AMOC-related interactions (Jochum and Malanotte-Rizzoli 2001).

1.1.3 Indian Ocean

In the Indian Ocean basin, the surface wind pattern at the Equator can vary considerably due to the monsoon oscillations (Miyama et al. 2003; Schott et al. 2009). Thus, the zonal component of the wind stress vanishes at the Equator for most of the year, and negative wind stress curl associated with the equatorward weakening of the trade winds (Miyama et al. 2003) drives a southward flow entirely composed of Ekman drift (Levitus 1987; Godfrey et al. 2001). An annual-mean equatorial upwelling is basically absent (Schott et al. 2004), and subtropical subduction only exists in the eastern part of the South Indian Ocean (SIO; Webster et al. 1999), since the limited extension of the Indian Ocean north of the Equator.

According to both observations and models (McCreary et al. 1993; Schott et al. 2002; Miyama et al. 2003), the resulting shallow overturning circulation, called Cross-Equatorial Cell (CEC), consists of a northward thermocline flow across the Equator (mostly along the western boundary), several upwelling branches in the Northern Hemisphere (outcropping near Somalia, Oman, and India), and a return flow at the surface towards the Southern Hemisphere (Fig. 1.8). In fact, upwelled water mostly comes from 200-300 m depth (Schott and McCreary 2001) and it is primarily originated in the Southern Hemisphere (Fischer et al. 1996), with main contributions given by the water subducted in the southeastern Indian Ocean and by the ITF transport (Miyama et al. 2003). Actually, a smaller overturning structure similar to an STC does exist in the South Indian Ocean (McCreary et al. 1993; Schott et al. 2002), along with a pair of very shallow equatorial rolls (Wacongne and Pacanowski 1996; Lee and Marotzke 1997). The southern Indian STC is driven by the Ekman pumping at the northern edge of the southeasterly trade winds (Schott et al. 2009).

The subtropical SIO accounts for almost the entire downward branch of both cells (Zhang and Talley 1998), while two upward branches exist between 10°S and the Equator, and in the North Indian Ocean (NIO; Schott et al. 2002). Moreover, there is a smaller upwelling zone in the eastern side of the

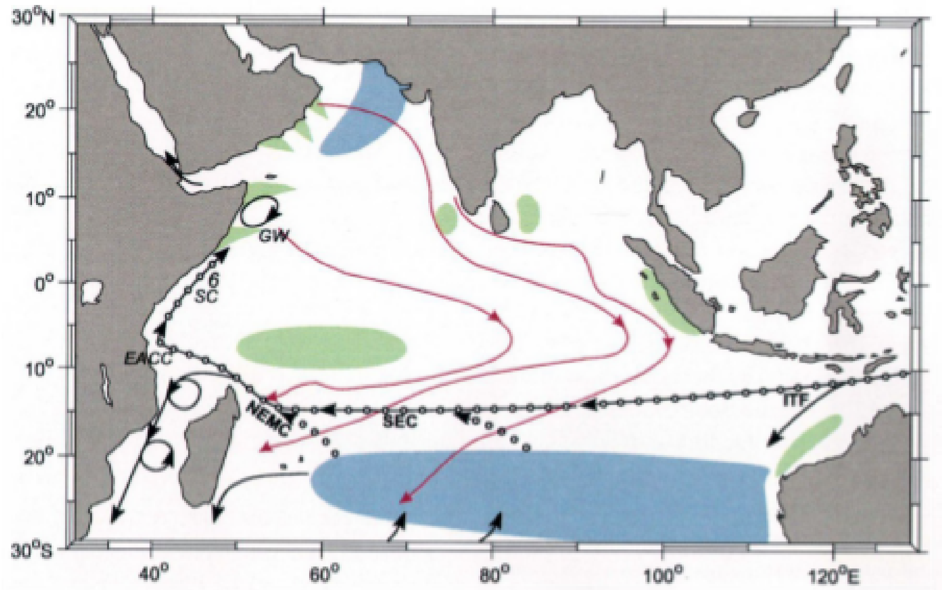

Figure 1.8: Schematics of the Indian CEC branches and associated mass transport (Sv), with subduction (blue) and upwelling (green) zones. Ocean currents names are ITF = Indonesian ThroughFlow, SEC = South Equatorial Current, NEMC = NorthEast Madagascar Current, EACC = East African Coastal Current, SC = Somali Current, GW = Great Whirl. Magenta lines are southward pathways. Taken from Schott et al. (2004).

Indian Ocean close to the Indonesian archipelago, related with an eastern branch of the southern STC; this branch is partly fed by the ITF, which is in turn influenced by the northern Pacific STC transport (Hong et al. 2014). The pathways followed by water parcels is in fact complicated by the presence of the ITF, which mostly flows in the upper ocean with a mass transport of about 10 Sv (Gordon et al. 1999; Gordon 2005). Both cells bring warm water southward and cool water northward, and their strength is regulated by the trade winds over the SIO; instead, the trade winds pattern over the NIO influence the transport of the CEC only (Lee 2004). In fact, the zonal component of the southeasterly trade winds in the SIO experienced a weakening over the 1990s, with a slowdown of the southern STC (Lee 2004). However, a rebound of the southern STC transport is documented by Lee and McPhaden (2008). The CEC transport also showed a significant slowdown over the last decades (Schoenefeldt and Schott 2006).

1.2 Tropical and Extratropical Variability

Earth's climate shows variability on many timescales. One of the main reasons for this variability lies in the non-linear interaction between the subcomponents of the climate system (Dijkstra 2013).

1.2.1 Tropical-Extratropical Interactions

Atmosphere-ocean coupled variability is particularly pronounced at the Tropics. In fact, coupled feedbacks result in an increased variability in both atmosphere and ocean, essentially related with the coupled nature of the system (Farneti and Vallis 2011). This is not only related with the local scale, but also with the global climate. In fact, many "teleconnections" mechanisms (Ångström 1935; Wallace and Gutzler 1981; Liu and Alexander 2007) are able to propagate tropical signals all over the world. On the other hand, extratropical regions can strongly influence the Tropics as well (Gu and Philander 1997; Kleeman et al. 1999; Pierce et al. 2000; Liu and Yang 2003).

Unlike the Tropics, climate variability at the Extratropics is mostly due to high-frequency weather disturbances, whose effect on long-term climate is basically related with the large ocean heat storage capability. Still, despite the chaotic nature of low-frequency variability at the midlatitudes (Molteni et al. 1993) and the large variance associated with transition between well-defined weather regimes (Molteni et al. 1990), the influence of the tropical ocean-atmosphere state on the Extratropics is large (Trenberth 1990; Graham et al. 1994; Cane 1998; Deser et al. 2004), mostly accomplished by the atmospheric *bridge* for what concerns SST (Lau and Nath 1996; Alexander et al. 2002; Liu and Yang 2003) and by the oceanic *tunnel* for the subsurface ocean response (Yang and Liu 2005). Many studies show in fact the link on different timescales between thermal anomalies in the equatorial Pacific Ocean and the extratropical Pacific (Trenberth 1990; Zhang et al. 1996; Zhang et al. 1998b; Deser and Phillips 2006), the Atlantic (Enfield and Mayer 1997; Klein et al. 1999; Alexander and Scott 2002) and the Indian oceans (Yu and Rienecker 1999; Meehl and Arblaster 1998; Deser et al. 2004).

As we mentioned, the Extratropics have an effect on the Tropics (e.g., Ferranti et al. 1990; Wu et al. 2007), and it can be as large as the tropical influence on the midlatitudes (Liu and Yang 2003). On short timescales, observations show that tropical convection can be affected by atmospheric wave trains originating at the midlatitudes (Lau and Phillips 1986), and extratropical atmospheric variability can force an SST "footprint" extending toward the Tropics (Vimont et al. 2001) as well as influence the trade winds strength (Meehl and Loon 1979). Also, extratropical SST and sea level pressure patterns influence ENSO space-time variability (Van Loon and Shea 1985; Trenberth and Hoar 1996; Yang et al. 2005; Anderson et al. 2013). Both atmosphere and ocean act to connect midlatitude and tropical disturbances from seasonal (Liu and

Xie 1994) to decadal timescales (Barnett et al. 1999; Wu et al. 2007), with the ocean accounting for one third of the total equatorial SST change (Liu and Yang 2003) and a larger contribution from the Southern Hemisphere (Liu and Yang 2003; Yang and Liu 2005). Furthermore, partially-coupled experiments performed by Yang and Wang (2008) show that the tropical SST response to extratropical forcing is basically linear, with only 10% of the signal due to non-linear effects.

On the ocean side, the communication between Tropics and Extratropics has been speculated from a long time (Ellis and Hales 1751; Rumford 1800; Lenz 1848; Stommel 1979; Luyten et al. 1983; McCreary and Yu 1992). Apart from the deep overturning circulation involving the whole global ocean (Warren 1981; Kuhlbrodt et al. 2007), the wind-driven gyres (Sverdrup 1947; Stommel 1960) and the shallow meridional overturning circulation (including STCs) play a fundamental role as teleconnection mechanisms in the upper layers. The heat transport related with those structures has great implication on the global climate (Hall and Bryden 1982; Klinger and Marotzke 2000). Waves propagation at the western boundary also provides an effective teleconnection mechanisms (Enfield and Allen 1980; Lysne et al. 1997; Capotondi and Alexander 2001; McGregor et al. 2007), which is even more effective than thermocline ventilation on short timescales (Liu and Alexander 2007).

1.2.2 Pacific Ocean Variability

So far, great interest in literature has been given to the tropical Pacific Ocean, which properties show strong variability on many timescales (Zhang et al. 1997). At the same time, the overlying atmosphere exhibits even more intense variations. Thus, air-sea interactions must play an important role (Palmer and Zhaobo 1985; Trenberth and Hurrell 1994; Latif and Barnett 1996; Farneti et al. 2014b).

High-frequency Variability

Despite the leading role played by low-frequency variability on climate, fluctuations from seasonal to interannual timescales are also key features of the tropical ocean-atmosphere state. It is worth to note that the annual cycle of solar radiation is not driving any large seasonal oscillations at the Equator, where the SST annual cycle is instead driven by ocean-atmosphere interactions through wind stress forcing (Mitchell and Wallace 1992; Chang 1996) and heat flux (Cayan 1992; Iwasaka and Wallace 1995). Moreover, despite the lack of consensus about magnitude and dynamics of the ocean heat transport seasonal cycle, it has been shown in several works that it is mainly driven by high-frequency wind stress variability (Jayne and Marotzke 2001).

ENSO is the most important climate phenomenon on interannual timescales, fluctuating between warm and cold phases at periods of 3-7 years (Zhang et al. 1997), and affecting atmospheric surface temperature and precipitation patterns all around the world (Dai and Wigley 2000; Sobel et al. 2002; Hansen et al. 2010). ENSO irregular nature can arise from a large number of factors, from nonlinear behaviours (Jin et al. 1994; Tziperman et al. 1994) to random effects excited by atmospheric weather (Kleeman and Power 1994; Zavala-Garay et al. 2003). Apart from local ocean-atmosphere interactions (Bjerknes 1969; Fedorov and Philander 2001), ENSO interannual variability is importantly influenced by water mass exchange processes between off-equatorial and equatorial regions. Among the different views about how this exchange occurs (Wang and Picaut 2004), an important role is played by the wind-induced ocean circulation, and the relationship between ENSO and Pacific STCs variability on interannual timescales has already been stated (Lee and Fukumori 2003; Schott et al. 2008; Zilberman et al. 2013). At the Extratropics, ENSO is able to induce part of the observed interannual atmospheric variability (Bjerknes 1969; Horel and Wallace 1981).

Focusing on the atmospheric side, a simple schematics of the ENSO modifications in the upper troposphere is shown in Fig. 1.9. Increased SST enhances atmospheric convection and upper-level divergence in the equatorial Pacific; the resulting response propagates as a wave train of alternating high and low geopotential anomalies on each hemisphere (Hoskins et al. 1977; Webster 1981; Hoskins and Karoly 1981), affecting the atmospheric state up to the midlatitudes by interacting with the storm track in the winter hemisphere (Webster 1982; Kok and Opsteegh 1985; Hoerling and Ting 1994; Kidston et al. 2015). The extratropical response can be very sensitive to the location of the tropical heating source (Simmons 1982; Geisler et al. 1985), with ocean-atmosphere interactions influencing the signal propagation outside the Tropics (Hoerling and Ting 1994; Alexander et al. 2002). The resulting atmospheric pattern at the Extratropics is able to change the ocean state by altering the latent and sensible heat flux at the air-sea interface (Deser et al. 1996); here, the ocean provides a modest (but complex) feedback on the extratropical response to ENSO (Alexander et al. 2002). We shall return later on the relationship between atmospheric variability at the midlatitudes and tropical Pacific Ocean in Chapter 4.

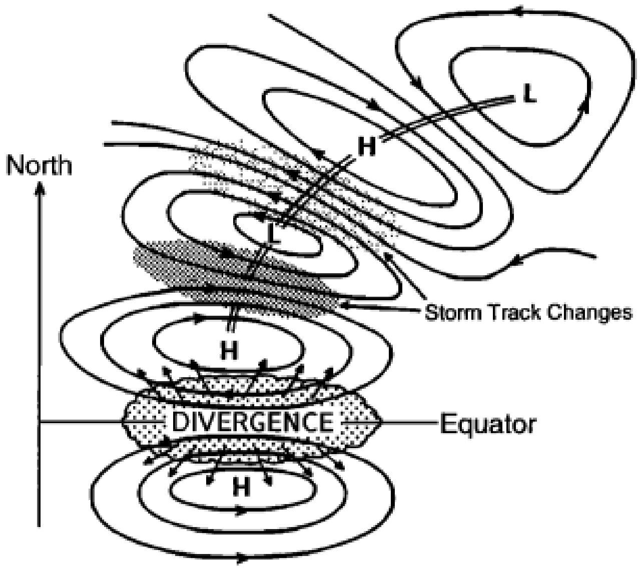

Figure 1.9: Schematic view of the dominant changes in the Northern Hemisphere upper troposphere in response to increases in SSTs, enhanced convection, and anomalous upper tropospheric divergence associated with a warm ENSO phase in the Pacific Ocean. A wave train of alternating high and low geopotential anomalies occurred in the surface wind stress and streamfunction anomalies results from the quasi-stationary Rossby wave response. Corresponding changes may occur in the Southern Hemisphere. Taken from Trenberth et al. (1998).

Low-frequency Variability

Low-frequency climate variability is affected by both natural and anthropogenic forcing, although most of it is thought to be driven by internal stochastic processes (Mikolajewicz and Maier-Reimer 1990; Power et al. 1995). The ocean, with its large thermal "inertia", contributes greatly to the observed low-frequency climate variability (Fraedrich et al. 2004), with basin-wide oscillatory modes arising through the collaboration of planetary waves propagation (Liu 2003; Yang et al. 2004), stochastic wind forcing (Cessi and Primeau 2001; Cessi and Louazel 2001), and baroclinic instability of the large-scale circulation (Colin de Verdière and Huck 1999).

In this respect, the Pacific Ocean is characterised by a pronounced variability on decadal-to-multidecadal timescales, mostly in terms of cyclic oscillations and regime shifts. Important examples of variability processes are ENSO decadal variability (Zhang et al. 1997; Kirtman and Schopf 1998; Yeh and Kirtman 2009), and the North Pacific decadal variability (Zhang et al. 1997; Mantua et al. 1997; Power et al. 1999a) of which the Pacific Decadal Oscillation (PDO) is the main manifestation. South Pacific Ocean also shows remarkable low-frequency variability (Zhang et al. 1997; Garreaud and Battisti 1999; Wong and Johnson 2003).

In the past, many hypotheses have been proposed on the mechanisms generating climate variability on decadal timescales in the Pacific Ocean (e.g., Trenberth and Hurrell 1994; Latif et al. 1998; Kirtman and Schopf 1998; Kleeman and Power 2000; Hazeleger et al. 2001b; Solomon et al. 2003; Lohmann and Latif 2005; Cheng et al. 2007; Farneti and Vallis 2011). Those speculations involved either atmosphere-only (Barnett et al. 1999; Pierce et al. 2000; Kushnir et al. 2002), ocean-only (Gu and Philander 1997; Lysne et al. 1997; Kleeman et al. 1999), and atmosphere-ocean processes (Knutson and Manabe 1998; Timmermann et al. 1998; Nakamura and Yamagata 1999; Liu et al. 2002; Timmermann and Jin 2002; Rodgers et al. 2004; Wu et al. 2007; Farneti et al. 2014b). Latif and Barnett (1994, 1996) hypothesise that Pacific decadal variability is mainly driven by unstable ocean-atmosphere interactions occurring in the North Pacific Ocean with the ocean thermocline intermediation, although analogous SST signatures are also observed in the tropical and South Pacific (Garreaud and Battisti 1999; Evans et al. 2001). Deser et al. (1996) actually show that decadal temperature anomalies can move equatorward from the North Pacific Ocean exploiting thermocline ventilation, a possibility already suggested by Welander (1959). Thermal anomalies can in fact propagate as passive tracers when they are density-compensated by salinity anomalies; in this case, they are called ocean "spicy" anomalies (Munk 1981). Schneider (2000) successfully exploit ocean spiciness to introduce a coupled ocean-atmosphere mode of decadal variability in the tropical Pacific, with anomalies originated in the Subtropics and reaching the Equator about 10 years later.

The Pacific Decadal Oscillation index is defined as the leading principal component of the monthly North Pacific Ocean sea surface temperature (Mantua et al. 1997; Zhang et al. 1997; Chao et al. 2000; Barlow et al. 2001). PDO oscillations are irregular, with periods ranging from 20 to 30 years. The spacial structure of the PDO index at the Tropics is similar to the canonical ENSO warm phase defined by Rasmusson and Carpenter (1982), with a warm phase characterised by cold SST anomalies in the Northwest Pacific and warm SST anomalies in the Northeast Pacific. Several works highlight the role of the PDO in the context of Pacific climate variability, for example by changing the Pacific Ocean heat content (Meehl et al. 2011; Balmaseda et al. 2013), the atmospheric state (Newman et al. 2003; Hazeleger et al. 2005), and affecting the evolution of regional climate regimes (Meehl and Hu 2006; Krishnan and Sugi 2003).

PDO time features are consistent with Hasselmann (1976)'s null hypothesis, as Pierce (2001) reproduce some observed characteristic of PDO using random-generated time series. The non-linear character of the Pacific decadal variability is confirmed by Power and Colman (2006), showing that ENSO-like variability modes can arise from random changes in ENSO activity. Nevertheless, part of the PDO variability must come from the tropical Pacific (Nakamura et al. 1997; Newman et al. 2003; Alexander et al. 2008), with Biondi et al. (2001) suggesting the necessity of positive ocean-atmosphere feedbacks to sustain the PDO oscillatory behaviour. It is then acknowledged that part of the PDO signal is extratropically-forced (Schneider et al. 1999a; Schneider and Cornuelle 2005; Zhang and Delworth 2007), and by now the PDO is considered a complex phenomenon resulting from the combination of different processes (Newman et al. 2003; Farneti 2017), with a third of the signal ascribed to equatorial dynamics and the remaining explained by ocean gyres and extratropical atmospheric variability (Schneider and Cornuelle 2005; Alexander 2010; Newman et al. 2016).

Similarly, PDO regime shifts are triggered and influenced by a large range of processes (Miller et al. 1994; Meehl and Hu 2006; Ding et al. 2013; Kucharski et al. 2016), and their occurrence is difficult to predict (Newman 2007). The 1976/1977 observed regime shift is responsible for an increase of 0.8°C in the tropical Pacific Ocean SST from the 1970s to the early 1990s (Zhang et al. 1997; McPhaden and Zhang 2002), with ocean-only and coupled simulations underestimating the observed SST increase while giving a subsurface warming up to 1.8°C (Solomon and Zhang 2006). Afterwards, a surface thermal decrease of several tenth of a degree due to another regime shift occurred in the late 1990s (Cheng et al. 2007). Similar regime shifts happened several times during the last century (Francis and Hare 1994; Zhang et al. 1997; Minobe 2000).

Although ENSO is primarily modulated by interannual variability, it also shows strong (inter)decadal variations (Wang and Ropelewski 1995; Power et al. 1999a; Vimont et al. 2002; Power et al. 2006). In fact, the interaction between ENSO and Pacific decadal variability is assessed in many studies (Trenberth 1990; Tziperman et al. 1994; Newman et al. 2003; Solomon et al. 2003; Schneider and Cornuelle 2005; Power and Colman 2006; Wang et al. 2008; Wang et al. 2013), as well as their joint effect on the Pacific Ocean (McGowan et al. 1998; Hare and Mantua 2000; Peterson and Schwing 2003) and the global climate (Kosaka and Xie 2013; Meehl et al. 2016). Assessing the impact of ENSO long-term modulation on Australian climate, Power et al. (1999a) highlight the interdecadal behaviour of the SST oscillation in the Pacific Ocean, of which the PDO is the Northern Hemisphere manifestation

(Folland et al. 2002). In accordance with the analysis performed by Zhang et al. (1997) and confirming some features already suggested by Mantua et al. (1997), Power et al. (1999a,b) and Folland et al. (2002) introduce the Interdecadal Pacific Oscillation mode (IPO), consisting in a warm tropical Pacific Ocean and weak trade winds during the positive phase, and a cool tropical Pacific and strong trade winds in the negative phase (Folland et al. 1999). Power et al. (1999a) suggest that the IPO essentially arise from ocean-atmosphere interactions, and its long-term oscillatory behaviour makes it susceptible to external forcing (Meehl et al. 2013; Song and Yu 2015). Furthermore, many studies attribute to the IPO a leading role about variable global warming rates in the early 2000s (Kosaka and Xie 2013; Fyfe et al. 2016), as well as in the past (Meehl et al. 2013; Kosaka and Xie 2016).

The Pacific Ocean also exhibits a strong multidecadal activity (Zhang et al. 1997; Minobe 1997; Deser et al. 2004), sometimes referred as Pacific Multidecadal Variability (PMV), coexisting with the aforementioned (inter)decadal Pacific variability (Minobe 1999) and driving large global climate effects (Meehl and Hu 2006). Tropical and extratropical PMV evolve independently (Latif 2006), basically responding to stochastic wind stress forcing (Power et al. 1995).

Role of STCs on Pacific Decadal Variability

The shallow meridional overturning circulation has been used to explain some of the decadal-scale variability within the Pacific Ocean (Nonaka et al. 2002; Capotondi et al. 2005; Zhang and McPhaden 2006; Cheng et al. 2007; Farneti et al. 2014a), due to their influence on ENSO and PDO variability (Kleeman et al. 1999; Meehl and Hu 2006; Wu et al. 2007; Farneti et al. 2014b; Hong et al. 2014). In particular, the anti-correlation between equatorial SST and equatorward mass transport, observed by McPhaden and Zhang (2002, 2004), is confirmed by several modelling studies (Capotondi et al. 2005; Zhang and McPhaden 2006; Cheng et al. 2007; Farneti et al. 2014a). In this respect, coupled simulations performed by Liu and Yang (2003) show that the signal coming from the Extratropics propagate toward the Equator exploiting both atmospheric and oceanic connections. In their modelling framework, the equatorial SST response (about a half of the forcing SST signal) is mostly due to the atmospheric bridge on monthly timescales, whereas the subsurface temperature response is forced by thermocline ventilation on decadal timescales, with the Southern Hemisphere having the largest influence on the equatorial ocean variability. In fact, the global warming trend observed during the last decades projects on a decadal mode of SST variability in the western equatorial Pacific Ocean, which is connected with both TCs and STCs circulation (Lohmann and Latif 2005), although other processes are involved on determining the tropical Pacific SST warming trend (Zhang and McPhaden 2006). However, finding the "smoking gun" of the STCs influence on equatorial SST in coupled simulations is still a challenge (Solomon and Zhang 2006), although models giving larger STCs convergence variations tend to simulate larger equatorial SST variability (Zhang and McPhaden 2006).

Solomon et al. (2003) provide a link between STCs, ENSO, and North Pacific decadal variability within an ocean-atmosphere coupled model. In fact, the application of an extratropical stochastic forcing on the sea surface affects ENSO decadal variability through an altered STCs transport, producing a more pronounced decadal variability. Furthermore, Wu et al. (2007) propose a joint teleconnection mechanism between STCs and the wind-evaporation-SST feedback (WES; Liu and Xie 1994) on driving Pacific climate variability on decadal timescales. For what concerns PDO, the regime transition occurred in the 1970s from a negative to a positive phase (Nitta and Yamada 1989; Graham 1994; Gutzler 1996; Wu et al. 2005) is related with a concomitant weakening of the STCs transport (McPhaden and Zhang 2002), with a "rebound" in the late 1990s (McPhaden and Zhang 2004) after another reversal of the PDO phase (Minobe 2002; Peterson and Schwing 2003; Yeh et al. 2011; Ding et al. 2013). According to the models comparison performed by Solomon and Zhang (2006), the reduced STCs transport observed from the 1970s to the 1990s is related to a reduction of subtropical wind stress forcing.

Gu and Philander (1997) exploit STCs dynamics to explain the propagation of thermal anomalies observed by Deser et al. (1996), subducting in the North Pacific to reach the equatorial regions through the so-called $\overline{v}T'$ mechanism. Although the observational study of Zhang et al. (1998a) corroborates this hypothesis, several studies (Schneider et al. 1999a,b; Tourre et al. 1999; Pierce et al. 2000; Hazeleger et al. 2001b) find instead that temperature signals would decay quickly away from their source region, way before reaching the equatorial region. In fact, despite the clear propagation of thermal anomalies from the subduction region up to 18°N shown by Deser et al. (1996), close to the Equator any correspondence is lost (Schneider et al. 1999a), whereas local (wind-induced) forcing accounts for most of the observed signal (Schneider et al. 1999b; Hazeleger et al. 2001b; Nonaka et al. 2002; McGregor et al. 2007, 2008). Gu and Philander (1997) mechanism is thus falling short in explaining the observed decadal variability in the Pacific Ocean (Capotondi et al. 2005;

Liu and Alexander 2007).

Another interpretation of the STCs observed influence on the tropical dynamics is given by Kleeman et al. (1999). Forcing a coupled model of intermediate complexity with an observed atmospheric dataset, they find that the decadal modulation of equatorial SST coincides with variations of subtropical wind stress, resulting largely from upwelling driven by thermocline ventilation. They also state that the wind stress forcing at the Subtropics is able to alter the equatorial temperature structure, changing the strength of the overturning cells through the so-called $v'\overline{T}$ mechanism. The framework introduced by Kleeman et al. (1999) is supported by several observational studies (McPhaden and Zhang 2002, 2004). In particular, the downward trend of the STCs transport observed from 1970s to the 1990s (McPhaden and Zhang 2002) coincided with an increase of the equatorial Pacific SST of about 0.8°C (Zhang et al. 1997), along with a decreased intensity of the trade winds and a IPO/PDO positive phase. Further, the observed SST increase can not be ascribed to changes in the surface flux, which usually act to damp rather than generate decadal variability at the Equator (McPhaden and Zhang 2002; Lohmann and Latif 2005). The reversal of the PDO phase in the late 1990s occurred together with an increase of the STCs-driven equatorial mass convergence (McPhaden and Zhang 2004; Cheng et al. 2007), but could be also due to decadal ENSO modulations (Kirtman and Schopf 1998).

England et al. (2014) link Pacific STCs dynamics to the recent global warming slowdown (Easterling and Wehner 2009; Trenberth and Fasullo 2013; Lewandowsky et al. 2016), likely induced by internal climate variability (Meehl and Teng 2014). Although Fyfe et al. (2016) and Hedemann et al. (2017) call for caution about hasty attributions for such complex event, the latest global warming slowdown nevertheless occurred during a negative phase of the IPO/PDO (Lee and McPhaden 2008; Meehl et al. 2013), corresponding to an enhanced trade winds forcing (L'Heureux et al. 2013; Boisséson et al. 2014), and an increased Pacific shallow overturning circulation strength in both observations (McPhaden and Zhang 2004; Meehl et al. 2011) and models (Capotondi et al. 2005; Farneti et al. 2014a). However, observational results from Chen and Tung (2014) does not support this Pacific-centric view, also corroborated by surface temperature analysis performed by Wu et al. (2011), while coupled simulations do not reproduce the observed strengthening of the Pacific trade winds (Yang et al. 2014; Kociuba and Power 2015). Anyway, by linearly increasing the zonal wind stress forcing on the Pacific Ocean between 45°N and 45°S, England et al. (2014) account for a substantial heat content increase in the Indo-Pacific Ocean below 125 m and a heat content decrease above 125 m. In fact, the deep ocean is thought to have played a more important role in the global warming slowdown, with respect to upper layers (Lyman et al. 2010; Balmaseda et al. 2013; Chen and Tung 2014). With a similar experimental setup, Maher et al. (2018) analyse the Pacific shallow overturning circulation (including both STCs and TCs) under different 20-years-long IPO conditions, showing a strengthening of the circulation during the negative IPO phase and a subsequent weakening for positive IPO. The subsurface temperature structure in the tropical Pacific is thus modified by the joint action of changes in thermocline depth and strengthening (weakening) of PSOC (also shown by Han et al. 2006), with the warm (cool) response found in the western Pacific between 100 and 300 m depth and cooling (warming) in the eastern Pacific.

Other explanations of tropical-extratropical relationship in the Pacific Ocean are given by Lysne et al. (1997), Liu et al. (1999), Capotondi and Alexander (2001), Hazeleger et al. (2001b), Wu et al. (2003), and McGregor et al. (2007) in terms of planetary waves propagation. Barnett et al. (1999) and Pierce et al. (2000) argue instead that decadal changes of the atmospheric circulation over the northern Pacific Ocean can extend so far equatorward to alter the wind stress in that region, ruling out any oceanic interaction.

1.3 Motivations and Objectives

The present Chapter included a literature review of the (rather extensive) state-of-the-art knowledge about Pacific STCs. However, a clear disambiguation of the role of different regions on forcing Pacific STCs is lacking, at least for what concerns modelling studies employing global ocean models. Further, a more detailed assessment of STCs properties under unforced conditions or future climate scenarios, with respect to what found in literature, is also needed.

In the present work, we tackle these aspects by setting up a hierarchy of numerical simulations of increasing complexity using a global ocean-ice model, starting with idealised perturbations and then moving to observed patterns. Finally, we assess several properties of STCs in ocean-atmosphere coupled models in two different configurations: the pre-industrial control implementation (in which the atmospheric radiative forcing is taken constant during the whole simulation), and an idealised future scenario characterised by a linear increase of the atmospheric CO_2 concentration.

Thus, the main objectives of the present work are:

1. To address the impact of the wind stress forcing acting on different regions of the Pacific Ocean on Pacific STCs, by comparing perturbation experiments with a climatological control simulation. These experiments are obtained employing both idealised and realistic anomalies.

2. To assess the transient response of the shallow meridional overturning circulation in the Pacific Ocean to both time-constant and time-varying wind stress forcing, as well as to evaluate the climatic impact of STCs anomalies on the tropical ocean state.

3. To study the Pacific STCs low-frequency variability in different implementations of state-of-the-art coupled models, evaluating both natural and forced aspects.

Chapter 2

Data and methods

Different data sources and analysis techniques are employed in the present study. It is also worth to underline that all numerical simulations are performed by the Ph.D. candidate. For what concerns the experiments performed for highlighting the role of (off-)equatorial wind stress forcing with idealised (Chapter 3) and realistic (Chapter 4) patterns, the description of the model is found in Section 2.1. A short description of the coupled models used to analyse simulated STCs properties (Chapter 5) is included in Sections 2.2.

2.1 The ocean model MOM5

For the first part of the study, we employed the NOAA/GFDL Modular Ocean Model version 5 (MOM5; Griffies 2012). It is a global-ocean, volume-conserving, primitive-equations model. MOM5 is written using generalised horizontal coordinates using a staggered B-grid type (Arakawa and Lamb 1977), as well as the tripolar configuration introduced by Murray (1996) to avoid any coordinate singularity at the North Pole. Bottom topography is represented using a partial bottom step technique (Adcroft et al. 1997; Pacanowski and Gnanadesikan 1998), along with quasi-horizontal rescaled height coordinates (Stacey et al. 1995; Adcroft and Campin 2004). The two-level time stepping scheme introduced by Griffies et al. (2005) is used, with a time step of 7200 s for inviscid and dissipative velocity components and a split-explicit time stepping scheme (80 s time step) employed as explicit barotropic solver (Griffies 2004).

The horizontal resolution is $1^\circ \times 1^\circ$, with a progressively increasing discretization toward the Equator (up to $1/3^\circ$) from 30°N to 30°S in the meridional direction. The model has 50 vertical levels in depth coordinates. Some variables are also remapped using the potential density referred at 2000 dbar as vertical coordinate, computed according to the IOC et al. (2010) equation of state. The model also includes a dynamic-thermodynamic sea-ice model.

2.1.1 Parametrisations

Mesoscale eddy processes are parametrised using the Gent-McWilliams (GM) skew-flux closure scheme (Gent and McWilliams 1990; Gent et al. 1995; Griffies 1998). The GM closure scheme accounts for some aspects of baroclinic eddies, able to convert available potential energy into eddy kinetic energy. Generally, baroclinic eddies correspond to the antisymmetric components of the tracer mixing tensor (Griffies 1998), with the tracer skew-flux directed along the isolines and perpendicularly to the gradient; this kind of mixing is often referred to as "stirring" (Eckart 1948). The skew-flux formulation introduced by Griffies (1998) supplements GM stirring algorithm with Redi (1982) and Cox (1987) isoneutral diffusion process, employed in many coarse-resolution models to parametrise tracer mixing.

We use a two-dimensional GM parametrisation, with maximum slope allowed for isoneutral density surfaces set to 0.05. GM diffusivity ranges from 100 to 800 m^2 s^{-1}, independent in depth but varying in latitude, longitude, and time. GM closure scheme is important in regions like the western boundaries or inside the Southern Ocean, where steep density surfaces can form and mesoscale eddies are smaller. At the Equator, however, most eddies are resolved, hence our model results are not affected by the choice of GM parameters. Submesoscale eddy fluxes related with re-stratification in the ocean mixed layer are parametrised following Fox-Kemper et al. (2008), Fox-Kemper and Ferrari (2008), and Fox-Kemper et al. (2011).

A combined scheme is used for tidal mixing, based on the algorithms introduced by Simmons et al. (2004) and Lee et al. (2006). The vertical mixing computation is provided by the KPP scheme introduced by Large et al. (1994) and Danabasoglu et al. (2006), with enabled double-diffusion mixing. A Smagorinski biharmonic scheme deals with horizontal friction (Griffies and Hallberg 2000), and a constant neutral diffusivity is used.

2.1.2 Surface boundary conditions

The climatological CORE-I Normal Year Forcing (NYF) atmospheric state (Griffies et al. 2009) is imposed as boundary conditions at the sea surface.

CORE-I NYF is a dataset specifically focused on long-term ocean simulations, obtained by Large and Yeager (2004) from a 43-years-long interannual-varying atmospheric state, with a seamless transition from 31 December to 1 January. CORE-I NYF design consists of a repeating annual cycle of atmospheric forcing, obtained as a combination of reanalysis and remote sensing products, producing near zero global-mean heat and freshwater fluxes when used in combination with observed SST.

Surface fluxes of heat, freshwater and momentum are thus determined using the CORE-I NYF atmospheric dataset, the model's prognostic SST and surface currents, as well as the Community Climate System Model (CCSM) bulk formulae described by Large and Yeager (2004), Large (2006), and Large and Yeager (2009). There is no restoring term applied to sea surface temperature. In contrast, surface salinity restoring is used to prevent unbounded local salinity trends, with a relaxation timescale of 60 days.

2.1.3 Control run

We performed a long control (reference) run in order to obtain a statistically-stable mean state, since deep ocean circulation must reach a quasi-equilibrium condition before any numerical experiments can be started. Equilibration takes from centuries to millennia to be reached, depending on the timescale of ocean ventilation and mixing (England 1995; Stouffer 2004). In this respect, Griffies et al. (2009) show that the typical timescale for ocean equilibration to the CORE-I NYF atmospheric state greatly varies among models, with a relatively-short surface adjustment time (50-100 years) whereas deep circulation properties keep drifting for more than 500 years.

After about 4000 years our model have adjusted in its deep layers, and standard metrics show minimal drift. Stability is evaluated in terms of mass transport of the Antarctic Circumpolar Current at the Drake Passage, and the global Meridional Overturning Circulation at some key locations. No significant drift is observed, although some low-frequency oscillations occur in some time series.

2.2 CMIP5 models

Coupled models are complex numerical algorithms, connecting different components of the climate system. Included in properly-set hierarchical modelling protocols (Held 2005; Cassou et al. 2018), coupled models are most valuable tools for the assessment of past, present and future climate variability, although deficiencies in model formulations and biases with observations still produce uncertainties in their results. In particular, since the very first attempts during the 1960s-1970s on assembling coupled models (Manabe and Bryan 1969; Manabe et al. 1975; Bryan et al. 1985), it seemed essential to include dynamically-varying ocean components for improving the representation of observed climate.

In the last decades, the emergence of a large number of different coupled models for climate simulations urged the establishment of ad-hoc model intercomparison projects, similar to other global-scale intercomparison efforts. As resumed by Meehl et al. (2000, 2005a), the first two Coupled Model Intercomparison Projects (CMIP1 and CMIP2) started respectively in 1995 and 1998, including almost all the coupled climate models of the time. Different groups of sub-projects were established, focusing on different aspects of climate variability and change. The following phases of the project enlarged the number of employed models and the tackled challenges (CMIP3 and CMIP4; Meehl et al. 2007), providing a key contribution for the International Panel for Climate Change (IPCC) Fourth Assessment Report (AR4).

Phase 5 of the project followed the same path (CMIP5; Taylor et al. 2012), introducing shorter integrations for climate prediction on decadal timescales, as well as long-term (centennial) simulations. Although there is little improvement with respect to CMIP3 concerning some key-aspects like cloud feedbacks (Andrews et al. 2012) and reproduction of observed climate variability and teleconnections (Qasmi et al. 2017), and despite the uncertainties affecting long-term projections (Knutti and Sedláček 2013), CMIP5 models provide unprecedented long datasets for analysing both climate state and variability.

Among the large number of available long-term simulations included in CMIP5, we chose to analyse the output from the control pre-industrial simulations performed with NOAA/GFDL coupled models, thus providing a continuity with our ocean-only perturbation experiments performed using MOM5. The main features of the models are shortly described as follows.

- CM2.1: Global coupled model described by Delworth et al. (2006) and Gnanadesikan et al. (2006), employing the NOAA/GFDL Modular Ocean Model version 4 (MOM4 Griffies et al. 2003) as ocean component, and a modified version of the AM2 model (The GFDL Global Atmospheric Model Development Team 2004) for the atmospheric part. The coupling between the components is provided by the Flexible Modeling System

(FMS; `https://www.gfdl.noaa.gov/~fms/`), as in all GFDL models.

- CM2.5: High-resolution global coupled model described by Delworth et al. (2012), which improves several aspects of CM2.1 by using an increased-resolution implementation of the atmospheric model and the Modular Ocean Model version 4p1 (MOM4p1; Griffies 2009). Among the selected models, CM2.5 is the only one not employing a parametrisation for mesoscale eddies.

- CM2.5-FLOR: Forecast-oriented Low Ocean Resolution version of CM2.5 model (Vecchi et al. 2014), incorporating high atmospheric resolution component from CM2.5 and relatively low-resolution ocean and sea-ice components from CM2.1.

- CM3.0: Global coupled model mostly focused on obtaining a better representation of aerosol-cloud and chemistry-climate interactions with respect to the CM2.1 formulation (Griffies et al. 2011). It includes an improved atmospheric representation (AM3; Donner et al. 2011), and the MOM4p1 as ocean model.

- ESM2M: Global climate model which uses the AM2 model as atmospheric component, MOM4p1 as ocean model, and an explicit representation of the carbon dynamics (Dunne et al. 2012).

2.3 Mass Transport and Energy Flux Diagnostics

This section include most of the metrics we employed throughout our analysis. We compute the total meridional mass transport (in Sverdrups; 1 Sv = 10^6 m^3 s^{-1}) as

$$\Psi(y, z) = -\int_{\lambda_1}^{\lambda_2} \mathrm{d}x \int_{-h}^{\eta} \mathrm{d}z' \, (v + v^*), \tag{2.1}$$

where λ_1, λ_2 define the longitudinal extension of the basin, h is the ocean's depth, η is the sea surface, and the transport includes both resolved v and parameterized v^* meridional velocities. Given that we are interested in the mass and energy anomalies reaching the equatorial upper layers, in most of our analysis we only consider the zonally and vertically integrated equatorward meridional transports in the uppermost 1000 m.

The meridional total energy transport (PW = 10^{15} W) is computed as an anomaly of the control run value, namely

$$E_{TOT}(y) = \rho_0 \, C_\mathrm{p} \int_{\lambda_1}^{\lambda_2} \mathrm{d}x \int_{-h}^{\eta} \mathrm{d}z \, (v\theta - v_c\theta_c), \tag{2.2}$$

where ρ_0=1035.0 kg m^{-3} is the reference density, C_p=3992.1 J kg^{-1} °C^{-1} is the heat capacity for seawater at constant pressure (Griffies 2012), v is now the total meridional velocity component and θ is potential temperature for the perturbation experiment, whereas v_c and θ_c relates to the control run. This diagnostic provides the full energy flux anomaly in the chosen latitudinal range. In order to isolate the contribution from STCs, the energy transport calculation proposed by Klinger and Marotzke (2000) is also used, where only zonal wind stress and SST values are needed. As we will show later, wind-driven meridional mass transports and meridional SST gradients are exploited to compute the meridional energy flux ascribed to STCs only.

Ocean heat content (OHC) is also evaluated as an anomaly, that is

$$OHC = \rho_0 \, C_\mathrm{p} \int\limits_{\lambda_1}^{\lambda_2} \mathrm{d}x \int\limits_{\phi_1}^{\phi_2} \mathrm{d}y \int\limits_{-h}^{\eta} \mathrm{d}z \, (\theta - \theta_c). \tag{2.3}$$

where ϕ_1, ϕ_2 define the latitudinal extension of the basin.

Finally, the Indonesian Throughflow (ITF) accounts for the exchange of water between Pacific and Indian basins. It is computed summing up the zonal transport crossing the passage between South Timor and Australia, and the meridional transport passing through Lombok and Ombai Straits.

2.3.1 Meridional energy transport by Subtropical Cells

The meridional energy transport provided by Equation 2.2 includes all dynamical processes, which in the Pacific mainly involves STCs and wind-driven gyres. In order to isolate the STCs contribution we employ the method developed by Klinger and Marotzke (2000), which allows the computation of the STC-related meridional energy transport using Ekman dynamics. The expression for the STCs meridional energy transport is

$$\mathrm{E_{STC}}(y) = C_\mathrm{p} \int\limits_{\lambda_1}^{\lambda_2} \mathrm{d}x \int\limits_{y_1}^{y} \mathrm{M_E} \frac{\partial \theta}{\partial y} \, \mathrm{d}y, \tag{2.4}$$

where $\mathrm{M_E} = -\tau(y)/f(y)$ is the Ekman mass transport and θ is the surface potential temperature. The energy transport is integrated zonally and for each model grid point between 10° and the latitude of zero wind stress (≈30°), although contributions to the STCs mass transport in the real ocean can also come from a more northern location (McCreary and Lu 1994; Liu et al. 1994). The estimates for the STC meridional energy transport given by Eq. 2.4 in our control run and for all ocean basins (Fig. 2.1) show that our model results compare well with the observational estimates given in Klinger and Marotzke (2000, c.f. Fig. 6). Because of their zonal extent, Pacific and Indian Ocean STCs stand out with the largest meridional fluxes.

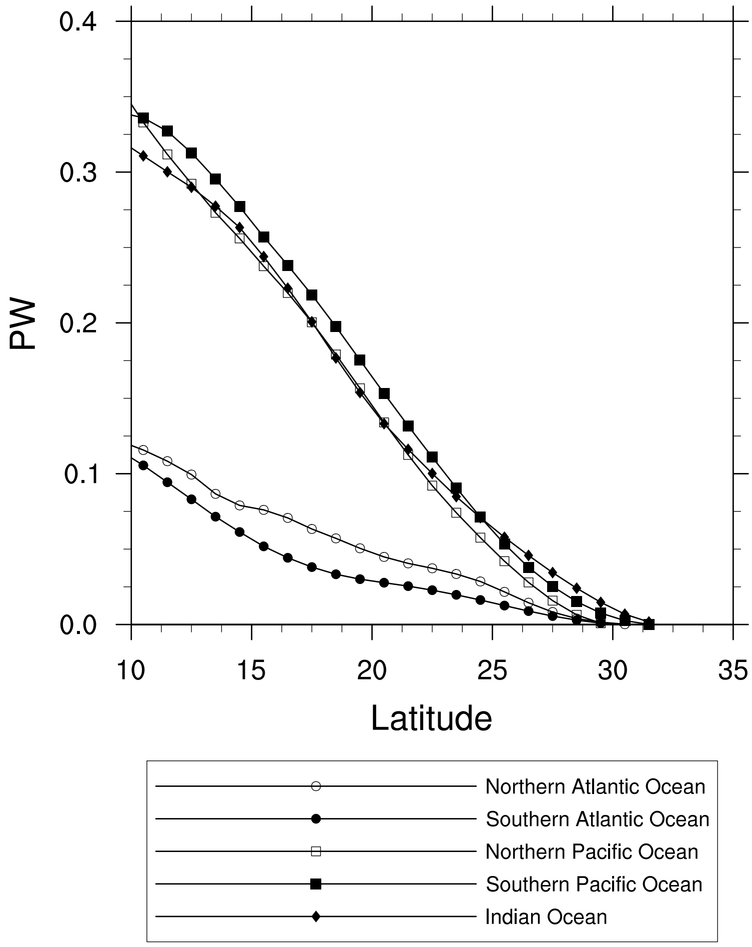

Figure 2.1: STC meridional energy transports in the control run computed for all basins (1 PW = 10^{15} W). Transports are estimated using Eq. 2.4 and are in agreement with previous observational estimates (Klinger and Marotzke 2000, c.f. Fig. 6).

A full derivation of Eq. 2.4 is provided here. The momentum balance in the Ekman boundary layer is expressed as in Vallis (2006)

$$f\,\mathbf{k} \times \mathbf{u}_\mathrm{E} = \frac{1}{\rho_0}\frac{\partial \boldsymbol{\tau}}{\partial z}, \tag{2.5}$$

where f is the Coriolis parameter, $\mathbf{u}_\mathrm{E}$ is the horizontal velocity vector in the Ekman layer, $\boldsymbol{\tau}$ the surface wind stress, ρ_0 a reference density and $\mathbf{k}$ the unit vertical direction.

Vertically integrating Eq. 2.5 yields

$$f\,\mathbf{k} \times \mathbf{M}_\mathrm{E} = \boldsymbol{\tau}, \tag{2.6}$$

and the integrated mass transport in the Ekman layer is

$$\mathbf{M}_\mathrm{E} = \int_{h_e}^{0} \rho_0 \mathbf{u}_\mathrm{E}\,\mathrm{d}z = \frac{\boldsymbol{\tau} \times \mathbf{k}}{f}, \tag{2.7}$$

where h_e is the characteristic depth of the Ekman layer and Eq. 2.7 defines the Ekman transport to be proportional to the magnitude of the wind stress.

Suppose now the wind stress to be zonal $\tau(y)$, providing a meridional mass flux $\mathrm{M}_\mathrm{E} = -\tau(y)/f(y)$. The wind stress τ is a function of latitude, generating a flow divergence at the surface and implying subduction into the ocean interior. Over a latitudinal interval δy, and using mass conservation, the mass flux subducted M_S is

$$\mathrm{M}_\mathrm{S} = \frac{\partial \mathrm{M}_\mathrm{E}}{\partial y}\delta y. \tag{2.8}$$

If a latitude at which $\tau = 0$ exists, as observed, then mass conservation requires all Ekman mass flux to be subducted. The flow beneath the Ekman layer exactly balances the mass flux in the Ekman layer, and the subducted mass flux M_S is equal and opposite to the Ekman mass flux M_E. Considering a full latitudinal extent

$$\mathrm{M}_\mathrm{S} = \int_{y}^{y_1} \frac{\partial \mathrm{M}_\mathrm{E}}{\partial y}\,\mathrm{d}y = -\mathrm{M}_\mathrm{E}(y), \tag{2.9}$$

where y_1 is a subtropical subduction latitude at which $\tau = 0$ and we have noted that $\mathrm{M}_\mathrm{E}(y_1) = 0$.

The temperature of the Ekman flow is $\theta(y)$, whereas the subducted flow conserves the surface temperature $\theta(y_1)$, assuming an interior adiabatic flow. The temperature flux associated with the Ekman flow is thus $\mathrm{T}_E(y) = \theta(y)\mathrm{M}_\mathrm{E}$, whereas the returning branch of the circulation has a temperature flux given by

$$\mathrm{T}_S(y) = -\int_{y}^{y_1} \theta(y)\frac{\partial \mathrm{M}_\mathrm{E}}{\partial y}\,\mathrm{d}y. \tag{2.10}$$

The net temperature flux, which we relate to the STC, is given by Klinger and Marotzke (2000) and Held (2001) as

$$\mathrm{T}_{\mathrm{STC}}(y) = \theta(y)\mathrm{M}_{\mathrm{E}} + \int_{y}^{y_1} \theta(y) \frac{\partial \mathrm{M}_{\mathrm{E}}}{\partial y} \,\mathrm{d}y \tag{2.11}$$

$$= -\int_{y}^{y_1} \mathrm{M}_{\mathrm{E}} \frac{\partial \theta}{\partial y} \,\mathrm{d}y = \int_{y}^{y_1} \frac{\tau(y)}{f} \frac{\partial \theta}{\partial y} \,\mathrm{d}y. \tag{2.12}$$

Or, in θ-space

$$\mathrm{T}_{\mathrm{STC}}(y) = -\int_{y}^{y_1} \mathrm{M}_{\mathrm{E}} \frac{\partial \theta}{\partial y} \,\mathrm{d}y = \int_{y_1}^{y} \mathrm{M}_{\mathrm{E}} \frac{\partial \theta}{\partial y} \,\mathrm{d}y = \int_{\theta(y_1)}^{\theta(y)} \mathrm{M}_{\mathrm{E}} \,\mathrm{d}\theta. \tag{2.13}$$

The last expression is the same as Eq. 11 in Klinger and Marotzke (2000) and Eq. 8 in Held (2001).

The meridional energy transport of the STC is obtained by zonally integrating the temperature flux and multiplying by C_{p}, the heat capacity of the ocean

$$\mathrm{E}_{\mathrm{STC}}(y) = C_{\mathrm{p}} \int_{\lambda_1}^{\lambda_2} \mathrm{d}x \int_{y_1}^{y} \mathrm{M}_{\mathrm{E}} \frac{\partial \theta}{\partial y} \,\mathrm{d}y. \tag{2.14}$$

Chapter 3

Impact of idealised zonal wind stress perturbations

In Chapter 1 we revised STCs properties as found in literature, showing that the importance of thermocline ventilation provided by STCs on connecting equatorial and off-equatorial regions is undoubted. Still, the role of local and non-local wind stress forcing on the equatorial ocean state and the relative role of STCs must be clarified, as long-lasting changes of the extratropical wind stress forcing can significantly affect tropical ocean variability (Alexander 2010). Bryan (1982) in fact show that changes in the zonally-integrated wind stress have a direct influence in the Ekman layer mass transport. The resulting wind-driven circulation is found in the thermocline (Pedlosky 1987), since the vertical structure of the thermocline is strongly linked to the horizontal structure of the ocean surface circulation (Luyten et al. 1983) and the ocean motion in the first 1000 m of depth is mostly wind-driven (Huang and Qiu 1994). Moreover, the compensating barotropic return flow occurring at relatively shallow depths involves STCs dynamics (Klinger and Marotzke 2000).

In the present chapter, we are going to assess the role of local and non-local wind stress forcing on the shallow meridional overturning circulation of the Pacific Ocean. Furthermore, the impact of the altered STCs transport on the equatorial surface and sub-surface ocean state will be evaluated. This chapter includes material published in Graffino et al. (2018).

3.1 Wind Stress Forcing of Pacific STCs

While McCreary and Lu (1994) crown the off-equatorial wind stress forcing as primary driving mechanism of Pacific STCs, Liu et al. (1994) specifically address the role of the equatorial wind stress the subtropical-tropical mass exchange. In particular, Liu et al. (1994) show that the absence of the equatorial forcing essentially cuts off the remote connection, thus giving a minor role to the subtropical wind stress forcing. However, wind stress patterns at the Subtropics can affect the tropical temperature field significantly by changing the mean depth of the equatorial thermocline (Liu and Philander 1995; Hazeleger et al. 2001b). Assessing the role of the thermocline in this respect is important, because of the observed correlation between upper-ocean heat content and thermocline depth (Rebert et al. 1985). Still, the properties of STCs in Liu and Philander (1995) model simulation are mainly determined by tropical easterlies, while the subtropical forcing is only able to slightly affect the EUC mass transport by changing the western boundary supply. By performing several sensitivity tests, Kleeman et al. (1999) nonetheless identify the wind stress variability in the subtropical Pacific Ocean as the source of STCs transport anomalies; in that region, anomalous latent heat fluxes forced by wind stress variations also provides a driving mechanism for ocean-atmosphere coupled decadal variability (Nakamura and Yamagata 1999).

The role of the wind stress forcing on STCs dynamics is further addressed by Klinger et al. (2002). In particular, despite the expected minor role of the extratropical wind stress on altering time-mean STCs properties, they acknowledge that it could have an important role on the transient phase by changing the inter-ocean circulation with the Indian basin. Using the same 3-1/2-layer model of Lu et al. (1998) over a simplified version of the Pacific Ocean, Klinger et al. (2002) in fact impose different wind stress patterns (both time-constant and time-oscillating) on the sea surface and compare the obtained results with a climatological control run. The amplitude of the generated signal at the Equator is found to be very sensitive to different oscillation periods, suggesting that a maximum response could be achieved with a properly-chosen forcing period. Moreover, the transient response of the circulation consists of a fast adjustment of the poleward surface flow, and a slower modification of both equatorward and upwelling motions, taking up to 10 years to reach an equilibrium value. Employing the same numerical setup of Lu et al. (1998), Solomon et al. (2003) further show that STCs variability responds almost linearly to changes in the wind stress forcing.

Klinger et al. (2002) also show that changing the intensity of the trade winds just modifies the longitudinal extent of the STCs-related equatorial upwelling, but it does not increase the upwelling intensity itself. However, this is not the case for other model studies (e.g., Capotondi et al. 2005). According to Lohmann and Latif (2005) simulations, a weakening of the trade winds could actually bring to a reduced Ekman transport divergence in the upper equatorial ocean, and the resulting negative wind stress curl anomaly at subtropical latitudes causes a local shoaling of the thermocline (Capotondi and Alexander 2001), with a consequent spin-down of STCs. Nonaka et al. (2002) show instead that SST at the Equator is not very sensitive to midlatitude wind stress variability (north of 25°N and south of 20°S), claiming that equatorial SST is more susceptible to tropical wind stress forcing, as also confirmed by the simulation study of Capotondi et al. (2005). Perhaps, as suggested by Nonaka et al. (2006), the wind stress anomalies employed by Nonaka et al. (2002) are not large enough to drive a substantial response. Nonaka et al. (2002) simulations also support the $v'\overline{T}$ mechanism introduced by Kleeman et al. (1999), since part of the equatorial ocean variability is driven by off-equatorial winds through STCs circulation. There is a lag of about 2 years between locally and remotely-forced equatorial SST anomalies, with Nonaka et al. (2002) suggesting that STCs act on maintain and eventually amplify anomalies driven by local winds, and not initiate them; this is also confirmed by McGregor et al. (2008) model simulations.

Nonaka et al. (2006) force a global ocean model with a climatological wind stress forcing on the tropical ocean and a modified forcing on the Extratropics, in order to study the role of strengthened and weakened midlatitude westerlies on the equatorial thermocline. They show that changes in the midlatitude wind stress pattern induce a striking alteration of the local mixed layer, bringing to the formation of mixed-layer-depth fronts and alteration of the subtropical stratification and water subduction. However, STCs mass transport does not change much during all experiments, with the resulting variations in the equatorial stratification mostly due to planetary waves propagation. According to McGregor et al. (2007, 2008) model simulations, the role of off-equatorial winds poleward of 12.5° is small but statistically significant in forcing Pacific low-frequency variability and generating thermocline depth anomalies at the Equator. Instead, western boundary reflection of planetary waves is important for the equatorial thermocline forcing just within 20° of latitude; poleward of this latitude, the role of waves reflection is negligible. However, perturbation experiments performed by Lübbecke et al. (2008) show that near-surface equatorial temperature anomalies are primarily governed by wind-driven changes in the EUC. More specifically, equatorward transport of subtropical thermocline water associated with STCs is significantly affected by low-frequency variability of the off-equatorial wind stress. Thus, STCs variability is driven by off-equatorial forcing and is anti-correlated with equatorial SST and EUC variability. The statistical relationship is weak on interannual timescales but stronger on decadal timescales, with equatorial and off-equatorial contributions becoming almost equal as also confirmed by Farneti et al. (2014a,b). Lübbecke et al. (2008) further speculate that discrepancies between computed net equatorward transport and equatorial SST trends among models could be due to the different employed horizontal resolution, especially for what concerns a correct reproduction of western boundary currents.

Farneti et al. (2014b) introduce an ocean-atmosphere feedback involving STCs intermediation. They show that wind stress anomalies in the North Pacific, generated by tropical SST forcing, can affect the subtropical gyre circulation, which in turn changes the Ekman transport altering the northern STC circulation and associated heat transport; finally, a thermal response is obtained at the Equator. In this way, decadal variability of the tropical SST can be driven by extratropical atmospheric circulation patterns; we will further explore this point in Chapter 4. The schematic of the mechanism proposed by Farneti et al. (2014b) is shown in Fig. 3.1. The initial forcing is provided by a tropical SST anomaly, which affects the atmospheric Hadley cell and the wind stress pattern over the Pacific Ocean. The altered STC circulation forces an equatorial anomaly, damping the initial one and giving way to a negative feedback process on decadal timescales. An equilibrium between forcing and response is reached after 5-10 years from the beginning of the simulation, consistent with both baroclinic adjustment and STCs forcing mechanisms.

3.2 Experimental Setup

In the present chapter, our main purpose is to assess the effect of subtropical and extratropical wind stress on STCs dynamics, and how their transport modifications propagate and influence the equatorial ocean state. We carried out similar analyses on a set of equatorial experiments, in order to have a direct comparison between locally and remotely-forced perturbation anomalies.

Starting from the last 200 years of the control run described in Chapter 2, we performed several perturbation experiments using time-constant wind stress

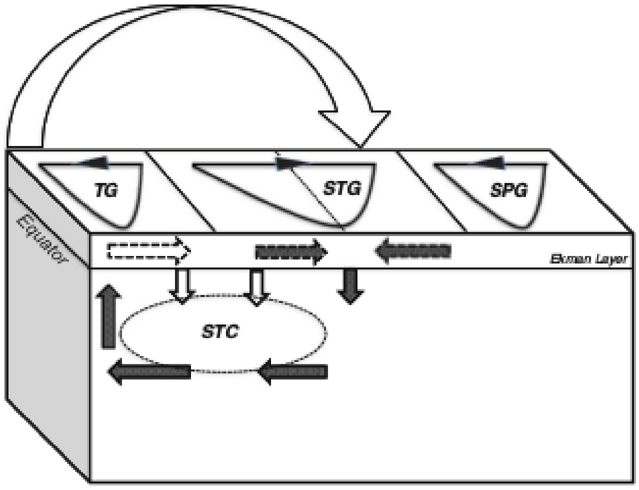

Figure 3.1: Schematic of the tropical-subtropical, ocean-atmosphere feedback in the Pacific Ocean, involving the horizontal gyres (TG: tropical gyre, STG: subtropical gyre, SPG: subpolar gyre) and subtropical vertical cell (STC: subtropical cell). Taken from Farneti et al. (2014b).

Experiment	τ_x	Time (years)
Control	NYF	1400
10	NYF±10%	20
20	NYF±20%	20
30	NYF±30%	20
40	NYF±40%	20
50	NYF±50%	20

Table 3.1: Main characteristics of the idealised perturbation experiments. τ_x is the zonal wind stress applied to the ocean surface during each experiment. The ocean model computes the zonal wind stress from the climatological zonal wind (NYF, CORE-I dataset; Griffies et al. 2009). Then, during the perturbation experiments, an anomaly is added to the climatological wind stress as a fraction, positive or negative, of the wind stress itself.

anomalies (Table 3.1). Each zonal wind stress anomaly used in the simulation is obtained as a fraction of the climatological value, and then added to or subtracted from the NYF field. Figure 3.2 shows the zonal average of the zonal wind stress anomalies. Zonal wind stress anomalies (Figure 3.3), superimposed on the NYF forcing, are chosen according to their geographical pattern and location, or by choosing a proper wind stress threshold that would maintain continuity with the climatological contours (Figure 3.3a). For each case, ten experiments are performed (Table 3.1) in order to assess the possibility of a linear relationship between the forcing applied and STCs response. Anomalous forcing experiments are 20 years long, and we show results averaged over the last 5 years.

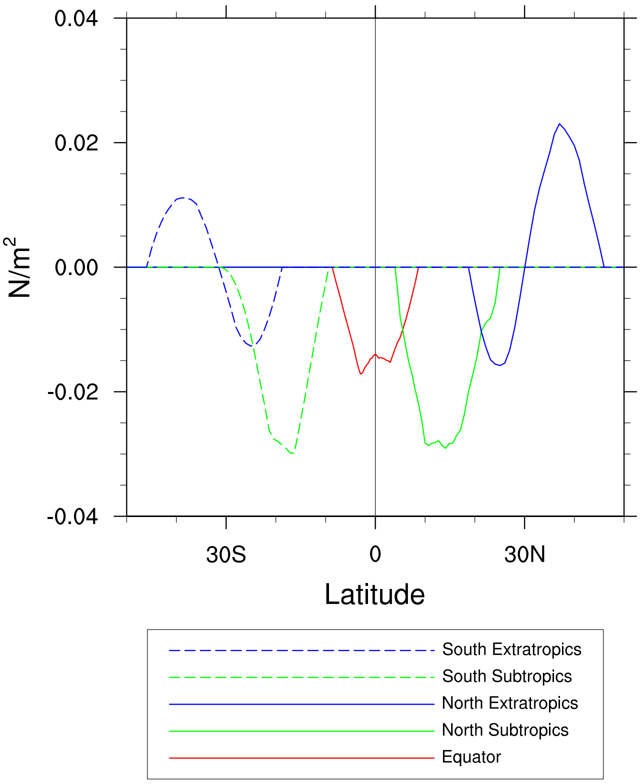

Figure 3.2: Zonal average of the zonal wind stress anomalies (N/m^2), computed from the climatological value of the zonal wind stress from the CORE-I dataset (Griffies et al. 2009). Each anomaly is added or subtracted to the NYF, after been multiplied by a factor.

3.3 Results

We designed our experiments to test the sensitivity of a time-constant zonal wind stress anomaly on STCs, located at some specific latitudinal range. Thus, they are not meant to reproduce any observed variability, but rather to quantify and test the sensitivity of STCs to idealised and realistic forcing anomalies. Although the absolute value of the imposed surface anomalies lies between the observed variability at both Subtropics and Extratropics (not shown), their duration is not realistic and serves the purpose of testing different hypotheses.

3.3.1 Equatorial Anomalies

Ten experiments are performed imposing a zonal wind stress anomaly at the Equator (Figure 3.3b). Five experiments have strengthened wind stress anomalies added on the climatological forcing in that region, five have instead weakened anomalies. The pattern extends from 8°N to 8°S in latitude and from 170°E to 100°W in longitude, with values smoothed linearly to zero at the edges. The shape is similar to the region defined by England et al. (2014)

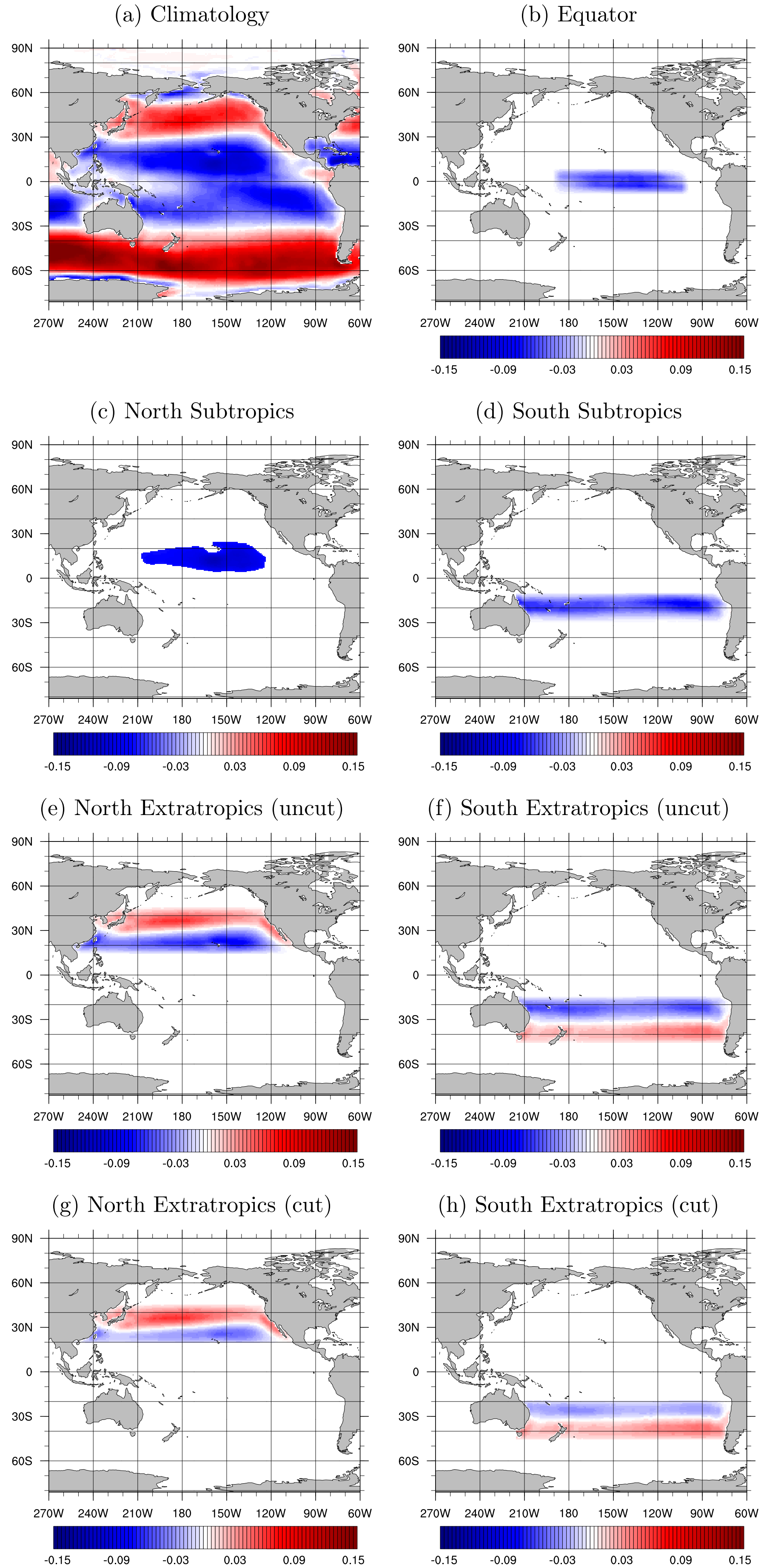

Figure 3.3: Climatological zonal wind stress (N m^{-2}) and zonal wind stress anomalies (N m^{-2}) from the CORE-I dataset (Griffies et al. 2009), which are multiplied by a factor and then added to or subtracted from the applied wind stress field.

as the IPO-related contribution to the strengthened trade winds circulation in the Pacific Ocean. The equatorial experiments assess the impact of zonal wind stress anomalies at the Equator on Pacific STCs.

The largest STCs mass transport is expected to be found at 15°N and 15°S (McPhaden and Zhang 2002). However, our equatorial wind stress anomalies do not give any substantial response at those latitudes. Figure 3.4 shows instead time series of the equatorward mass transport at 9°N and 9°S, close to the boundaries of the anomaly. The meridional transport from each experiment is zonally-integrated on the whole Indo-Pacific basin, vertically-integrated in the first 1000 m, and finally subtracted from the control value. At 9°N an increasing divergence of the equatorward mass transport from the control value is observed as the magnitude of the zonal wind stress anomaly increases. Instead, at 9°S the behaviour is more chaotic, probably due to the contribution of the Indian Ocean in the computation. However, equatorial mass transport anomalies are less than a tenth of the control value.

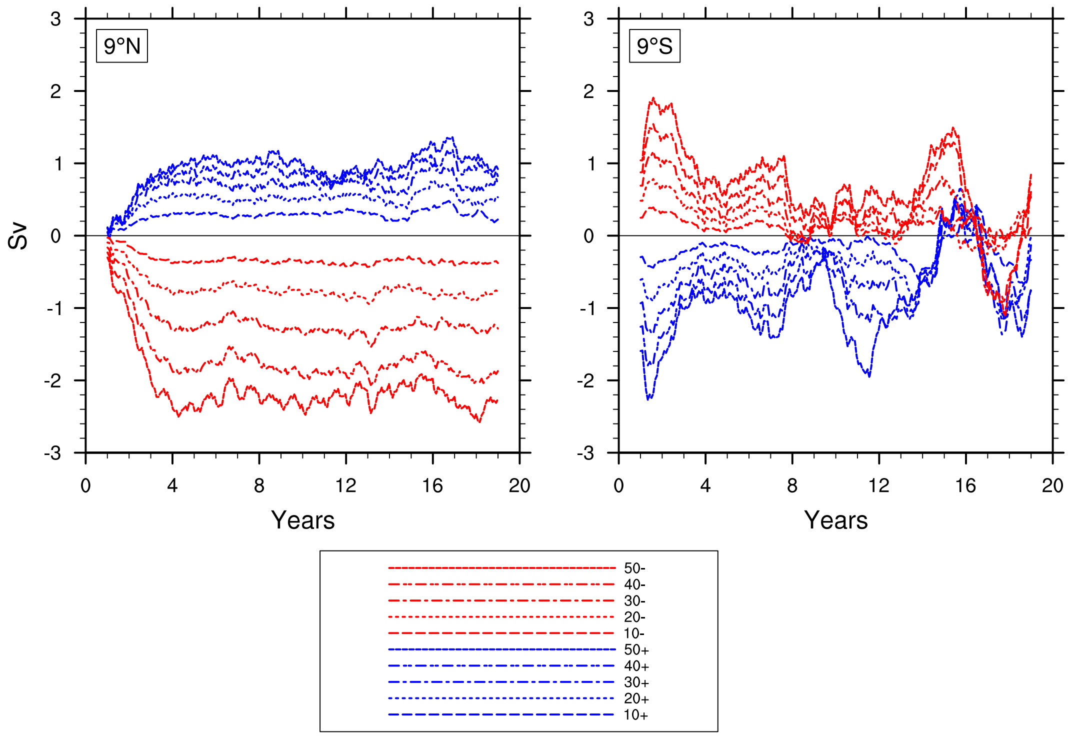

Figure 3.4: Time series (25-months running mean) of the zonally and vertically-integrated anomalous equatorward transport (Sv) for the equatorial experiments at 9° of each hemisphere in the Indo-Pacific Ocean. Anomalies are computed as deviations from the control value. In the legend, + refers to strengthened anomalies and - to weakened anomalies.

The top panels in Figure 3.5 show the anomalous transports for some selected experiments. For convenience, we just show results for the strengthened anomalies. Although the impact of the equatorial wind stress anomalies on the overturning circulation is significant, the signal is confined to 10°N-10°S and to a limited potential density range (1030-1032kg m^{-3}), and thus does not involve the Subtropics. Therefore, our experiments suggest that an equatorially-confined wind stress anomaly, however strong, is only able to force local overturning structures very close to the Equator such as TCs, but not STCs, with meridional energy transport anomalies restricted to a small latitudinal range across the Equator. Since TCs act over a weak temperature gradient, their energy transport is limited even in the case of strong wind stress forcing.

The zonal velocity structure driven by equatorial wind stress anomalies has a dipolar shape. In Fig. 3.5 (middle panels), positive (negative) velocity anomalies in the lower (upper) pycnocline are obtained from the strengthened experiments; the pattern is instead reversed for weakened anomalies.

A thermal response at the Equator is clearly shown in Figure 3.5 (bottom panels), larger in the western Pacific Ocean and with anomalies up to 3°C. As we will show later, these signals are different from a typical STCs response (see Fig. 3.9), being related with a local adjustment of the thermocline to the wind stress forcing, rather than to a remote advection involving STCs. In fact, a stronger (weaker) zonal wind stress at the Equator pushes more (less) efficiently the surface water towards the west, and the equatorial thermocline tilt is enhanced (reduced). For strengthened wind stress anomalies, a steeper thermocline results in a warm anomaly in the West Pacific and a cold anomaly in the East Pacific.

At the surface, a typical La-Niña condition develops for strengthened anomalies (Figure 3.6), with a cold SST anomaly (up to 1°C) developing at end of the simulations along the Equator. Conversely, weakened wind stress patterns build up an El-Niño SST pattern. This temperature response is quite remarkable, since the NYF atmospheric state at the surface is constantly damping any ocean thermal anomaly, constraining the simulated SST toward the climatological atmospheric state.

By changing the equatorial wind stress strength, we are also changing the mass transport across the Indonesian straits (Fig. 3.7). The anomaly of the ITF mass transport from the strongest experiments is up to 2 Sv, or about 15% with respect to the control transport of 11-12 Sv. Furthermore, the strength of the transport anomaly is similar to what has been estimated by previous studies (Meyers 1996; England and Huang 2005). It also explains the different behaviour between STCs mass transport time series in the Northern Hemisphere (Fig. 3.4, left panel) and in the Southern Hemisphere (Fig. 3.4, right panel). In fact, as the mass transport integration (Eq. 2.1) is performed over the whole Indo-Pacific basin, time series at 9°N are poorly influenced by the Indian Ocean part, whereas the altered ITF transport and the related changes in the Indian Ocean circulation strongly affects the computation at 9°S. As soon as the wind stress anomaly sets on, the ITF transport is modified with little delay. Then, it decays for some time before stabilisation. The effect of an altered ITF transport on the Indian Ocean is displayed by a remarkable SST signal, as well as a modified ocean heat content in the upper Indian Ocean (not shown).

3.3.2 Subtropical Anomalies

The main STCs driving mechanism occurs through changes of the wind stress at the Subtropics, as first suggested by McCreary and Lu (1994). Therefore, we expect to obtain the largest STCs response by locating a wind stress anomaly in these regions. We performed twenty experiments (ten in each hemisphere, Figure 3.3c,d), employing both strengthened and weakened anomalies.

As shown in Figure 3.8, the effect of subtropical wind stress anomalies is large on STCs mass transport, up to 10-12 Sv at 15° in each hemisphere; at its maximum, the anomalous transport is roughly one third of the control value for both hemispheres. The stabilisation of the trends occur on a decadal time scale, and is faster for the Northern Hemisphere experiments.

Some examples of the structure of the STCs response are shown in Figure 3.9. Compared to the signal generated by equatorial anomalies (Figure 3.5), here we can see a proper response of STCs involving the whole overturning structure from the Equator to the subtropical region. Only the Northern Hemisphere strengthened experiments are shown, being the response obtained from other experiments very similar.

A broad meridional ocean energy transport anomaly, straddling the whole subtropical and tropical regions, is obtained for both Northern and Southern Hemisphere experiments (not shown). The anomalous energy transport spans the whole subtropical region, with anomalies ranging from 0.03 PW (10% of the control value) for the 10% experiment to 0.3 PW (60% of the control value) for the 50% experiment. It should be noted that the computation includes the Indian Ocean transport, mostly affecting the Southern Hemisphere estimate. A linear relationship between meridional energy transport and wind stress holds, mainly for small anomalies. For larger anomalies (40% and 50%) this relationship is lost. In fact, large wind stress anomalies are affecting not only STCs, but significantly modify energy transports related to the wind-driven gyre.

By changing STCs transport, subtropical wind stress anomalies are able to drive a considerable response at the Equator (Figure 3.9, central and bottom panels). Comparing our subtropical results with the equatorial ones (Figure 3.5), we can see how the two responses are significantly different. In the equatorial experiments, although the thermal signal can be stronger locally, as in the West Pacific, we do not see any STC-related effect. Instead, cold anomalies arising in the equatorial thermocline from the strengthened subtropical wind stress anomalies can be traced to a remote response due to STCs. In fact, an accelerated STC is able to draw deeper (and colder) water to the Equator, by feeding the EUC (Fig. 3.9, middle panels). Similarly, weakened subtropical wind stress anomalies drive warm anomalies at the Equator by slowing down the EUC and reducing the local upwelling of relatively cold waters. In this respect, our results differ from the conclusions given by Liu and Philander (1995), whose EUC response to off-equatorial wind stress forcing is said to be very limited, whereas in our experiments EUC is accelerated (decelerated) for strengthened (weakened) wind stress (not shown).

Looking at the sea surface (Figure 3.10), a cold SST signature develops from the 20% strengthened experiment onwards. A warm response is instead obtained in the weakened experiments (not shown). Considering only the north-subtropical experiments, both strengthened and weakened 50% wind stress anomalies force a response up to 0.48°C in the Niño 3.4 region. South-subtropical experiments drive a slightly smaller thermal signal. These values are very close to the threshold (0.5°C) associated to a warm or cold ENSO phase. The equatorial SST adjustment time is faster for the northern subtropical experiments (not shown), because part of the wind stress anomaly is very close to the Equator. Instead, the southern subtropical wind stress anomaly takes up to 10 years to force an equatorial response.

There is no significant anomaly in the ITF transport in any of the subtropical experiments (not shown). This result suggests that strengthening or weakening subtropical wind stress does not lead to any appreciable modification of the ITF mass transport.

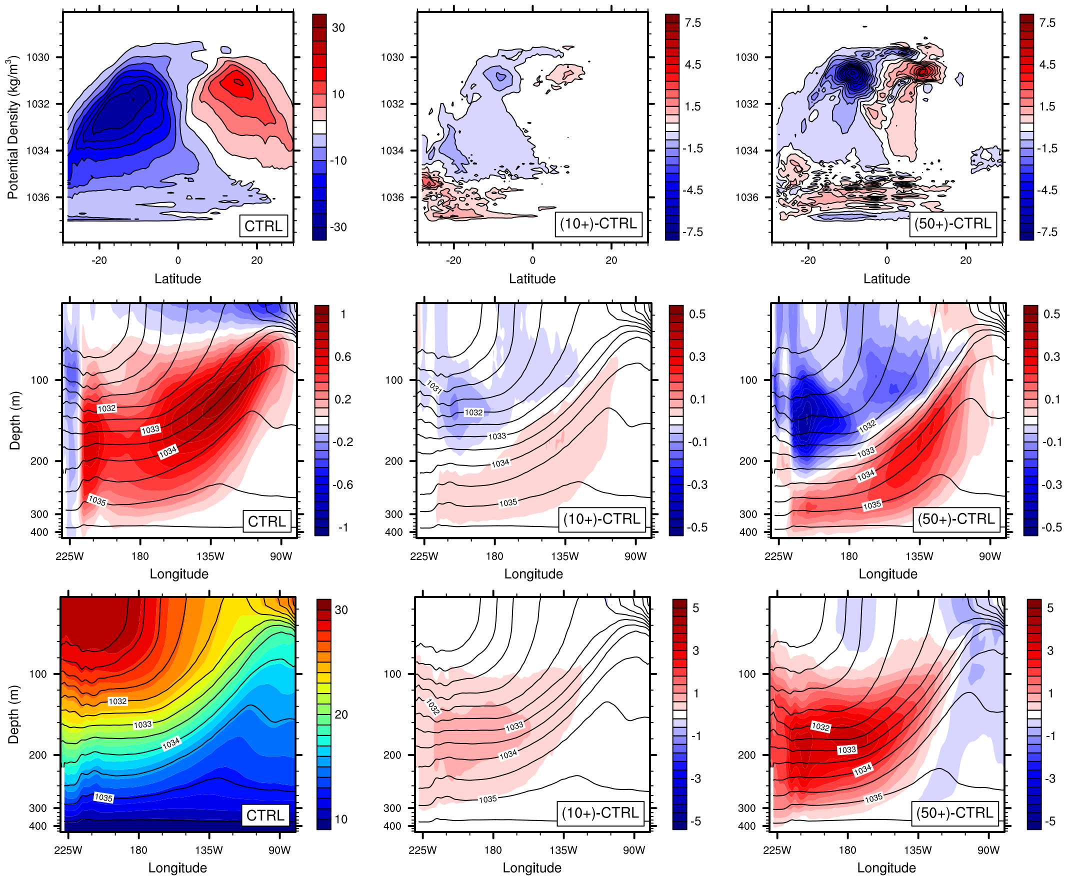

Figure 3.5: (Top panels) Zonally-integrated mass transport on potential density coordinates (kg m^{-3}, referred to 2000 dbar) over the Indo-Pacific Ocean. Time-mean overturning (left), 10% (center) and 50% (right) anomalies for the strengthened equatorial experiments. Red structures are clock-wise cells and blue ones are counterclock-wise. Units are Sverdrup (1 Sv = 10^6 m^3 s^{-1}). (middle panels) Zonal cross sections of zonal velocity (m/s) at the Equator for the control run (left panels, contours), and anomalies for the 10% and 50% (middle and right panels, contours) strengthened equatorial experiments, superimposed on isolines of potential density (kg m^{-3}, referred to 2000 dbar). (Bottom panels) Zonal cross sections of temperature (°C) at the Equator for the control run (left panels, contours), and anomalies for the 10% and 50% (middle and right panels, contours) strengthened equatorial experiments, superimposed on isolines of potential density (kg m^{-3}, referred to 2000 dbar).

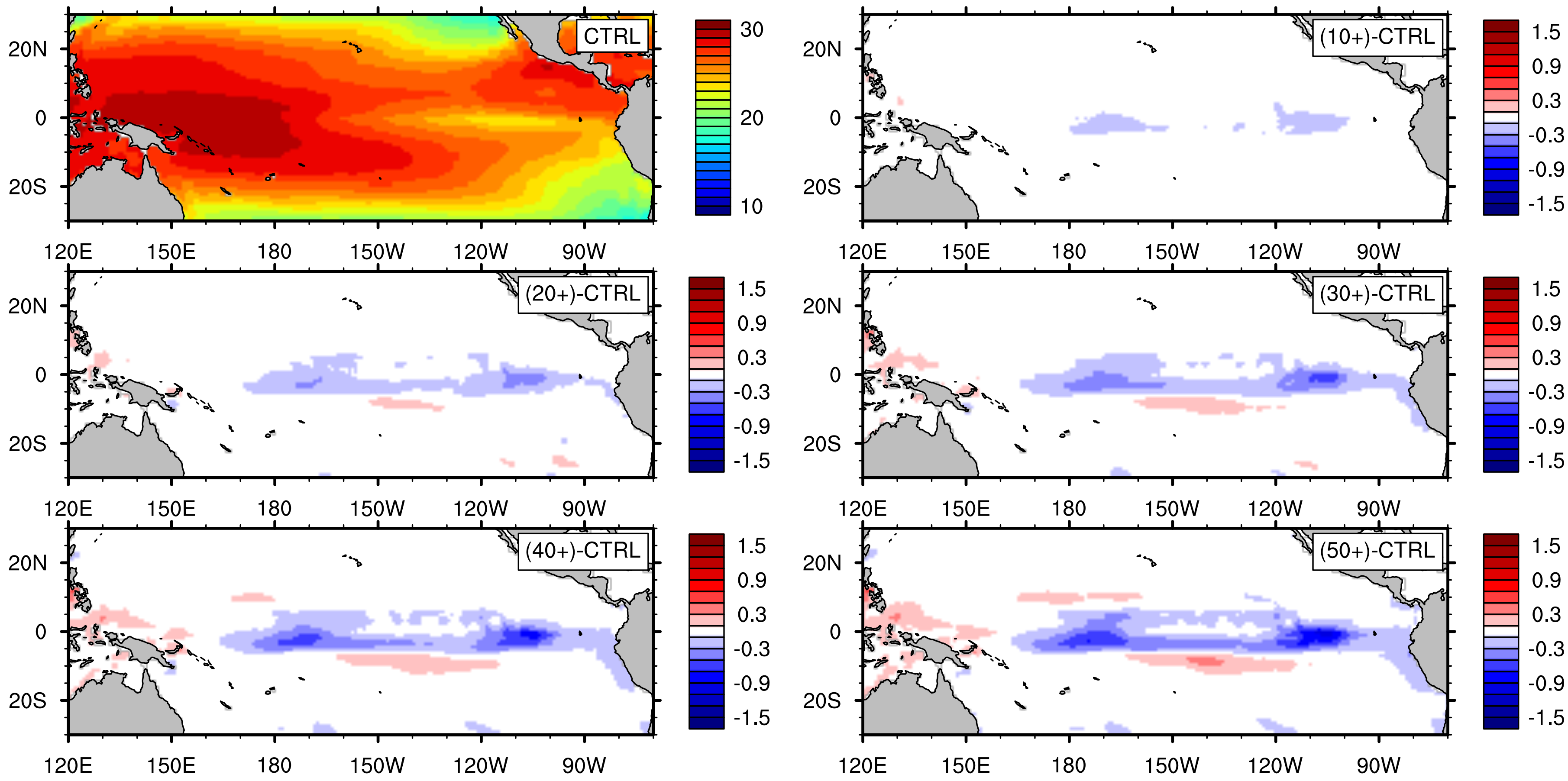

Figure 3.6: Sea surface temperature (°C) for the control run (top-left panel), and anomalies for the strengthened equatorial experiments.

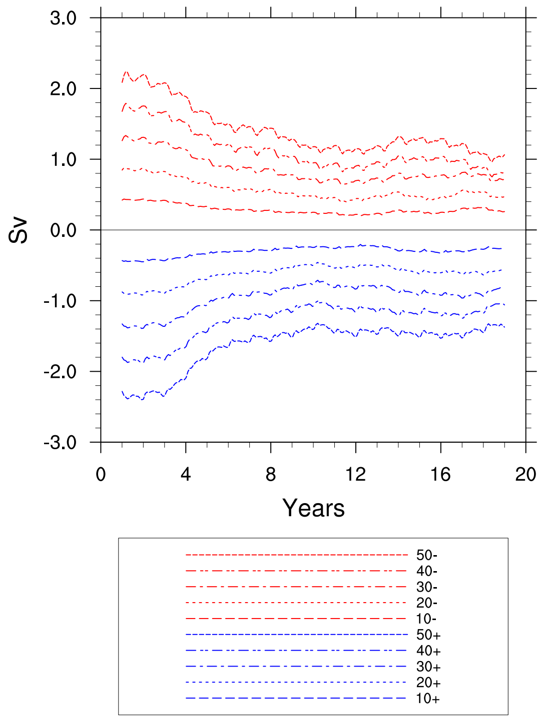

Figure 3.7: Time series (25-months running mean) of the Indonesian Throughflow mass transport (Sv) for the equatorial experiments, shown as anomalies relative to the control run. In the legend, + refers to strengthened anomalies and - to weakened anomalies.

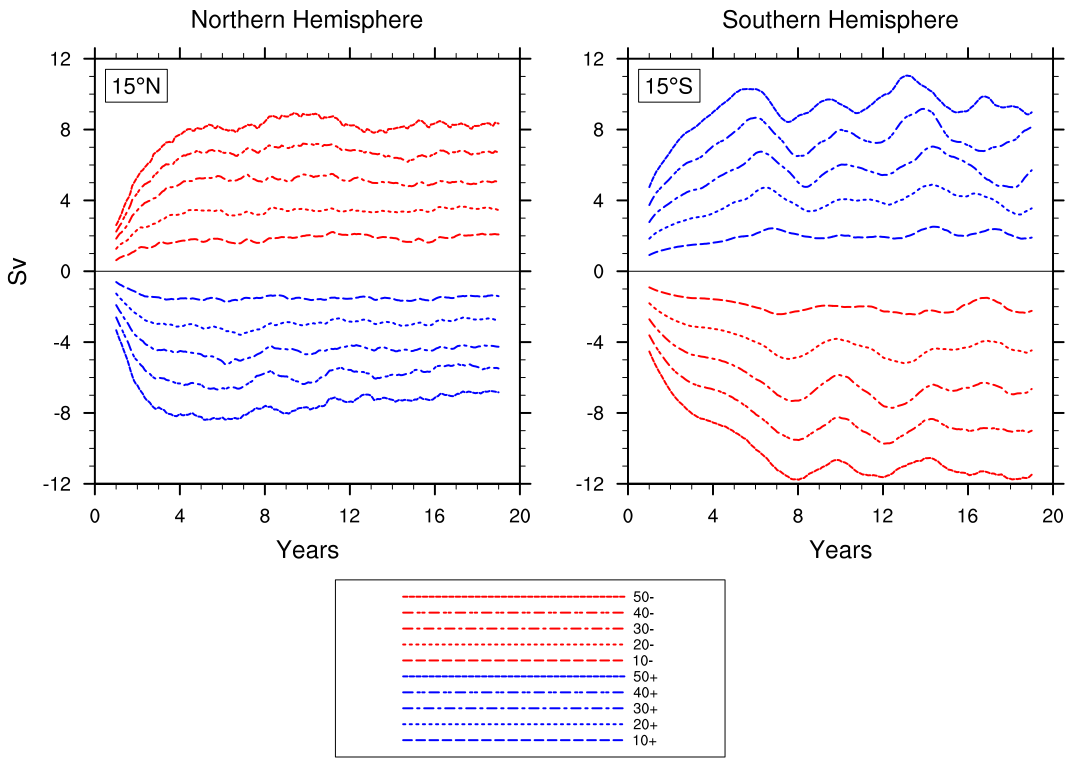

Figure 3.8: As in Fig. 3.4 but for the northern subtropical (left panel) and the southern subtropical (right panel) experiments at 15° of each hemisphere in the Indo-Pacific Ocean.

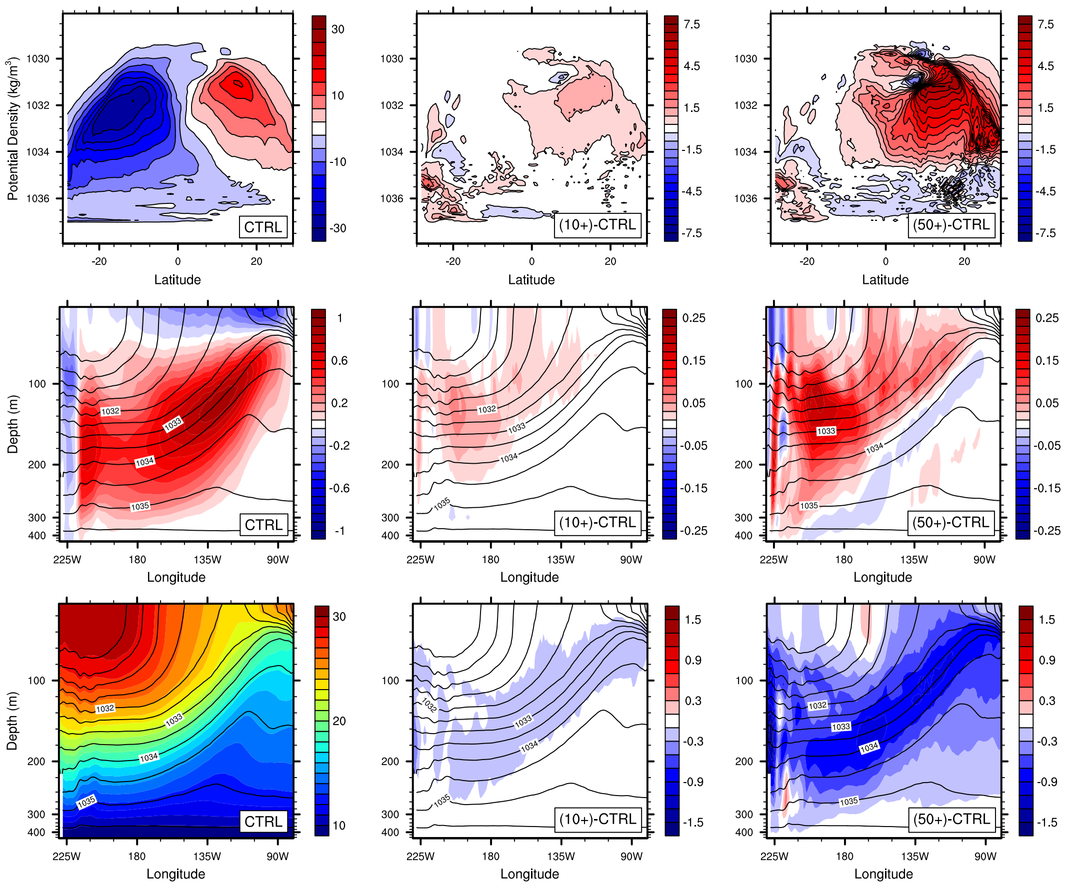

Figure 3.9: As in Fig. 3.5 but for the northern subtropical experiments.

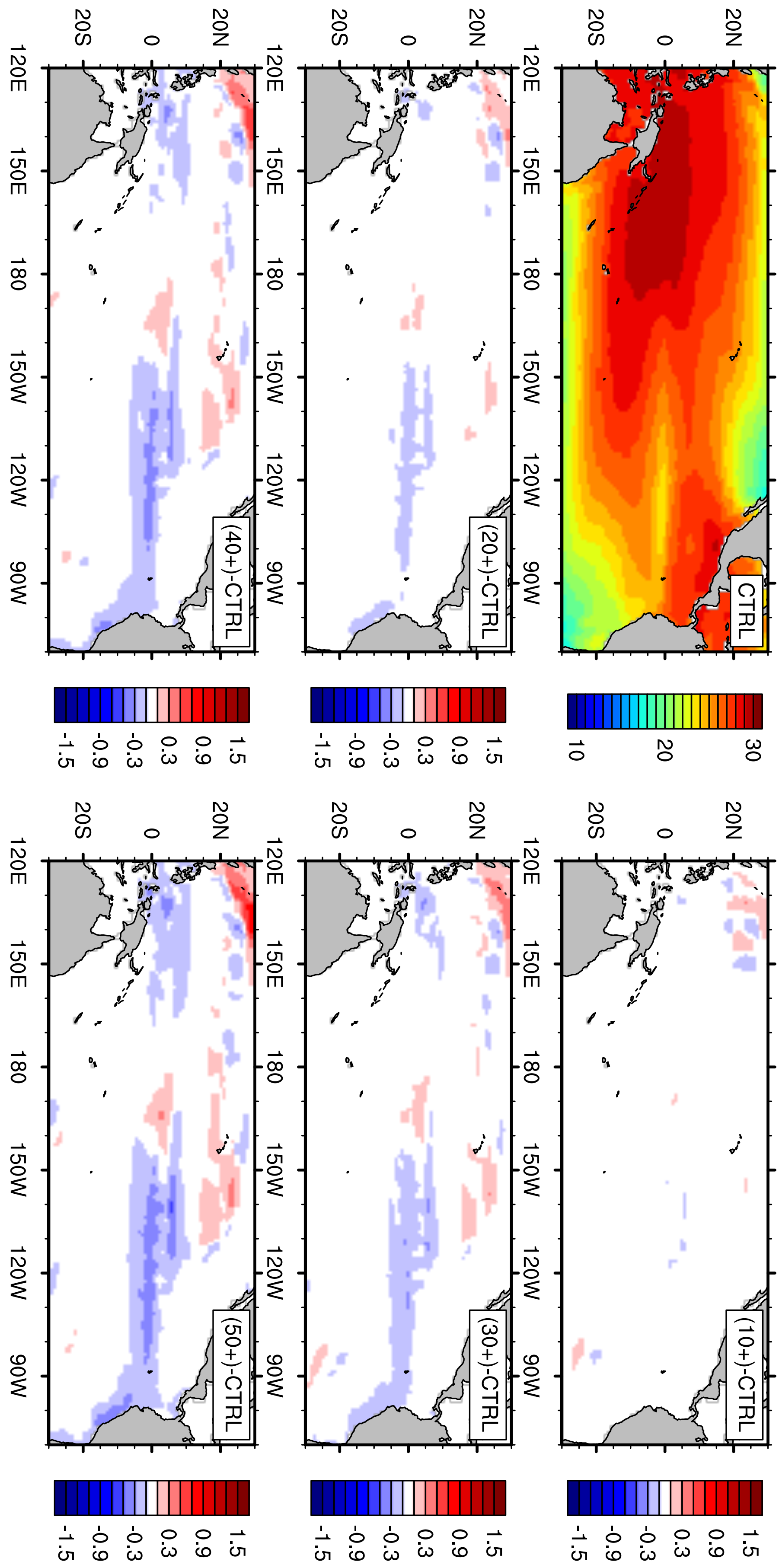

Figure 3.10: As in Fig. 3.6 but for the northern subtropical experiments.

3.3.3 Extratropical Anomalies

We showed how a subtropical zonal wind stress anomaly can influence STCs dynamics. Our next purpose is to verify whether such influence can be observed with an anomaly located further poleward. In fact, many midlatitude weather regimes are related with characteristic zonal wind stress patterns in the Pacific sector, possibly affecting STCs circulation as shown in Chapter 4.

We perform two sets of experiments imposing idealised extratropical wind stress anomalies, extending up to 45° in each hemisphere, with a linear smoothing at the edges of the anomaly. As before, the intensity of the anomaly was a fraction of the climatological zonal wind stress (Table 3.1). In one set, the wind stress anomaly reaches into the Subtropics, as far as 15° (Fig. 3.3e,f), whereas the second set starts at 20°, and it is considered purely extratropical (Fig. 3.3g,h). The first set is called *UNCUT*, the second is named *CUT*.

A remarkable response, able to force a stable thermal signal in the equatorial thermocline up to the surface within 12 years, is only found in the case where anomalies reach the edge of the subtropical gyre (*UNCUT* experiments). Using the *CUT* anomalies instead, any significant STC response is vanished, as well as the thermal equatorial signal. This is clearly shown in Fig. 3.11 for the equatorial ocean structure, and in Fig. 3.12 for the sea surface temperature. Presumably, all anomalous mass transport generated by the *CUT* wind stress anomaly is recirculating within the subtropical gyre, without reaching the equatorial region. This confirms that STCs are mainly forced by wind stress at the cutoff latitude for subtropical subduction, ranging from 15° to 20°, at the edge of the subtropical gyre.

3.3.4 STCs Meridional Energy Transport

In Figure 3.13 we show STCs meridional energy transport anomalies generated by equatorial and subtropical wind stress anomalies according to the metrics introduced in Chapter 2.

As expected, equatorial experiments show very weak associated anomalies (Fig. 3.13a,c), with some significant deviations from the control state only within the equatorial region. Subtropical experiments are instead associated with large STC meridional energy transport anomalies, extending up to 20°(Fig. 3.13b,d). Meridional energy transport anomalies directly related to STCs account for $\approx 1/3$ of the total transport anomaly (not shown). The relative role of STCs is larger for modest anomalies, whereas it becomes less important for the strongest cases. As we already mentioned, this is probably

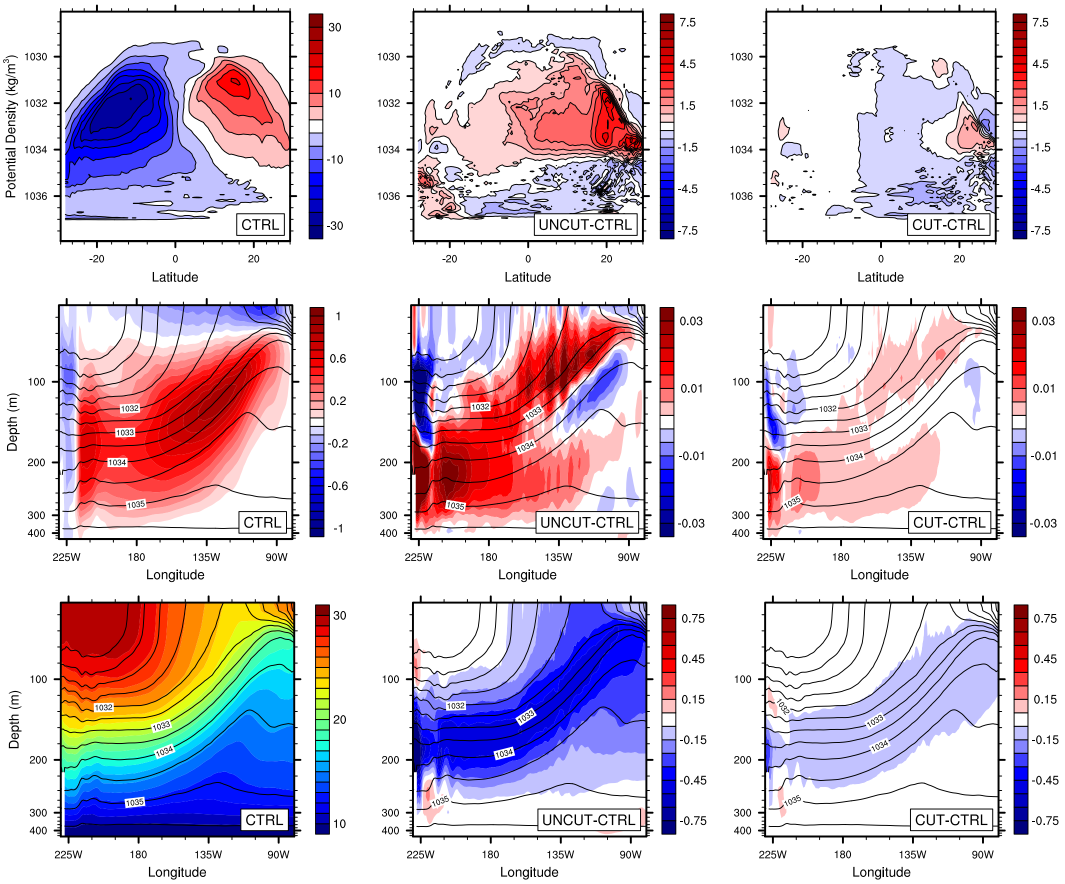

Figure 3.11: As in Fig. 3.5 but for the 50% strengthened *UNCUT* and *CUT* northern extratropical experiments.

due to the intensification of the wind-driven subtropical gyre, transporting larger and larger amount of heat poleward. For what concerns the extratropical experiments, although *UNCUT* wind stress anomalies are able to generate remarkable energy transport anomalies, even similar in magnitude to the subtropical experiments, *CUT* wind stress anomalies instead give basically no signal (not shown). This further emphasise the importance of the wind stress forcing acting on the 15°-20° latitudinal region on altering STCs dynamics.

3.4 Discussion

The overall behaviour of the northern-hemisphere idealised experiments is summarised in Figure 3.14, where anomalies in equatorward mass transport, northern STC energy transport and equatorial SST are plotted against values of anomalous wind stress forcing. The agreement between the regression lines and our key metrics in Fig. 3.14 supports a linear relationship with the applied wind stress forcing (angular coefficients are showed for each regression line).

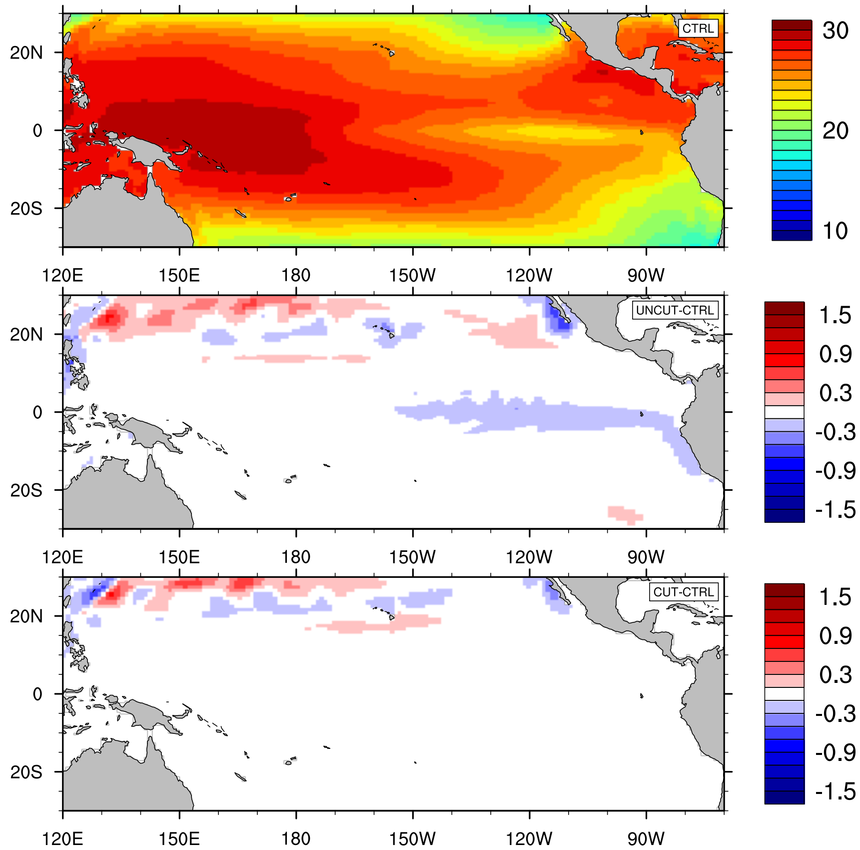

Figure 3.12: As in Fig. 3.6 but for the for the 50% strengthened *UNCUT* and *CUT* northern extratropical experiments.

Subtropical experiments show a symmetric behaviour between strengthened and weakened experiments, in both equatorward mass transport and STC energy transport. Instead, equatorial SST anomalies induced by the equatorial experiments does not show similar behaviours for strengthened and weakened experiments, making harder the interpretation of STCs influence on SST in terms of a linear response.

Equatorial experiments are not able to drive a substantial response in terms of either mass or energy transport. In fact, however strong, equatorial wind stress anomalies are always related to a local dynamical adjustment, with a thermal signal due to local adjustments of the thermocline to changing wind stress forcing. Thus, here only the shallower Tropical Cells are excited. Although equatorial wind stress anomalies do not involve modifications of STCs transports, they could in fact set up the appropriate initial conditions for a tropical-extratropical teleconnection, whereby the thermally-direct Hadley cell anomalies can produce subtropical wind stress and wind-stress curl changes leading to STCs anomalous transports feeding back to the Equator, resulting in opposite anomalies as hypothesised in Farneti et al. (2014b). The oceanic

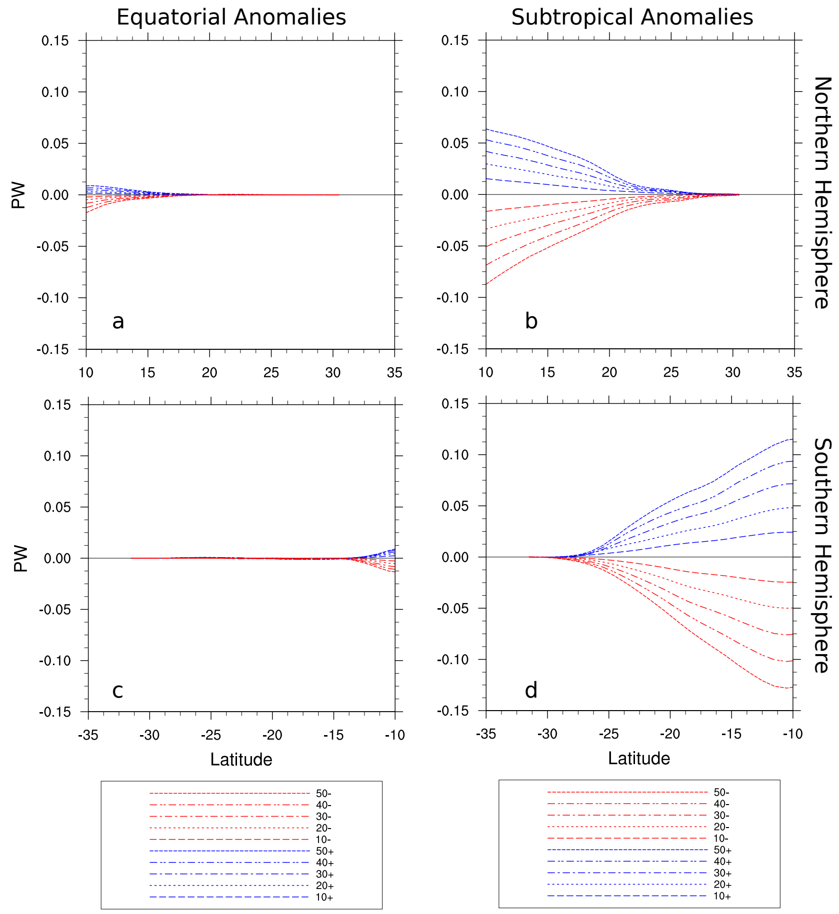

Figure 3.13: STC meridional energy transport (1 PW = 10^{15} W) for all northern (top row) and southern (bottom row) idealised experiments, estimated using Eq. 2.4. Anomalies shown are from the equatorial (left column) and subtropical (right column) experiments.

component of this oscillation is tested and quantified here, however the complete cycle can only be reproduced within a coupled model, and not in our ocean-only setup which is also damping our surface anomalies due to the imposed atmospheric state.

SST anomalies in the Niño 3.4 region are larger in the equatorial experiments with respect to other regions, stressing the importance of local wind stress forcing on the equatorial ocean state. Despite the climatological atmospheric surface temperature applied to the model, remotely-induced thermal anomalies in the equatorial thermocline are able to propagate to the surface, with values up to 0.5°C in the central Pacific Ocean. These values are comparable with those found by Farneti et al. (2014a) using an OGCM forced by the interannual CORE-II forcing during the period 1948–2007.

Subtropical wind stress anomalies produce the largest values of STCs mass and energy transport anomalies. Overall, subtropical zonal wind stress anomalies are found to be the strongest forcing mechanism of STCs in the Pacific Ocean, as predicted by previous theoretical studies (e.g., McCreary and Lu 1994). On the other hand, extratropical wind stress anomalies are also capable of driving a substantial response in the overturning cells. Nevertheless, the signal reaching the Equator is generated within the 15°-20° region, at the equatorward edge of the subtropical gyre, whereas any anomalous transport generated north of that latitude recirculates within the gyre.

Our ocean-only idealised experimental setup proved very useful in highlighting some fundamental properties of STCs dynamics and its connection to the tropical ocean. However, the time-independent and idealised character of the applied wind stress anomalies and the absence of ocean-atmosphere coupling are strong limitations. These points are addressed in the following chapters.

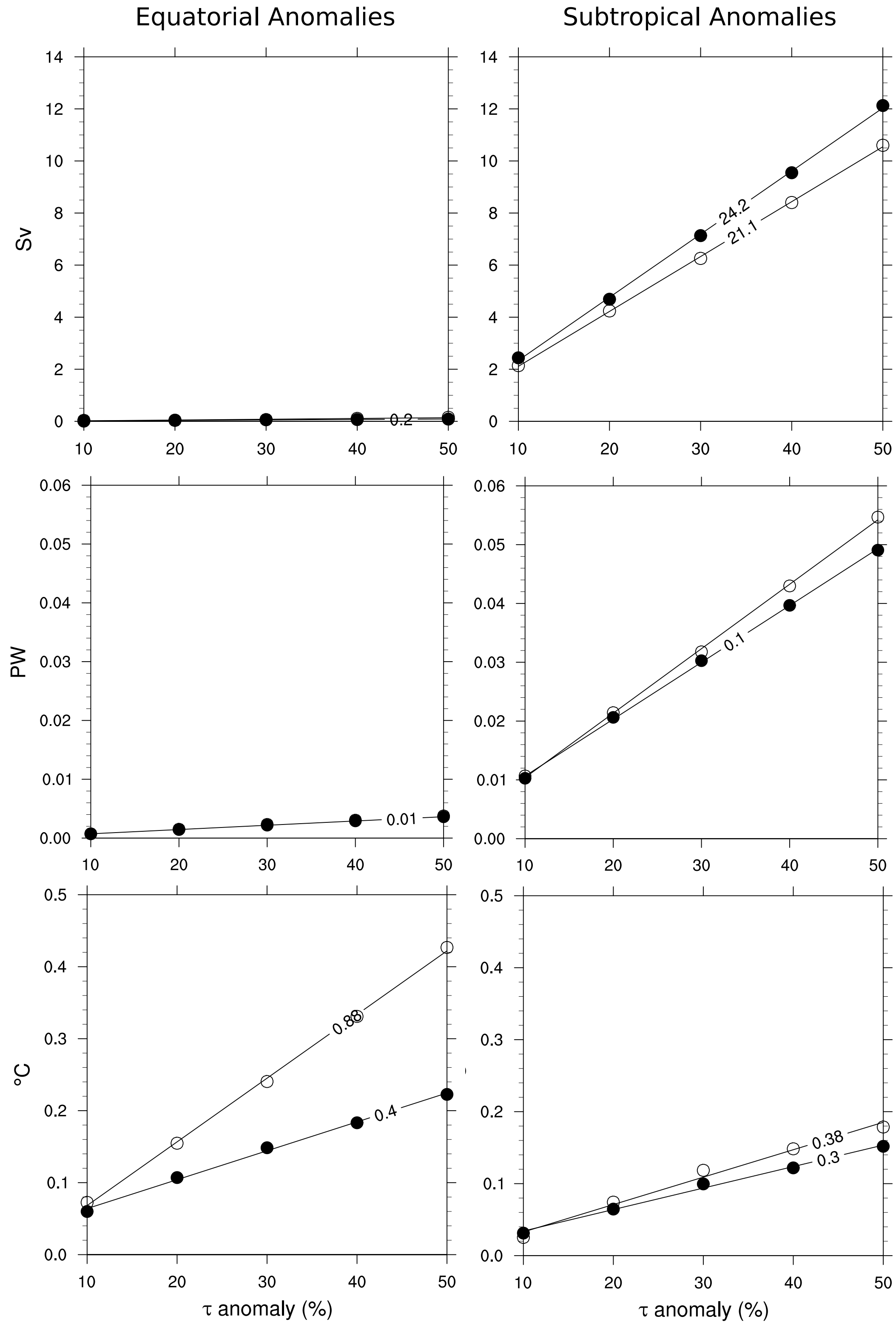

Figure 3.14: Absolute value of anomalies in equatorward mass transport (top row), northern STC meridional energy transport (middle row) and equatorial SST (bottom row) plotted against wind stress anomaly for equatorial (left column) and subtropical (right column) wind stress patterns. Mass transports are evaluated as the maximum time-averaged, zonally-integrated, vertically-integrated equatorward mass transport anomaly in the region 10°- 30°N. STC energy transport are evaluated as the time-averaged, zonally-integrated energy tranport anomaly at 15°N. Equatorial SST anomalies are evaluated in the Niño 3.4 region (5°N - 5°S, 120°- 170°W). Solid and empty circles denote strengthened and weakened experiments, respectively. Linear fits are showed for each experimental set, together with the angular coefficient a of the regression line $y = ax$.

Chapter 4

Impact of COWL-related zonal wind stress perturbations

In Chapter 3 we explored the impact of the off-equatorial wind stress forcing on STCs employing idealised wind stress patterns. However, intensity and duration of the applied anomalies were not realistic, and they were meant to assess the specific role of different regions on Pacfic STCs forcing. On the other hand, observed atmospheric patterns are known to have a large impact on the equatorial Pacific Ocean state, possibly involving STCs dynamics (Farneti et al. 2014b; Molteni et al. 2017). In particular, low-frequency variations over the North Pacific Ocean and associated teleconnections have large impact on the global climate, with air-sea interactions playing a leading role (Namias 1959, 1969; Lanzante 1984) especially during winter (Van Loon 1979; Wallace et al. 1990). The main source of decadal variability in the North Pacific has always been matter of debate between local (Bjerknes 1964; White and Barnett 1972; Latif and Barnett 1996) and remote (Nitta and Yamada 1989; Graham 1994; Yukimoto et al. 1996) perspectives. However, sensitivity experiments by Liu et al. (2002) and Wu et al. (2003) show that tropical Pacific and North Pacific have separated oscillation mode, not originated but still influenced by tropical-extratropical interactions.

In the present chapter we will evaluate the impact of an observed atmospheric pattern on the Pacific STCs using similar metrics employed in Chapter 3, performing several ad-hoc perturbation experiments with the same global ocean model (MOM5). This chapter includes material published in Graffino et al. (2018).

4.1 The Cold Ocean-Warm Land Pattern

Wallace et al. (1993) suggest that some of the Northern Hemisphere wintertime warming trend observed from the 1960s to the 1980s (Manabe and Stouffer 1980; Ingram et al. 1989) can be attributed to a recurrent atmospheric pattern over the North Pacific Ocean. In fact, by examining land station datasets of the Northern Hemisphere during anomalously warm winters, Wallace et al. (1995) determine that about half of the temporal variance of the monthly-averaged surface air temperature is related to a specific spatial pattern, in which oceans are anomalously cold and continents are anomalously warm. Furthermore, Wallace et al. (1996) show a monthly mean analysis of the Northern Hemisphere 500 hPa geopotential height field from 1946 to 1993, which is characterised by positive anomalies over Russia and North America, and negative anomalies over the North Pacific and the Barents Sea. Because of its spatial structure, by then this atmospheric regime has been referred to as the Cold Ocean-Warm Land (COWL) pattern. Its occurrence and spatial properties are confirmed by observations (Corti et al. 1999; Wu and Straus 2004), as well as by modelling studies (Broccoli et al. 1998).

Although at the beginning it has not been considered an atmospheric modal structure on its own (Wallace et al. 1996), later on COWL gained a more "rigorous" definition in terms of Empirical Orthogonal Function (EOF) of the sea level pressure and 500-hPa geopotential height fields over the Northern Hemisphere (Wu and Straus 2004). From a more dynamical perspective, Molteni et al. (2011a) interpret COWL as a thermally-balanced wave mode in terms of thermal equilibration of planetary waves (Charney and DeVore 1979; Mitchell and Derome 1983; Marshall and So 1990), defining a COWL index related to the zonal-wavenumber 2 of the net surface heat flux over regions of large land-sea contrast; the "traditional" definition of the COWL pattern corresponds to the positive phase of this index. The importance of the wintertime large-scale structure of atmospheric planetary waves on surface temperature variations (especially on winter) has been firstly highlighted by Van Loon and Williams (1976, 1977).

By using the ERA-interim reanalysis dataset (Dee et al. 2011), Molteni et al. (2017) confirm that half of the spatial variance of the decadal variations of 500 hPa geopotential height from the late 1990s to the early 2010s is in fact explained by the COWL index defined by Molteni et al. (2011a), as shown in Fig. 4.1. Some features of the observed decadal changes analysed by Molteni et al. (2011a), Farneti et al. (2014b), and Molteni et al. (2017) show a phase shift of the COWL index towards a negative phase at the beginning of the twenty-first century. Part of this pattern reversal could be SST-forced, as the corresponding DJF 500 hPa geopotential height difference between 2000-2009 and 1990-1999 has a strong projection onto the Pacific Ocean, along with a negative PDO pattern in the corresponding SST field (Farneti et al. 2014b).

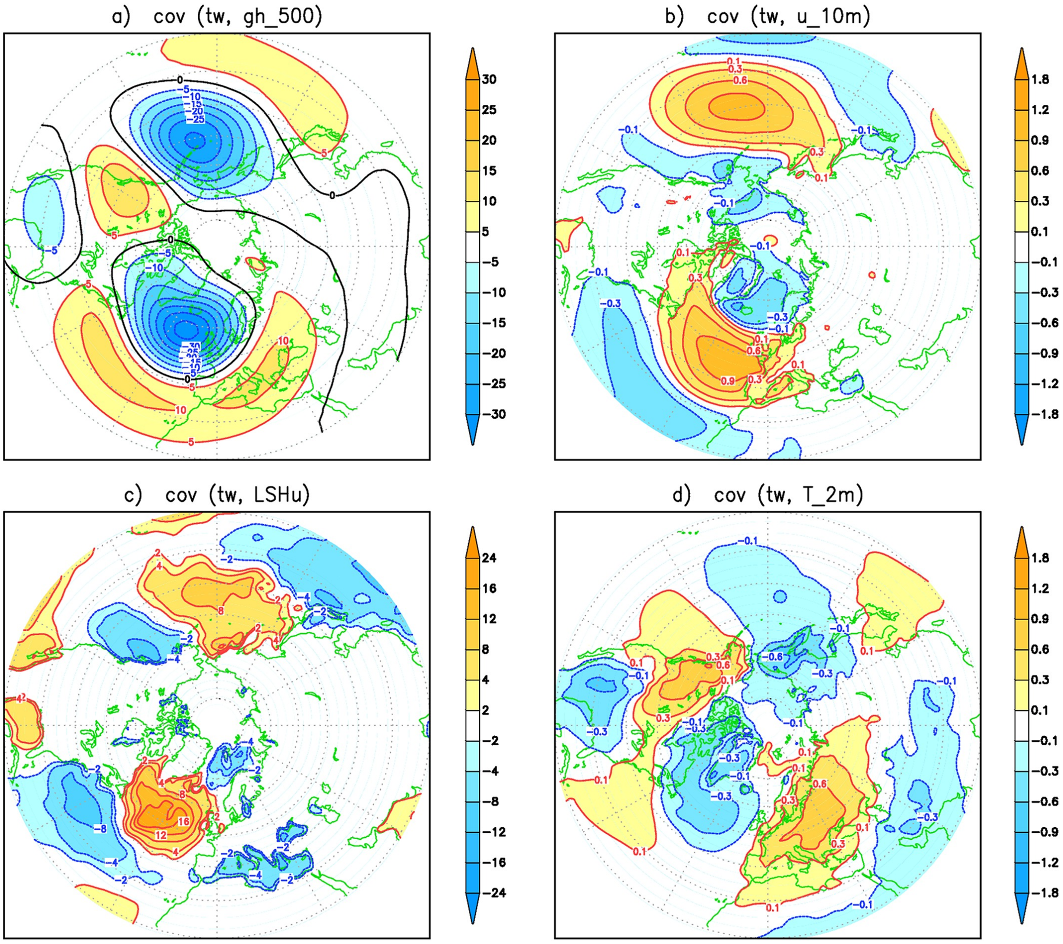

Figure 4.1: Covariance of Northern Hemisphere fields with the normalized wavenumber-2 heat flux index introduced by Molteni et al. (2017) in ECMWF System-4 (Molteni et al. 2011b): (a) 500 hPa geopotential height (m), (b) 10 m zonal wind (m s−1), (c) upward latent and sensible heat flux (W m^{-2}), and (d) 2 m temperature (°C) for DJF from 1981/1982 to 2012/2013. Taken from Molteni et al. (2017).

Wallace et al. (1995, 1996) explain the strong linear correlation between the amplitude of COWL and hemispheric-mean temperature in terms of the smaller heat capacity of land with respect to ocean: on monthly timescales, lands would equilibrate faster with the overlying surface air temperature, experiencing larger temperature variability in response to the atmospheric circulation dynamics with respect to oceans (Barnett 1978). Thus, variations of the hemispheric-mean temperature associated with COWL occur in response to changes in configuration of warm and cold air masses relative to the land-ocean distribution below (Wallace et al. 1995). Wallace et al. (1995) also mention the potential influence on the observed COWL pattern arising from regional anomalies induced in the Northern Hemisphere by large climatic patterns, such as ENSO (Trenberth 1990) and NAO (Deser and Blackmon 1993; Hurrell 1995), with Wallace et al. (1996) further claiming that extratropical coupled interactions contributes to COWL interdecadal variability. However, cluster analysis performed by Corti et al. (1999) show that ENSO does not directly force any midlatitude atmospheric pattern (COWL included), although a modification can occur in the frequency of occurrence of such modes. Using a long coupled integration, Broccoli et al. (1998) underline a minor role for air-sea interactions in driving the observed COWL variability, in favour of land-sea contrast. By employing ensemble simulations, Molteni et al. (2017) further show that forcing from tropical SST is not the main source of the COWL variability.

Molteni et al. (2011a) give some insight of the potential large-scale effects of COWL on the ocean circulation: for example, the negative phase of their COWL index would be the atmospheric driver of the North Pacific Gyre Oscillation (NPGO; Di Lorenzo et al. 2008). Moreover, a positive feedback may arise between the North Pacific Ocean and the atmosphere, reinforcing the existing COWL pattern (Molteni et al. 2011a). According to Molteni et al. (2017), COWL has been relevant also for the global warming slowdown, because of its different seasonal impact on the Northern Hemisphere (Kosaka and Xie 2013; Trenberth et al. 2014) and, more importantly for our analysis, the potential influence of COWL on ocean tropical-extratropical interactions (Farneti et al. 2014b; Molteni et al. 2017).

Molteni et al. (2017) further address the role of the COWL pattern during the recent global warming slowdown, by employing the 32-year re-forecast dataset of the ECMWF seasonal forecast (System-4; Molteni et al. 2011b). Heat flux and temperature fields resulting from 51 realisations of the Northern Hemisphere wintertime atmospheric conditions are considered, showing that simulated SST in the Tropics maintain a strong consistency in the different ensemble members, whereas the extratropical responses vary significantly. Thus, alternative dynamical realisations with very similar tropical SST can be used to assess the associated decadal trends at the midlatitudes. Two a-posteriori ensemble means are also computed by Molteni et al. (2017) by giving different weights to specific members: in one case (*ENS_A*) higher weights are given to ensemble members reproducing observed COWL anomalies, in the other case (*ENS_0*) to members with no COWL response. In this way, Molteni et al. (2017) show that *ENS_A* more closely reproduces the observed ocean-atmosphere heat exchange decadal variability than *ENS_0*, highlighting the important role of the COWL pattern in the climate of the last decade and, at the same time, the influence of the heat flux in driving extratropical planetary waves affecting wintertime atmospheric conditions. Observed trends of surface air temperature and winds at the Extratropics also show features strictly related to COWL anomalies.

4.2 Experimental Setup

In Chapter 3 we employed idealised wind stress anomalies to assess the role of different regions on forcing a proper STCs response. We now make a step further, considering the effect of realistic decadal wind stress anomalies on STCs. Wind stress patterns associated with observed decadal COWL variability are selected because of its potential to contribute to global climate variability and STCs dynamics (Farneti et al. 2014b; Molteni et al. 2017).

Two zonal wind stress anomaly patterns, originally called *ENS_A* and *ENS_0*, are obtained from the ECMWF seasonal forecasting System-4 by Molteni et al. (2017), as we briefly explained before. One wind-stress anomaly pattern (*COWL*) is generated to match as close as possible the observed COWL-related wind stress difference between the two periods 2009/2013 and 1996/2000 (Fig. 4.2, left panel), while the other (*NOCOWL*; Fig. 4.2, right panel) is designed to have no projection on the COWL pattern. We choose to use different names with respect to Molteni et al. (2017) study, in order to make easier the interpretation of results related with each wind stress anomaly. It should be noted that both anomalies have very similar equatorial wind stress pattern, while they differ substantially in subtropical regions. Furthermore, being derived from ensemble members of the ECMWF seasonal forecast, they are dynamically consistent wind stress patterns. Anomalies are added or subtracted from the NYF field, as explained in Chapter 2. Thus, by analysing the difference in the response between the experiment *COWL* and *NOCOWL*, we are able to investigate the impact of observed decadal off-equatorial wind-stress anomalies on STCs as well as on equatorial thermocline and sea surface temperature.

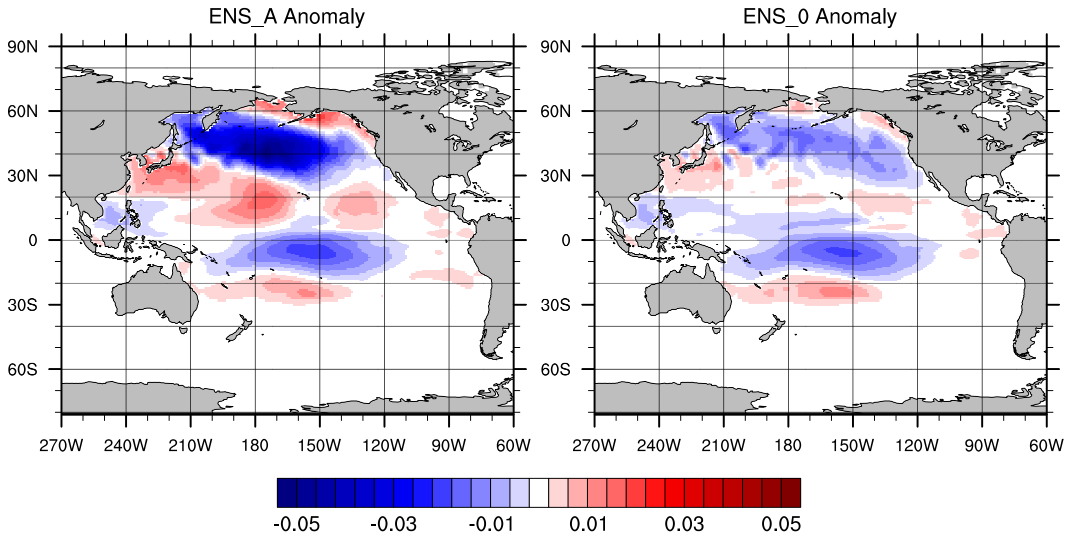

Figure 4.2: Ensemble means obtained from the ECMWF seasonal forecast System-4 (Molteni et al. 2011b). One ensemble-mean is representative of observed decadal changes that can be described by a shift of the COWL-like pattern (Molteni et al. 2017), and is composed of members reproducing closely the observed COWL anomalies (*COWL*; left panel). The second ensemble-mean results from members whose response along the COWL pattern is close to zero (*NOCOWL*; right panel).

Experiment	τ_x	Time (years)
Control	NYF	1400
COWL	NYF±ENS_A	20
NOCOWL	NYF±ENS_0	20

Table 4.1: Main characteristics of the realistic perturbation experiments. τ_x is the zonal wind stress applied to the ocean surface during each experiment. The ocean model computes the zonal wind stress from the climatological zonal wind (NYF, CORE-I dataset; Griffies et al. 2009). Then, during the perturbation experiments, an anomaly is added to the climatological wind stress as a fraction, positive or negative, of the wind stress itself. Employed wind stress anomalies are taken from Molteni et al. (2017).

4.3 Results

Table 4.1 briefly summarizes the main features of the performed simulations. More specifically, a series of numerical experiments is performed by adding *COWL* and *NOCOWL* anomalies to or by subtracting them from the NYF field, without altering their intensity (time-constant experiments). In a different set (time-varying experiments), the intensity of the wind stress anomalies changes in time following a sinusoidal function, completing a half-cycle in 20 years. Unless otherwise stated, results are averaged over the last 5 years of the simulation.

4.3.1 Time-constant Anomalies

Time series at 15°N (Fig. 4.3) shows the response of the equatorward mass transport to the applied time-constant wind stress anomalies. The *COWL* pattern modified the mass transport by about 2 Sv, stabilising after about 5 years. The signal generated by the *NOCOWL* pattern stabilises earlier with a maximum value of 0.8 Sv.

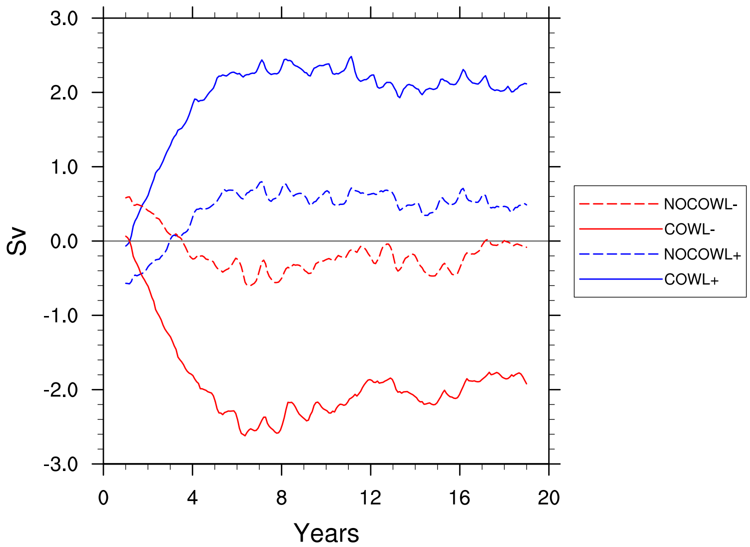

Figure 4.3: Time series (25-months running mean) of the zonally and vertically-integrated anomalous equatorward transport (Sv) for the time-constant COWL experiments at 15°of each hemisphere in the Indo-Pacific Ocean. Anomalies are computed as deviations from the control value. In the legend, *COWL+* and *COWL-* refer to strengthened and weakened anomalies, respectively. *NOCOWL+* and *NOCOWL-* refer to the ensemble mean not projecting on the COWL pattern.

The main difference between the two applied wind stress patterns lies outside the Equator. Our results in Chapter 3 showed local wind stress forcing as the main driver of thermal and velocity anomalies at the Equator. Hence, the potential signal forced at the Subtropics is likely to be obscured by the locally-generated response. Therefore, in the following we analyse the difference between both ensemble means, so highlighting any subtropically-generated signal.

As seen in Fig. 4.4 (top panels), the off-equatorial zonal wind stress related to the COWL regime is able to force a distinct STC response in the Northern Hemisphere. This anomalous mass transport alters the velocity structure in the equatorial thermocline (Fig. 4.4, central panels), driving a thermal signal through the same process we described in Chapter 3 in terms of the $v'\overline{T}$ mechanism (Kleeman et al. 1999) up to 0.4°C (Fig. 4.4, bottom panels). The response is nearly symmetrical for strengthened and weakened experiments.

At the surface, a warmer (colder) SST signal is generated at the Equator in

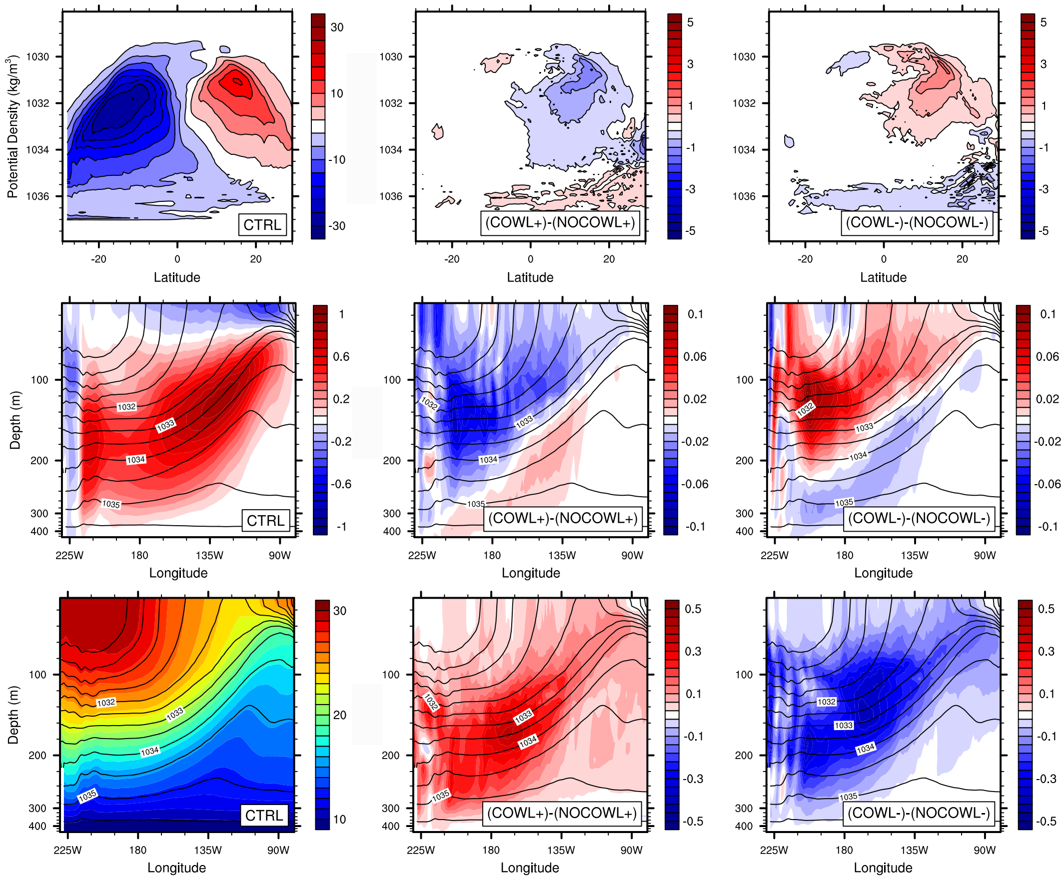

Figure 4.4: As in Fig. 3.5 but for the realistic time-constant wind stress anomalies. Results are presented as the difference between the ensemble mean reproducing the COWL pattern (*COWL* experiments) minus the ensemble mean not projecting on COWL (*NOCOWL* experiments).

the Pacific Ocean in response to strengthened (weakened) *COWL* wind stress anomalies, compared to *NOCOWL* (Fig. 4.5). The equatorial response develops along the whole basin, with a maximum value of 0.1°C in the eastern Pacific. Also, the sign of the anomaly is consistent with the sign of the subtropical wind stress of the *COWL* pattern (Fig. 4.2, left panel). The response time of both *COWL* and *NOCOWL* experiments is very similar to what obtained with our idealised equatorial wind stress anomalies (not shown), again highlighting the fundamental role of the local wind stress forcing on the equatorial ocean state.

STC meridional energy transport anomalies obtained from *COWL* realistic wind stress patterns extend up to 25°N, and are comparable to the 20% anomaly of our idealised subtropical experiments (not shown). *NOCOWL* induced anomalies are close to zero, confirming the significant role played by the subtropical sector of the COWL regime on STCs.

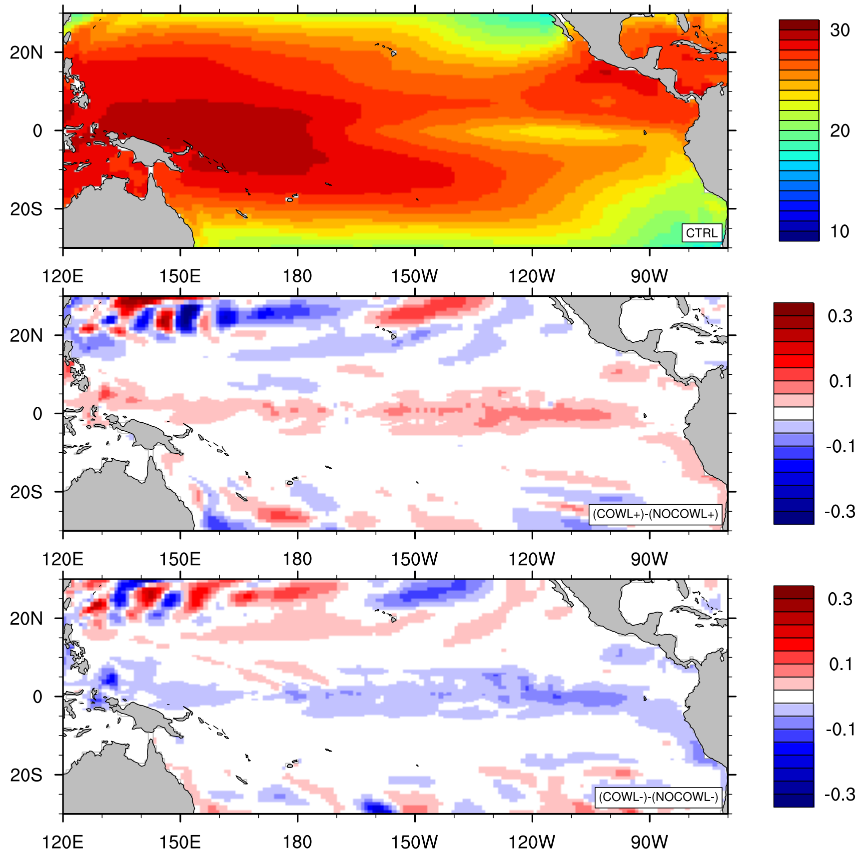

Figure 4.5: As in Fig. 3.6 but for the realistic time-constant wind stress anomalies. Results are presented as the difference between the ensemble-mean reproducing the COWL pattern (*COWL* experiment) minus the ensemble-mean not projecting on COWL (*NOCOWL* experiment).

4.3.2 Time-varying Anomalies

Two different kinds of time-varying wind stress anomalies are employed for both *COWL* and *NOCOWL* patterns. The first type (*COWL+* and *NOCOWL+*) concerns a sinusoidal strengthening of the wind stress anomaly during the first half of the simulation (10 years), with a subsequent weakening in the second half for vanishing at the end of the simulation (20 years). The second type of experiments (*COWL-* and *NOCOWL-*) is implemented in the opposite way: weakening first and strengthening then, with the same temporal structure. In this way, we aim to assess the transient response of STCs to changing wind stress forcing, as well as the residual STCs dynamics for zero wind stress forcing. Again, in order to highlight the off-equatorial response we analyse the difference between both ensemble means.

Time series of the equatorward mass transport (Sv) at 15°N show an increased (decreased) circulation during the strengthening (weakening) phase of the oscillation, with a reversal of the trend during the second half of the simulation (Fig. 4.6). However, there is some residual transport at the end of the simulations, due to the slow STC-related mass transport adjustment. Compared with the time-constant anomalies shown in Fig. 4.3, we see that a stable configuration of STC mass transport can not be achieved in the time-varying *COWL* simulations, although the maximum transport intensity is comparable with the time-constant one, whereas in the *NOCOWL* experiments after a slow increase in mass transport intensity there is no clear sign of a decreasing trend.

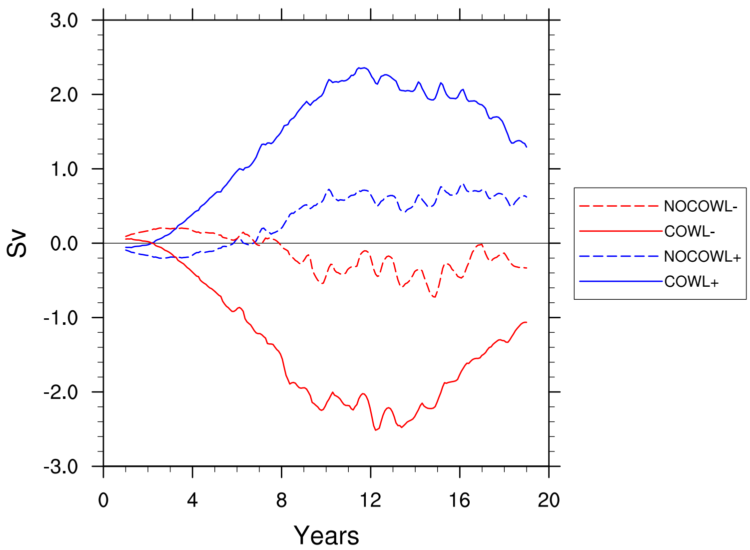

Figure 4.6: As in Fig. 4.3 but for the realistic time-varying wind stress anomalies.

The residual transport is more effectively shown in Fig. 4.7. The overall picture is similar to what shown in Fig. 4.4. However, there are few notable differences. In the top panels of Fig. 4.7, zonally-integrated mass transport computations display a stronger northern STC structure for both *COWL+* and *COWL-* patterns, with respect to *NOCOWL+* and *NOCOWL-* anomalies. The difference fields of the velocity structure at the Equator (middle panels of Fig. 4.7) shows smaller values with respect to Fig. 4.4, with similar patterns in *COWL+* and *NOCOWL+* experiments, and a larger tendency for positive zonal velocities for *COWL-* and *NOCOWL-* anomalies. The residual STCs circulation also results in a thermal response up to 0.1°C in the equatorial thermocline in *COWL+* and *COWL-* experiments (bottom panels), as well as in a small signal the equatorial sea surface temperature (not shown).

Focusing on the temperature trend, in Fig. 4.8 we show that both *COWL+* and *NOCOWL+* patterns produce significant decadal trends in all considered regions (East Indian, West Pacific, and East Pacific Ocean). However, some features are shared by both patterns (top and middle panels), like the east-

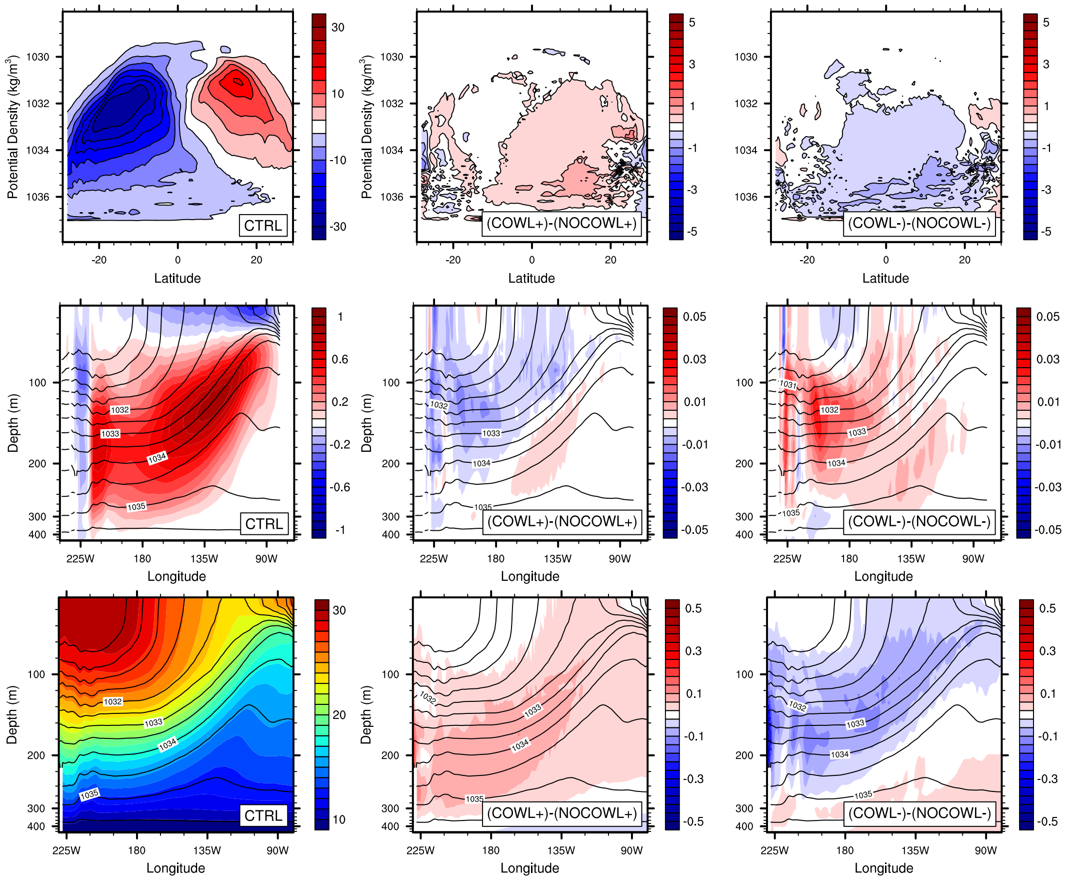

Figure 4.7: As in Fig. 3.5 but for the realistic time-varying wind stress anomalies, time-averaged over the last year of the simulation. Results are presented as the difference between the ensemble-mean reproducing the COWL pattern (*COWL* experiment) minus the ensemble-mean not projecting on COWL (*NOCOWL* experiment).

ern Indian Ocean warming trend (stronger close to the Indonesian Straits) and the remarkable signal obtained in the southern subtropical Pacific Ocean. The difference between the two patterns (bottom panels) highlights the strong trends located in the northern subtropical Pacific Ocean, along with a warming tendency of the lower equatorial thermocline in both western and, more weakly, eastern Pacific basin. A specular picture is obtained from the *COWL-*/*NOCOWL-* experiments, in which a cold trend is obtained in the lower equatorial thermocline (not shown).

The decadal thermal trend along the Equator is shown in Fig. 4.9, where all time-varying patterns are shown (top and middle panels) with the respective differences (bottom panels). Remarkable temperature trends are produced by all time-varying wind stress anomalies, with a warm tendency for *COWL+* and *NOCOWL+* patterns, and a cold trend for *COWL-* and *NOCOWL-* patterns. Focusing on the difference fields, a larger warming tendency located in the lower thermocline of the western/central Pacific Ocean is obtained from the

COWL+ experiment with respect to the *NOCOWL+* experiment, along with a weak cold signal in the eastern Indian Ocean. The colder trend obtained from the *COWL-* experiment with respect to the *NOCOWL-* experiment is instead located at upper depths and is stronger in the central Pacific Ocean.

4.4 Discussion

In the present chapter we showed how the COWL pattern, an observed atmospheric regime particularly prominent over the extratropical Northern Hemisphere (Wallace et al. 1996; Molteni et al. 2011a), is actually able to force the North Pacific STC and affect the equatorial ocean state, as suggested by Farneti et al. (2014b) and Molteni et al. (2017). This further suggests a potential role of midlatitude atmospheric modes on forcing STCs decadal variability. In fact, although high-frequency atmospheric processes may have a larger effect on short timescales, signals generated by low-frequency atmospheric variability, however small, are much more important on longer timescales.

The response given by the subtropical sector of the COWL pattern confirms what obtained with our idealised experiments (Chapter 3), although the use of a single wind stress intensity does not allow an assessment of an eventual linear relationship with the response magnitude. A remarkable signal is seen at the Equator when we subtract *COWL* and *NOCOWL* response, the main difference between the two wind stress patterns being found at the Subtropics (Fig. 4.2). It is worth noting that the intensity of our realistic wind stress anomalies is smaller with respect to our idealised ones, the subtropical sector of *COWL* having a zonal wind stress comparable to the 10%-20% experiments shown in Chapter 3. In fact, velocity and thermal response magnitude from our realistic experiments is similar to what obtained with the 10% idealised wind stress anomalies.

On the other hand, our realistic experiments also confirm the prominent influence of the local wind stress forcing onto the equatorial ocean state. As a matter of fact, there is no much difference in terms of equatorial SST response between *COWL* and *NOCOWL* anomalies, and all simulations exhibit an altered tilting of the equatorial thermocline (not shown), which however does not involve any substantial STCs change as we explained in Chapter 3. Instead, the northern STC is certainly involved on forcing the COWL-related response at the Equator (Fig. 4.5), because of the thermal signal shown in Fig. 4.4 (bottom panel) and the larger STC meridional energy transport compared with the *NOCOWL* case (not shown). However, we can not properly assess eventual effects due to other tropical-extratropical interaction mechanisms, involving for example planetary waves propagation. We also stress that any thermal signal generated at the sea surface is locally damped by the climatological atmospheric forcing.

Time-varying wind stress experiments highlight some properties of STCs transient response. Largest mass transport intensities are achieved a couple of years later the reversal of the wind stress forcing on *COWL+* and *COWL-* cases, and a STC residual anomalous transport is observed even at zero-forcing in all experiments. This shows that realistic wind stress variations do not immediately induce a significant alteration of STCs dynamics, although the equatorial SST responds quickly to the altered local forcing and its adjustment is much faster (not shown).

For what concerns temperature trends, employing time-varying anomalies it becomes evident that the largest effect related with COWL variations is found at the Subtropics (Fig. 4.8, bottom panels), where the main difference between *COWL* and *NOCOWL* wind stress anomalies is located. However, in the lower thermocline of the equatorial Pacific a zonally-averaged decadal trend of 0.1°C is found in both *COWL+/NOCOWL+* and *COWL-/NOCOWL-* configurations. The decadal trend is also evident from a zonal perspective along the Equator (Fig. 4.9), although the response tends to be larger at 5-10° of latitude (not shown).

Numerical experiments performed with a global ocean model using realistic wind stress anomalies basically confirm what obtained with the idealised setup, and further provide an evaluation of the effect of an observed atmospheric weather regime on low-frequency STCs variability, also from a time-dependent perspective. Nevertheless, the use of a global ocean model forced with prescribed atmospheric forcing does not allow an evaluation of potential feedback mechanisms. Furthermore, long-term STCs variability can not be addressed with our 20-years numerical experiments. In the next chapter we assess STCs properties as simulated using state-of-the-art coupled models, in pre-industrial and future scenario multi-century integrations.

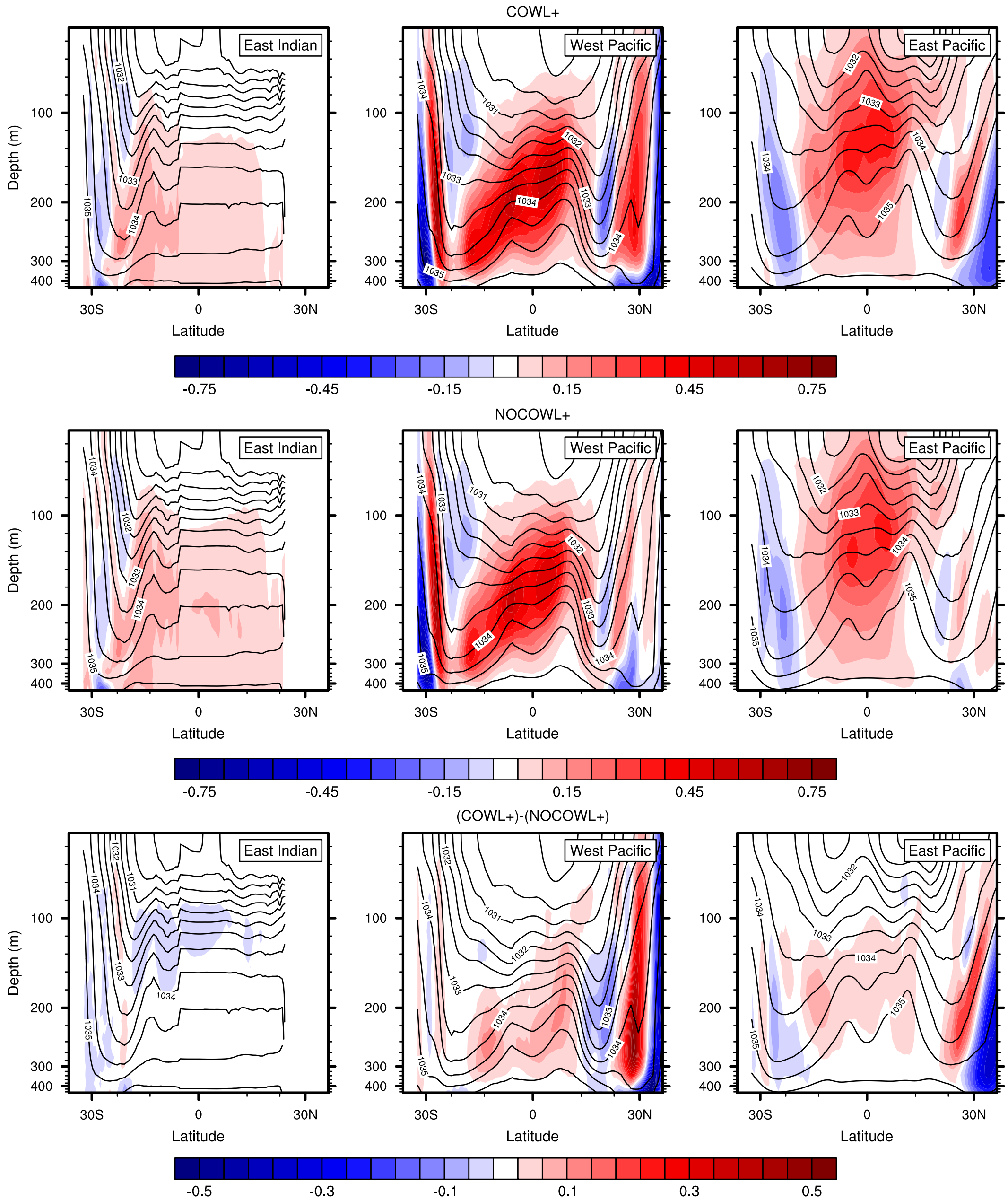

Figure 4.8: Time-averaged, zonally-averaged temperature trend (°C/10 yr) for the realistic time-varying wind stress anomalies. The regions shown are eastern Indian (80°E-150°E, left column), western Pacific (115°E-160°W, middle column), and eastern Pacific Ocean (160°W-70°W, right column). The top row concerns the *COWL+* wind stress anomaly, the middle row the *NOCOWL+* wind stress anomaly, and the bottom row the difference between *COWL+* and *NOCOWL+* anomalies.

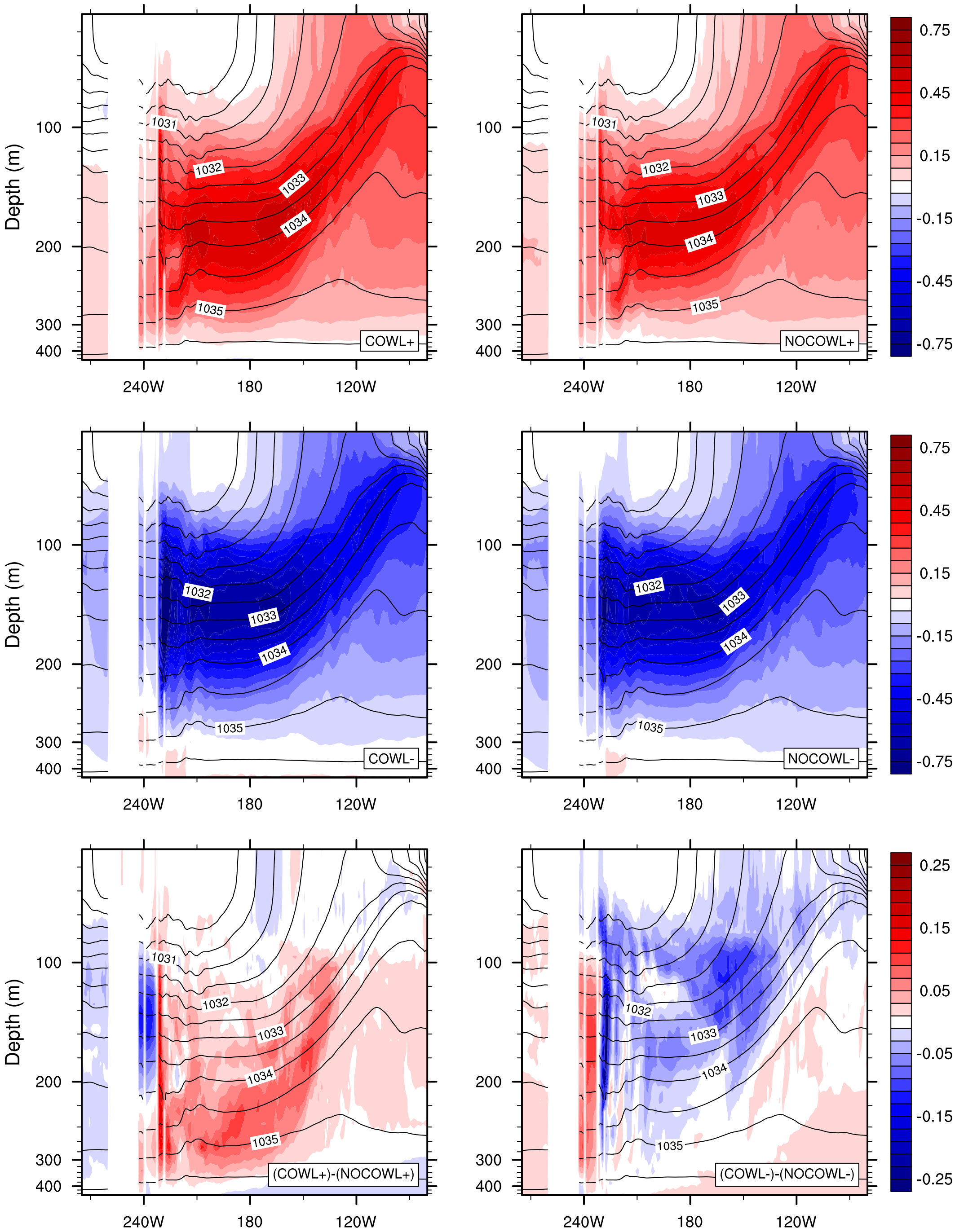

Figure 4.9: Time-averaged equatorial temperature trend (°C/10 yr) for the realistic time-varying wind stress anomalies. The top row concerns the *COWL+* wind stress anomaly, the middle row the *NOCOWL+* wind stress anomaly, and the bottom row the difference between *COWL+* and *NOCOWL+* anomalies.

Chapter 5

STCs simulated by CMIP5 models

In Chapters 3 and 4 we showed how a global ocean model is able to reproduce several STCs properties, also providing an estimate of the impact of idealised and realistic wind stress patterns on the Pacific shallow overturning circulation. On the other hand, several studies highlight problems in coupled ocean-atmosphere simulations of STCs (Solomon and Zhang 2006; Zhang and McPhaden 2006; Yang et al. 2014) and, generally speaking, tropical-extratropical interactions (Farneti 2017). In particular, Zhang and McPhaden (2006) attribute the large variability of simulated STCs transport exhibited by climate models to uncertainties on reproducing the tropical pycnocline, which in turn largely depends on model resolutions and parametrizations, as well as on the surface wind forcing. Similar problems actually affect also ocean models forced with the CORE-I NYF dataset (introduced in Chapter 2), poorly reproducing the observed western Pacific Ocean thermocline due to an imperfect representation of the South American coastal upwelling (Griffies et al. 2009). Still, the multi-model correlation between tropical SST (9°N-9°S, 90°W-180°W) and Pacific STCs transport standard deviations analysed by Zhang and McPhaden (2006) is 0.79, higher than the 95% significance level. However, they also note inconsistencies between modelled trends of SST and STCs transport during the recent past.

In the present chapter we analyse several coupled simulations performed by NOAA/GFDL models included in CMIP5 (Taylor et al. 2012). In particular, we want to assess long-term STCs variability in unforced integrations, as well its impact on equatorial climate. Moreover, we shall compare STCs meridional energy transport in both pre-industrial and global-warming future scenario simulations.

5.1 STCs Variability in Coupled Models

We already discussed some aspects of low-frequency STCs variability in Chapter 1. However, despite their potential importance for climate, in literature only few studies assess STCs centennial-scale variations, harder to evaluate because of the short available observational record, as well as predicted changes of STCs in future scenarios. An increasing number of studies instead attempts an evaluation of STCs decadal-scale variability in historical simulations (e.g., Solomon and Zhang 2006; Zhang and McPhaden 2006; Yang et al. 2014).

By analysing Simple Ocean Data Assimilation reanalysis (SODA; Carton and Giese 2008), Yang et al. (2014) find a positive trend of the equatorial convergence mass transport from 1900 to 2008, with a stronger increase in the Northern Hemisphere with respect to the Southern Hemisphere. They also find a strengthening of the zonal SST gradient at the Equator, which in turn accelerates the Walker circulation and, according to them, the oceanic STCs transport. However, we showed in Chapter 3 that a stronger equatorial wind stress forcing would result in a change of the equatorial thermocline tilting, not involving STCs dynamics. Comparing results from a subset of CMIP5 models, Yang et al. (2014) also compute a multiple model ensemble mean of equatorial Pacific Ocean temperature from the 1871-2008 historical runs, obtaining a warming trend at the surface and a cooling trend at the subsurface. According to the models, this occurred together with a weakening of the trade winds, in contrast with SODA reanalysis which shows instead intensified northeast and southeast trades west of 120°W. Thus, the subset of models analysed by Yang et al. (2014) does not capture well long-term STCs variations.

Farneti (2017) shows that different unforced coupled models gave a weaker equatorial mass convergence during the second half of the twentieth century compared to observations, along with a weak correlation between equatorial SST and STCs interior mass transport; a possible reason could be an incorrect representation of the off-equatorial wind stress variability. In fact, results from uncoupled models forced by atmospheric reanalysis are in better agreement with the observed STCs properties, and give larger correlation between tropical SST and STCs convergence.

Few studies assessed STCs response to future global warming and increasing greenhouse emissions, using either single coupled model simulations or ensembles. Meehl et al. (2005b) simulate a strong reduction of STCs equatorward transport in the interior ocean, using a coupled model forced by anthropogenic global warming from 1900 to 2100. Lohmann and Latif (2005) find a weakening (strengthening) STC circulation in the Northern (Southern) Hemisphere in a 240-yr global warming scenario simulated by a coupled model, as confirmed by Park et al. (2009) and Wang and Cane (2011) simulation studies.

With a multi-model intercomparison study on the second half of the twentieth and twenty-second centuries, Luo et al. (2009) show a redistribution of equatorward transport in a warmer climate from the interior to the western boundary contribution, but with a relatively small change in the total STCs transport. Using a subset of CMIP3 models (Meehl et al. 2007), Wang and Cane (2011) question those results by showing no compensation between western boundary and interior components, with the former depending more on the modelled shoaling of the equatorial pycnocline base in the western Pacific and the latter related with wind-driven changes of the equatorial ocean vertical structure (Vecchi et al. 2006; Vecchi and Soden 2007; Clarke 2010). In particular, weakening interior trends would be responsible for a decreased STCs equatorward transport, as already shown by McPhaden and Zhang (2002) using observations, and by Zhang and McPhaden (2006) using coupled simulations. There are also interhemispheric contrasting trends of the STCs poleward branches obtained by Wang and Cane (2011), confirming Lohmann and Latif (2005) model results and attributed to changes in the off-equatorial wind stress forcing. Overall, opposing results coming from different observational and modelling studies suggest that the STCs response to past, present, and future global warming is not easy to discern with available models and observations.

5.2 Experimental setup

Among the models available in CMIP5, in Chapter 2 we mentioned our choice to analyse outputs coming from NOAA/GFDL coupled models, listed in Table 5.1. This choice has two motivations. First of all, it fits with our previous studies concerning STCs properties modelled by a global ocean model; in fact, results shown in Chapters 3 and 4 have been obtained from MOM5 simulations, and all NOAA/GFDL coupled models considered in the present study employ the same ocean code (see Chapter 2 for details). Second, among the outputs analysed in Zhang and McPhaden (2006) coupled models comparison, NOAA/GFDL coupled simulations were able to better reproduce several STCs properties.

The simulations used differ in both spatial resolution and length of integra-

Model	Control Integration Length (years)	Scenario Integration Length (years)	Oceanic Resolution (°)	Atmospheric Resolution (km)
CM2.1	4000	600	1	200
CM2.5	1000	—	0.25	50
CM2.5-FLOR	920	—	1	50
CM3.0	6000	5900	1	200
ESM2M	1500	200	1	200

Table 5.1: List of simulations used in the present study, obtained with NOAA/GFDL coupled models and included in CMIP5.

tion (Tab. 5.1). The oceanic component has a 1° resolution (up to 1/3° from 30°N to 30°S) for all models except CM2.5, which has a higher horizontal resolution (0.25°). The model CM2.5 also employs a higher resolution atmospheric component, also shared by its FLOR version, with respect to other models.

We analyse outputs coming from two different types of simulations. The first type is the control pre-industrial integration, in which the atmospheric radiative forcing is prescribed during the whole coupled simulation to observed conditions of 1860 (Stouffer et al. 2011). These simulations are used to assess natural climate variability, and they are suitable for our purpose of studying long-term unforced STCs variations. The second kind of climate simulations we employed is called *1%to2xCO*$_2$. Basically, in these integrations the CO_2 global concentration is increased by 1% per year starting from the end of the respective control simulation, until a doubling of the initial CO_2 concentration is reached; afterwards, CO_2 global concentration is kept fixed. This idealised scenario has been specifically introduced in the CMIP5 experimental protocol (Taylor et al. 2009) to study transient effects on global climate arising from simplified greenhouse forcing. However, we will focus on the last part of the *1%to2xCO*$_2$ integrations to assess STCs meridional energy transport in a warmer climate, using the same metrics introduced in Chapter 2.

We are going to evaluate low-frequency Pacific STCs variability in unforced simulations, by computing equatorward mass transport and separating western boundary and interior contributions; the interior component is computed from the South American coastline to 145°E in the Northern Hemisphere and to 165°E in the Southern Hemisphere, according to Zhang and McPhaden (2006). The relationship between mass transport and equatorial SST in those simulations will also be assessed. Then, we shall move to analyse future scenario integrations, addressing the problem of STCs meridional energy transport variations in a warmer climate.

5.3 Results

We evaluate here some properties of STCs simulated by NOAA/GFDL coupled models included in CMIP5 (Table 5.1). First we focus on the control simulations, then we analyse future scenario integrations.

5.3.1 Long-term STCs Variability

We compute equatorward mass transport (Eq. 2.1) from five control pre-industrial simulations performed by several NOAA/GFDL coupled models included in CMIP5 and described in Chapter 2. These long unforced integrations allow an evaluation of STCs low-frequency variability.

The strength of simulated STCs by evaluated coupled models is shown in Fig. 5.1. With respect to our control simulation described in Chapter 2 and shown here in the CTRL panel, we see a slightly stronger overturning circulations in all coupled simulations, along with incongruities in the Southern Hemisphere for potential density larger than 1035 kg m^{-3}, thus outside the STCs characteristic density range.

Fig. 5.2 shows the equatorward mass transport at 15°N from the five evaluated simulations, integrated over the Pacific Ocean. There is a large variability among models for what concerns both mean and standard deviation. In particular, time-averaged mass transport ranges from about -19 Sv for CM2.5 to about -40 Sv for CM2.1. These two models also stand out for what concerns standard deviation, with CM2.1 exhibiting the largest value (5 Sv) and CM2.5 the smallest value (1 Sv). Some of these considerations also apply for the equatorward mass transport computed at 15°S (Fig. 5.3), in which the standard deviation is about 2-3 Sv for all models. However, in the Southern Hemisphere the largest transport is given by the CM3.0 simulation (38 Sv), while the smallest is given by the CM2.5_FLOR model (30 Sv). All models show remarkable interannual and interdecadal variability, but no centennial-scale variations. Both CM2.5 formulations actually exhibit a slight decreasing trend of equatorward mass transport in the Southern Hemisphere, along with a warming trend in the equatorial SST (not shown). However, it must be noted that these two simulations are shorter than other integrations, which show instead no appreciable trends.

In Tabs. 5.2, 5.3, 5.4, and 5.5 we focus on mass transport diagnostics for all control pre-industrial simulations at different latitudes. Computed values refer to the Pacific basin only, differently from the previous chapters, in or-

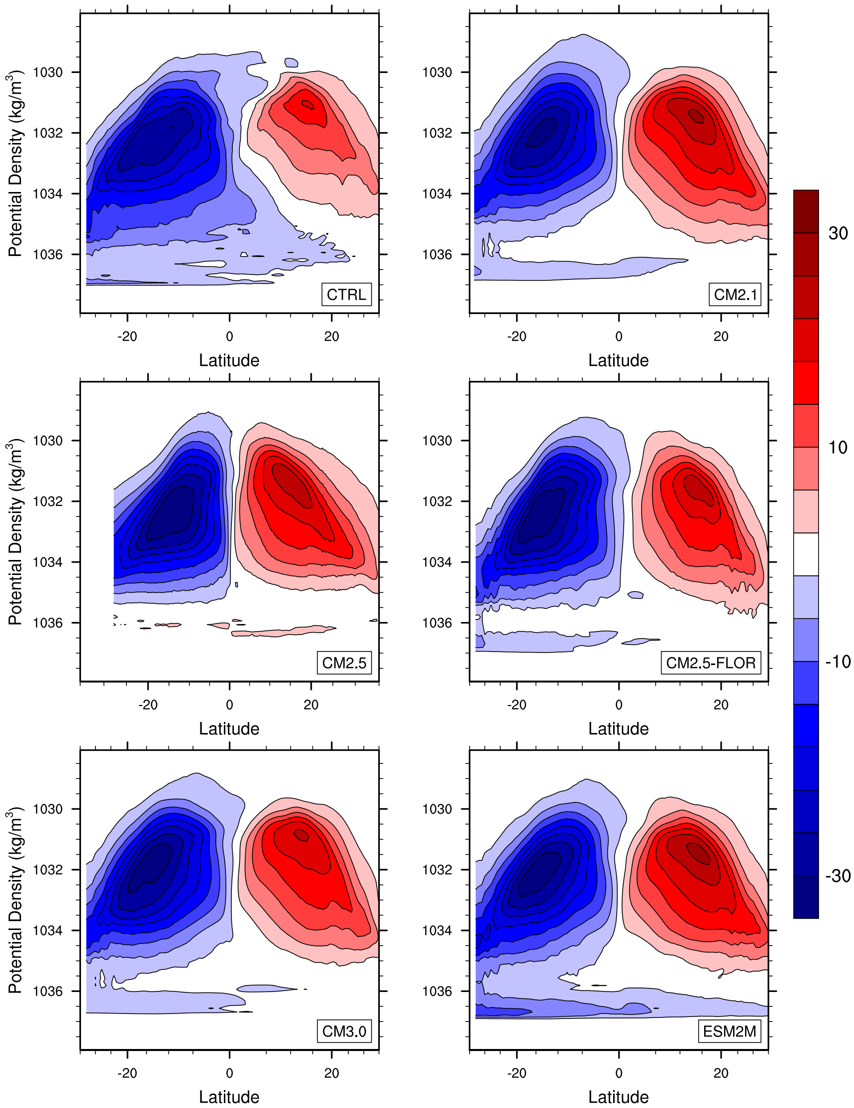

Figure 5.1: Zonally-integrated mass transport (Sv) on potential density coordinates (kg m^{-3}, referred to 2000 dbar) for the control pre-industrial NOAA/GFDL simulations included in CMIP5. Red structures are clock-wise cells and blue ones are counterclock-wise.

der to better assess western boundary and interior contributions. Few models show a reduction of the total equatorward mass transport from 15° to 9° of latitude, particularly prominent for CM2.1 and CM3.0. This is probably due to the recirculation of part of the equatorward flow within the subtropical gyre, and to interactions with the Indian Ocean at the Indonesian Straits. In general, we also see how in the Northern hemisphere there is a large reduction in the interior component moving closer to the Equator, in favour of the western boundary part. This is consistent with the presence of a high potential vorticity ridge close to 9°N (Lu and McCreary 1995). However, an analogous equatorward reduction of the interior mass transport also occurs in the Southern Hemisphere, but in a lesser extent.

	Total		Int		WB	
Model	Avg	STD	Avg	STD	Avg	STD
CM2.1	-40	5	-29	9	-11	5
CM2.5	-19	1	-17	3	-2	3
CM2.5-FLOR	-23	2	-19	4	-4	4
CM3.0	-28	3	-15	4	-13	3
ESM2M	-34	3	-22	7	-12	5

Table 5.2: Equatorward mass transport (Sv) of Pacific STCs at 15°N as simulated by control pre-industrial simulations performed by NOAA/GFDL coupled models. All mass transports are computed using Eq. 2.1 in the Indo-Pacific Ocean. *Tot* refers to the total equatorward mass transport, *Int* to the interior component, and *WB* to the western boundary contribution.

	Total		Int		WB	
Model	Avg	STD	Avg	STD	Avg	STD
CM2.1	-22	4	-2	2	-20	3
CM2.5	-22	2	-4	3	-18	2
CM2.5-FLOR	-23	3	-3	3	-20	3
CM3.0	-22	3	-5	3	-17	2
ESM2M	-28	4	-4	3	-24	4

Table 5.3: As in Tab. 5.2 but at 9°N.

5.3.2 STCs Energy Transport in a Warmer Climate

In this section we use the STCs meridional energy transport metrics introduced in Chapter 2, employing Eq. 2.4 in future climate scenario simulations from the evaluated subset of NOAA/GFDL coupled models. As explained in the experimental setup section of the present chapter, these integrations are characterised by a linear increase of the CO_2 global concentration until reaching a doubling with respect to pre-industrial values. In this way, we are able to evaluate eventual change in STCs energy transport under global warming conditions.

Before doing that, we assess STCs energy transport in all control pre-industrial simulations using the same metrics for different basins (Fig. 5.4). Further, we compare them with values obtained from observations: we employed the NOAA Optimum Interpolation (OI) SST V2 (Reynolds et al. 2002) dataset provided by NOAA/OAR/ESRL PSD (Boulder, Colorado, USA) for

	Total		Int		WB	
Model	Avg	STD	Avg	STD	Avg	STD
CM2.1	31	3	15	3	16	3
CM2.5	27	3	23	3	4	2
CM2.5-FLOR	30	2	14	4	16	3
CM3.0	38	3	16	3	22	2
ESM2M	32	3	12	3	20	3

Table 5.4: As in Tab. 5.2 but at 15°S.

	Total		Int		WB	
Model	Avg	STD	Avg	STD	Avg	STD
CM2.1	31	3	7	4	24	4
CM2.5	37	3	9	2	28	4
CM2.5-FLOR	32	3	7	3	25	4
CM3.0	29	2	4	2	25	2
ESM2M	31	2	8	4	23	4

Table 5.5: As in Tab. 5.2 but at 9°S.

the sea surface temperature, and the International Comprehensive Ocean-Atmosphere Data Set (ICOADS; Freeman et al. 2017) provided by NOAA/OAR/ESRL PSD (Boulder, Colorado, USA) for the zonal wind stress. A word of caution must be spent, being the results shown in Fig. 5.4 a comparison between observed values (affected by both internally and externally-forced climate variability) and pre-industrial simulations (not including any external forcing). As such, Fig. 5.4 just serves as a benchmark for Eq. 2.2 before assessing future climate scenario integrations.

In general, we see that model-generated STCs meridional energy transports tend to show larger values than observed estimates. This is true especially for Pacific and Indian STCs, giving the largest values of meridional energy transport in both models and observations, whereas Atlantic STCs associated transports are smaller and closer to observational values. Observations estimate shown in Fig. 5.4 is very similar to an analogous estimate performed by Klinger and Marotzke (2000, Fig. 6).

STCs meridional energy transport estimates from observations and two different types of coupled simulations (control and *1%to2xCO*$_2$) are compared in Fig. 5.5 for three models listed in Table 5.1. The period considered in the computation is the same for all future-scenario integrations. All models give an increase of meridional energy transport in a warmer climate for the Indian and

South Pacific STC. Different increase tendencies are also observed among the models, with CM3.0 (ESM2M) giving the largest (smallest) difference between control and *1%to2xCO*$_2$. On the other hand, future scenario computations give slightly smaller values of STCs meridional energy transport for the North Pacific STC. Again, CM3.0 computations show larger separation from observations, with CM2.1 and ESM2M respective lines almost overlapped.

Looking more carefully on the Pacific basin, these changes are concurrent with a slight weakening (strengthening) of the zonal wind stress in the northern (southern) subtropical ocean in future-scenario integrations, with respect to pre-industrial simulations (not shown). At the same time, a stronger SST increase in the North Pacific Ocean with respect to South Pacific is also seen in all future-scenario simulations, but with no substantial difference in terms of SST meridional gradient. Therefore, the different behaviour of northern and southern Pacific STCs meridional energy transport is attributable to distinct zonal wind stress changes.

5.4 Discussion

The picture drawn by our preliminary analysis of state-of-the-art coupled models about STCs variability provides several interesting insights, but also few controversial aspects. Results coming from two different types of NOAA/GFDL coupled models integrations have been shown. The first consists of a control pre-industrial implementation, with no external forcing and prescribed global CO_2 concentration to pre-industrial values. The second is a future scenario simulation, in which the CO_2 concentration is increased by 1% per year until the global value is doubled with respect to the initial (pre-industrial) value, and is then kept fixed thereafter.

Tabs. 5.6 and 5.7 include correlation coefficients relating several STCs mass transports metrics (total transport, western boundary and interior contributions) at different latitudes, as well as the correlation of equatorial mass transport convergence with Niño3.4 SST. In general, correlation between total equatorward mass transport and interior components tend to deteriorate moving toward the Equator in the Southern Hemisphere, with the CM2.5-FLOR value even reversing its sign, while being more stable in the Northern Hemisphere. However, we show that total equatorward mass transport and interior component are well correlated, confirming what found by several studies (McPhaden and Zhang 2002; Lee and Fukumori 2003; Cheng et al. 2007;

Hong et al. 2014). Interior and WB components are anti-correlated in all models as suggested by many observational and modelling works, although with some ambiguities among models and with a drastic equatorward deterioration in the Northern Hemisphere, probably due to the Indian Ocean influence, whereas values are found increasing in the Southern Hemisphere moving from 15° to 9°. Anti-correlation between equatorial mass convergence and Niño3.4 SST is rather poor in most models, with the only exception of CM2.5-FLOR and ESM2M, with respect to other estimates obtained by observations and historical coupled simulations (McPhaden and Zhang 2002, 2004; Zhang and McPhaden 2006). However, our poor representation of STCs mass transport and tropical SST relationship is not entirely surprising in the context of coupled models (Solomon and Zhang 2006; Farneti 2017). Furthermore, interannual SST variability in the equatorial Pacific Ocean is dominated by ENSO fluctuations, with a more important role of STCs on regulating equatorial ocean dynamics on longer timescales.

	Tot vs Int		Int vs WB		Conv vs SST	
Model	15°N	15°S	15°N	15°S	Tot	Int
CM2.1	0.80	0.60	-0.79	-0.57	-0.19	-0.17
CM2.5	0.45	0.84	-0.90	-0.57	-0.13	-0.53
CM2.5-FLOR	0.60	0.72	-0.93	-0.80	-0.26	-0.24
CM3.0	0.68	0.71	-0.70	-0.39	-0.16	-0.10
ESM2M	0.62	0.55	-0.87	-0.61	-0.48	-0.38

Table 5.6: Pearson correlation coefficients relating different aspects of Pacific STCs variability as simulated by control pre-industrial simulations performed by NOAA/GFDL coupled models. All mass transports are computed using Eq. 2.1 at 15° of latitude in the Pacific Ocean. *Tot* refers to the total equatorward mass transport, *Int* to the interior component, and *WB* to the western boundary contribution. *Conv* refers to the equatorward mass convergence, computed as the sum of the Northern and Southern Hemisphere contributions for both total and interior transports. *SST* represents the sea surface temperature computed in the Pacific Niño3.4 region.

Here we further resume our major findings for each evaluated model.

CM2.1 Time-averaged equatorward mass transport at 15° of latitude is the largest of all analysed models, with intensity larger than 30 Sv in both hemispheres. However, at 9°N the equatorward mass transport is almost halved, whereas at 9°S the reduction is much smaller. Mass transport correlations show a good agreement of total transport and interior component at 15°, deteriorating going closer to the Equator. A similar behaviour is shown by the relationship between WB and interior components, although in the Southern Hemisphere their anti-correlation even

	Tot vs Int		Int vs WB		Conv vs SST	
Model	9°N	9°S	9°N	9°S	Tot	Int
CM2.1	0.55	0.34	-0.08	-0.75	-0.06	-0.22
CM2.5	0.61	0.19	-0.55	-0.65	-0.33	-0.54
CM2.5-FLOR	0.65	-0.27	-0.47	-0.84	-0.41	-0.74
CM3.0	0.70	0.12	-0.44	-0.56	0.03	-0.04
ESM2M	0.56	0.21	-0.21	-0.82	-0.42	-0.69

Table 5.7: As Tab. 5.6 but at 9°of latitude.

increases moving equatorward. The same pattern is observed for the equatorial convergence anti-correlation with Niño3.4 SST.

CM2.5 Unlike all other models, we see here an increase of equatorward mass transport moving from 15° to 9°, up to 10 Sv in the Southern Hemisphere. Total and interior transports show a contrasting behaviour, with an increasing (descreasing) correlation moving equatorward in the Northern (Southern) Hemisphere. Interior and western boundary contribution show a rather good anti-correlation, as well as equatorial mass convergence and SST especially in the Southern Hemisphere.

CM2.5-FLOR Equatorward mass transports computed at 15° only change slightly going closer to the Equator. Anti-correlation between interior and WB components is particularly good at 15°, although deteriorating moving equatorward especially in the Southern Hemisphere, where a small anti-correlation is found at 9°S. Anti-correlation between equatorial convergence and SST instead increases going equatorward.

CM3.0 We observe a remarkable decrease of the total equatorward mass transport going toward the Equator, from 6 Sv (Northern Hemisphere) to 9 Sv (Southern Hemisphere). A drastic reduction is seen in the relationship between total transport and interior component in the Southern Hemisphere as we move toward the Equator, whereas in the Northern Hemisphere the reduction affects the WB-Int anti-correlation value. There is basically no relationship between equatorward convergence and Niño3.4 SST.

ESM2M The Northern Hemisphere estimation of the equatorward mass transport is affected more evidently than the Southern Hemisphere by gyre recirculation. The WB-Int anti-correlation is very good at 15°N, but greatly reduced at 9°N; instead, an opposite behaviour is seen in the Southern Hemisphere. The equatorial convergence - SST anti-correlation is the largest of all considered models.

Overall, linear correlations do not give us a coherent picture of the long-term STCs variability, as well as the relationship between STCs strength and equatorial surface ocean state. Many effects can contribute to these inconsistencies, ranging from ocean model formulation and resolution to atmospheric feedbacks. A more thorough analysis must be performed, and is currently under way.

So far we assessed STCs dynamics under unforced climate conditions, but how are STCs expected to change under global warming? Future scenario assessments in a warmer climate give an ambiguous response to this question. North Pacific STC shows a decreased meridional energy transport in future integrations with respect to pre-industrial simulations, whereas South Pacific and Indian STCs exhibit increased associated energy transports. The same patterns is also given by Atlantic STCs (not shown). This potentially suggests a different behaviour of STCs future changes, with a weakening (strengthening) in the Northern (Southern) Hemisphere in terms of meridional energy transport. This is consistent with previous modelling studies (Lohmann and Latif 2005; Park et al. 2009; Wang and Cane 2011).

On the other hand, although faithfully reproducing previous assessments from other studies, our observational estimate could underestimate STCs meridional energy transport in the Southern Hemisphere with respect to models. A further evaluation using ocean reanalysis (as ORAP5, Zuo et al. 2017) is already scheduled. Furthermore, at the moment our analysis does not include historical simulations of the last century, which would be a more consistent comparison with observations-derived computations, due to the lack of any external forcing in control pre-industrial integrations. As such, results coming from the present chapter should be seen as an initial attempt to study low-frequency STCs variability in CMIP5 models, as part of a larger analysis study.

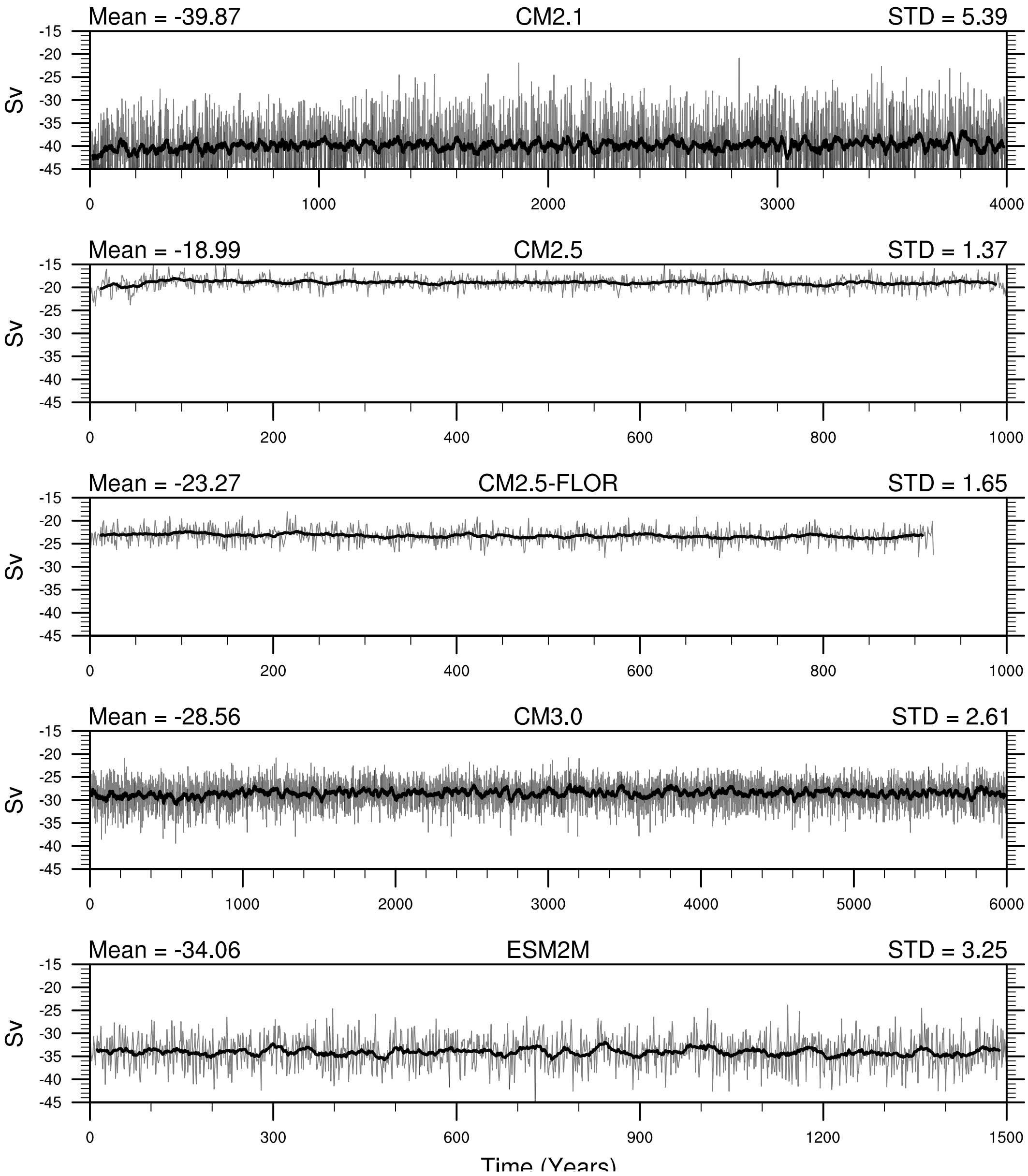

Figure 5.2: Annual mean (thin lines) and 25-years running mean (thick lines) of zonally, vertically-integrated equatorward mass transport (Sv), computed at 15°N for the control pre-industrial from a subset of NOAA/GFDL simulations included in CMIP5. Temporal mean and standard deviation are also given for each time series.

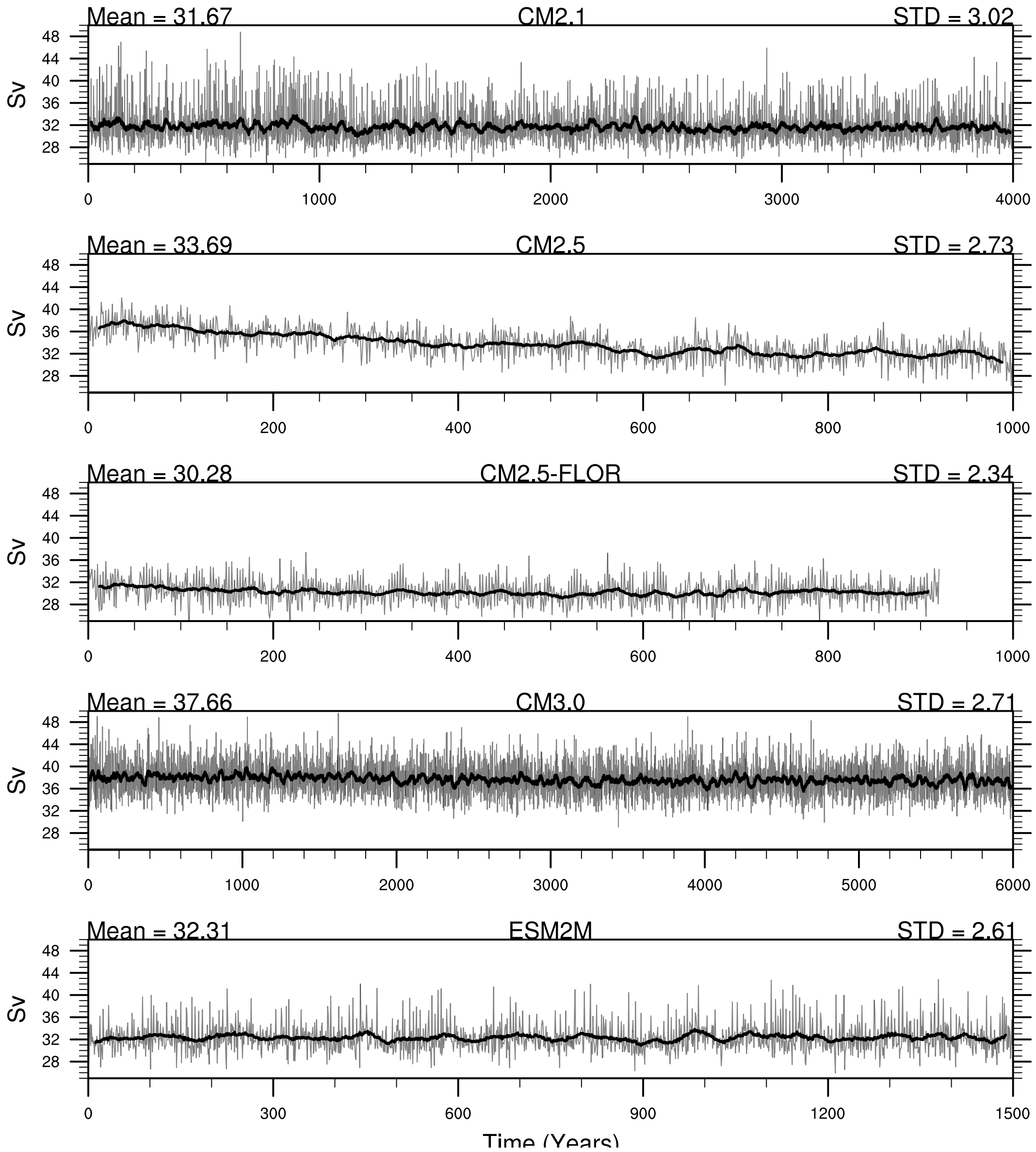

Figure 5.3: As in Fig. 5.2 but at 15°S.

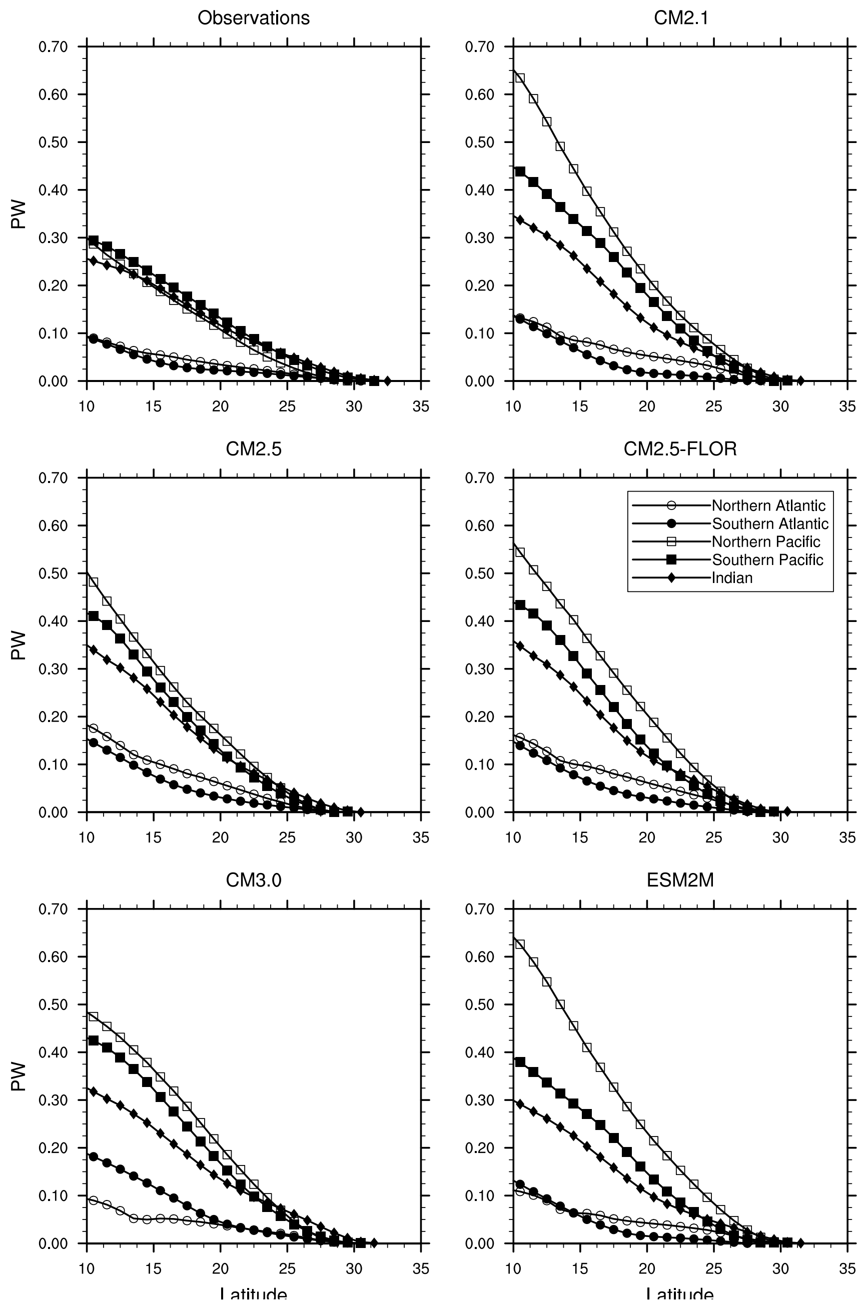

Figure 5.4: STCs meridional energy transports (PW) from observations and all control pre-industrial coupled simulations, estimated using Eq. 2.4 and plotted against latitude.

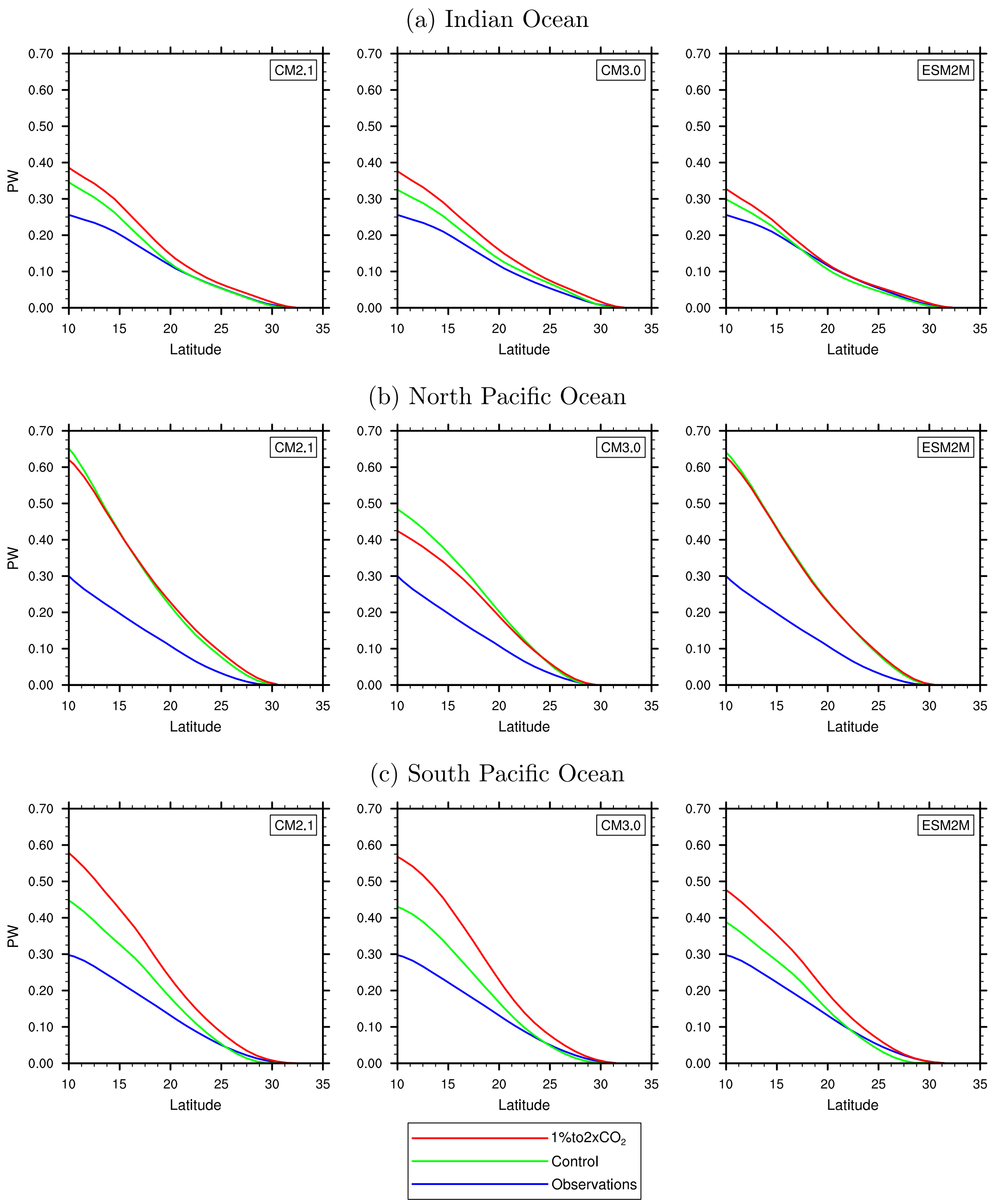

Figure 5.5: STCs meridional energy transport intensity (PW) from observations, control pre-industrial and *1%to2x*CO_2 coupled simulations, estimated using Eq. 2.4 and plotted against latitude.

Chapter 6

Conclusions and Outlook

During the present dissertation, we studied the effect of wind stress forcing on Pacific Subtropical Cells (STCs) using numerical models of different complexity. In fact, one of the most pressing issues concerning climate modelling is about dealing with inherent uncertainties of ocean-ice models. Perhaps, the best way for tackling the problem is suggested by Griffies et al. (2009): acknowledging the limitations of ocean-ice models and incorporating them in a hierarchical structure of numerical tools, in which fully-coupled climate models lies on top. The present study tried to follow those guidelines: we started with an analysis of ad-hoc experiments performed with a global ocean model, employing idealised wind stress patterns and intensities to emphasise their impact on STCs dynamics; we then moved to a more realistic experimental setup using the same model, highlighting the necessarily smaller STCs response to employed wind stress anomalies with respect to idealised ones; finally, we assessed several STCs properties as reproduced by different implementations of state-of-the-art climate models.

First of all, employing a global ocean model (MOM5; Griffies 2012) we applied idealised and realistic time-invariant zonal wind stress anomalies at the sea surface, in order to strengthen or weaken the climatological forcing. It is worth to note that the observed interannual variability of the zonal wind stress in Pacific subtropical and extratropical regions can produce larger anomalies than the ones used in this study (not shown). Results from the different perturbation experiments were compared with respect to a climatologically-forced long control run, obtained with the same model. In a similar way, England et al. (2014) applied a zonal wind stress anomaly to the entire Pacific basin from 45°N to 45°S. However, we chose here to test the STCs response by using selected forcing locations, in order to understand which region gives the strongest response. This is a key aspect, since in general the equatorial response produced by trade winds anomalies is stronger than the one generated from outside the Tropics. In fact, by changing the wind stress forcing on a very large area, the largest part of the off-equatorial signal could be hidden by the (relatively larger) locally-generated response. Actually, the structure of the meridional overturning circulation trend in England et al. (2014) is very similar, in terms of spatial extension, to what is obtained here with equatorial wind stress anomalies (Fig. 3.5).

Our results from idealised experiments can be summarised as follows.

- Equatorial wind stress anomalies located between 8°S and 8°N do not extend poleward enough in order to force STCs. Zonal cross sections at the Equator show large thermal anomalies (up to 3°C) in some cases, but they are related to an adjustment of the thermocline in response to the different local wind stress forcing. Appreciable changes in ITF transport are also obtained (up to 2 Sv), leading to a remarkable temperature anomaly in the Indian Ocean (not shown).

- Among all experiments, subtropical wind stress anomalies have the strongest impact on STCs. Equatorward mass transport anomalies reach 12 Sv, roughly one third of the control value. The generated STCs motion develops mainly in the thermocline, with a striking thermal signal appearing at the Equator: up to 1°C at depth and 0.5°C at the surface. In terms of energy transport, anomalies reach close to half of the control value for the experiment with the strongest wind stress anomaly (not shown). However, if a diagnostic for STC-related meridional energy transport is used, then STCs energy flux is quantified to be $\approx 1/3$ of the total transport anomaly. Finally, subtropical wind stress anomalies – and the associated STC dynamical changes – do not have an appreciable effect on ITF transport.

- Extratropical wind stress anomalies are found to exert a weak influence on both mass and energy STCs transport, as compared to subtropical experiments. In particular, most of the signal is forced within the 15°-20°latitudinal region, as evidenced by a set of forcing anomalies located north to those latitudes which did not produce appreciable changes in STC dynamics. In the latter case, transport anomalies likely recirculate within the subtropical gyre.

For what concerns realistic wind stress anomalies, zonal wind stress patterns related with COWL are able to force a signal from the northern STC reaching the Equator, with a thermal anomaly of 0.4°C in the thermocline and 0.1°C at the surface. Obviously, the generated response is smaller than what obtained in our strongest idealised experiments, being the wind stress intensity much smaller in this case. On the other hand, a time-varying implementation of the COWL wind stress anomalies highlights important aspects about STCs transient properties, with the equatorward mass transport showing a large inertia to changing wind stress forcing, but still showing a stronger response to wind stress variations in the subtropical region. However, subsurface temperature trends driven by the COWL-related wind stress anomalies are mainly found at the Subtropics, although a small signal is also found in the equatorial thermocline.

Among the different processes connecting the Subtropics to the tropical ocean, our numerical experiments suggest the interaction mechanism proposed by Kleeman et al. (1999) as able to explain remotely-driven thermal anomalies at the Equator in terms of anomalous STCs mass transports. That is, an anomalous STC transport drives a surface thermal signal at the Equator by altering the feeding of subsurface water to the thermocline. Our idealised subtropical experiments drive a substantial STC response in the equatorial thermocline, where the bulk of the Equatorial Undercurrent flows and forms part of the returning branch of the STC circulation. A more modest response is found in our realistic experiments, due to the subtropical sector of the COWL wind stress pattern.

In order to further demonstrate the role of different wind stress forcings on the upper ocean, we now compare ocean heat content anomalies in the equatorial Pacific (10°N-10°S), integrated at different depths during the final stage of the simulation for several numerical experiments (Table 6.1). We see a strong heat content increase in the first 300 m for the equatorial idealised set, accounting for the whole increase in the total ocean column. Furthermore, the ITF advects part of the generated signal into the Indian Ocean, leading to significant heat content anomalies in the top 1000 m for all idealised equatorial experiments (not shown). In the strengthened subtropical experiments is instead generated a negative heat content anomaly, since a strengthened STC circulation draws deeper (and colder) water to the surface. Again, the heat content change is mostly located in the uppermost 300 meters. In the realistic case, heat content anomalies in the surface layers are even larger than total column integrations. We also notice that the both strengthened and weakened

COWL/*NOCOWL* anomalies can drive a heat content response comparable to the strongest idealised experiments, with a reversed sign due to the shape of the employed patterns. Furthermore, the difference between *COWL* and *NOCOWL* anomalies is about 60-70 10^{21} J, comparable to 20% idealised subtropical experiments and completely attributable to the subtropical sector of the COWL pattern.

	Equatorial		Subtropical		*COWL*		*NOCOWL*	
Depth	10%	50%	10%	50%	+	-	+	-
0 - 300 m	154	717	-52.5	-275	299	-283	226	-215
0 - 1000 m	153	717	-56	-284	297	-272	229	-211
Total	153	717	-55.5	-280	289	-267	220	-208

Table 6.1: Ocean heat content anomaly (10^{21} J) in the equatorial Pacific Ocean (10°N-10°S) resulting from several idealised (strengthened Equatorial and Subtropical) and realistic (time-constant *COWL* and *NOCOWL*) experiments, averaged over the last 5 years of simulation. Values are given for the upper 300 m, upper 1000 m and the total water column. Only the weakest and strongest wind stress anomaly experiments are considered for the idealised setup.

Building on the results coming from idealised and realistic wind stress experiments, we computed several STCs diagnostics from two different implementations of a subset of GFDL/NOAA coupled models included in CMIP5. The first type is a control simulation meant to reproduce natural climate variability, the second is an idealised global-warming future scenario. The response obtained presents both positive and negative aspects. On one hand, coupled models successfully reproduce the separation of western boundary and interior contributions in the equatorward transport, as well as their anti-correlation. Moreover, some aspects of predicted STCs changes are consistent with previous studies. On the other hand, the obtained relationship between equatorial mass convergence and SST is very weak, and computed STCs meridional energy transport do not match observational estimates. A comparison of both control and future scenario integrations with historical simulations is also lacking, as well as an assessment of the role of off-equatorial wind stress forcing on simulated STCs.

In conclusion, several points of our analysis deserve a more thorough examination, in order to understand their implications on local and global climate. Although our analysis shed light on important, and sometimes underrated, aspects of Pacific Ocean dynamics, tropical-extratropical connections, and ocean-atmosphere interactions, much can still be done.

Bibliography

Adcroft, A., C. Hill, and J. Marshall (1997). “Representation of Topography by Shaved Cells in a Height Coordinate Ocean Model”. In: *Mon. Wea. Rev.* 125, pp. 2293–2315.

Adcroft, A. and J.M. Campin (2004). “Rescaled height coordinates for accurate representation of free-surface flows in ocean circulation models”. In: *Ocean Model.* 7, pp. 269–284.

Alexander, M.A., I. Bladé, M. Newman, J.R. Lanzante, N. Lau, and J.D. Scott (2002). “The Atmospheric Bridge: The Influence of ENSO Teleconnections on Air-Sea Interaction over the Global Oceans”. In: *J. Climate* 15, pp. 2205–2231.

Alexander, M.A., L. Matrosova, C. Penland, J.D. Scott, and P. Chang (2008). “Forecasting Pacific SSTs: Linear Inverse Model Predictions of the PDO”. In: *J. Climate* 21, pp. 385–402.

Alexander, M.A. (2010). “Shallow Overturning Circulations of the Tropical-Subtropical Oceans”. In: *Climate Dynamics: Why Does Climate Vary?* Ed. by D.Z. Sun and F. Bryan. Washington D.C., USA: American Geophysical Union.

Alexander, M.A. and J. Scott (2002). “The influence of ENSO on air-sea interaction in the Atlantic”. In: *Geophys. Res. Lett.* 29.14.

Alory, G., S. Cravatte, T. Izumo, and K.B. Rodgers (2005). “Validation of a decadal OGCM simulation for the tropical Pacific”. In: *Ocean Model.* 10, pp. 272–282.

Anderson, B.T., J.C. Furtado, K.M. Cobb, and E. Di Lorenzo (2013). “Extra-tropical forcing of El Niño-Southern Oscillation asymmetry”. In: *Geophys. Res. Lett.* 40, pp. 4916–4921.

Anderson, D.L., K. Bryan, A.E. Gill, and R.C. Pacanowski (1979). “The transient response of the North Atlantic: Some model studies”. In: *J. Geophys. Res.* 84.C8, pp. 4795–4815.

Anderson, D.L. and A.E. Gill (1975). "Spin-up of a stratified ocean, with applications to upwelling". In: *Deep Sea Res.* 22.9, pp. 583–596.

Andrews, T., J.M. Gregory, M.J. Webb, and K.E. Taylor (2012). "Forcing, feedbacks and climate sensitivity in CMIP5 coupled atmosphere-ocean climate models". In: *Geophys. Res. Lett.* 39, p. L09712.

Ångström, A. (1935). "Teleconnections of Climatic Changes in Present Time". In: *Geogr. Ann. A* 17, pp. 242–258.

Arakawa, A. and V.R. Lamb (1977). "Computational design of the basic dynamical processes of the UCLA general circulation model". In: *General circulation models of the atmosphere.* Ed. by J. Chang. Vol. 17. Geophysical Monograph Series. Amsterdam, Netherlands: Elsevier, pp. 173–265.

Bacon, S., W.J. Gould, and Y. Jia (2003). "Open-ocean convection in the Irminger Sea". In: *Geophys. Res. Lett.* 30.5.

Baines, P.G. and S. Condie (1999). "Observations and Modelling of Antarctic Downslope Flows: A Review". In: *Ocean, Ice, and Atmosphere: Interactions at the Antarctic Continental Margin.* Ed. by S.S. Jacobs and R.F. Weiss. Antarctic Research Series. Washington D.C., USA: American Geophysical Union.

Balmaseda, M.A., K.E. Trenberth, and E. Källén (2013). "Distinctive climate signals in reanalysis of global ocean heat content". In: *Geophys. Res. Lett.* 40, pp. 1754–1759.

Barlow, M., S. Nigam, and E.H. Berbery (2001). "ENSO, Pacific Decadal Variability, and U.S. Summertime Precipitation, Drought, and Stream Flow". In: *J. Climate* 14, pp. 2105–2128.

Barnett, T.P. (1978). "Estimating Variability of Surface Air Temperature in the Northern Hemisphere". In: *Mon. Wea. Rev.* 106, pp. 1353–1367.

Barnett, T.P., D.W. Pierce, M. Latif, D. Dommenget, and R. Saravanan (1999). "Interdecadal interactions between the tropics and midlatitudes in the Pacific basin". In: *Geophys. Res. Lett.* 26.5, pp. 615–618.

Biondi, F., A. Gershunov, and D.R. Cayan (2001). "North Pacific Decadal Climate Variability since 1661". In: *J. Climate* 14, pp. 5–10.

Bjerknes, J. (1964). "Atlantic Air-Sea Interaction". In: *Adv. Geophys.* 10, pp. 1–82.

— (1969). "Atmospheric teleconnections from the equatorial Pacific". In: *Mon. Wea. Rev.* 97, pp. 163–172.

Böning, C.W. and P. Herrmann (1994). "Annual Cycle of Poleward Heat Transport in the Ocean: Results from High-Resolution Modeling of the North and Equatorial Atlantic". In: *J. Phys. Oceanogr.* 24, pp. 91–107.

Broccoli, A.J., N. Lau, and M.J. Nath (1998). “The Cold Ocean-Warm Land Pattern: Model Simulation and Relevance to Climate Change Detection”. In: *J. Climate* 11, pp. 2743–2763.

Bryan, K., S. Manabe, and R.C. Pacanowski (1985). “A Global Ocean-Atmosphere Climate Model. Part II. The Oceanic Circulation”. In: *J. Phys. Oceanogr.* 5, pp. 30–46.

Bryan, K. (1982). “Seasonal variation in meridional overturning and poleward heat transport in the Atlantic and Pacific Oceans: A model study”. In: *J. Mar. Res.* 40, pp. 39–53.

— (1991). “Poleward heat transport in the ocean: A review of a hierarchy of models of increasing resolution”. In: *Tellus* 43.4, pp. 104–115.

Butt, J. and E. Lindstrom (1994). “Currents off the east coast of New Ireland, Papua New Guinea, and their relevance to regional undercurrents in the western equatorial Pacific Ocean”. In: *J. Geophys. Res.* 99.C6, pp. 12503–12514.

Cane, M.A., A.C. Clement, A. Kaplan, Y. Kushnir, D. Pozdnyakov, R. Seager, S.E. Zebiak, and R. Murtugudde (1997). “Twentieth-Century Sea Surface Temperature Trends”. In: *Science* 275.5302, pp. 957–960.

Cane, M.A. (1998). “A role for the tropical Pacific”. In: *Science* 282.5386, pp. 59–61.

Capotondi, A. and M.A. Alexander (2001). “Rossby Waves in the Tropical North Pacific and Their Role in Decadal Thermocline Variability”. In: *J. Phys. Oceanogr.* 31, pp. 3496–3515.

Capotondi, A., M.A. Alexander, C. Deser, and M.J. McPhaden (2005). “Anatomy and Decadal Evolution of the Pacific Subtropical-Tropical Cells (STCs)”. In: *J. Climate* 18.18, pp. 3739–3758.

Carissimo, B.C., A.H. Oort, and T.H. Vonder Haar (1985). “Estimating the Meridional Energy Transports in the Atmosphere and Ocean”. In: *J. Phys. Oceanogr.* 15, pp. 82–91.

Carton, J.A., X. Cao, B.S. Giese, and A.M. Da Silva (1996). “Decadal and interannual SST variability in the tropical Atlantic Ocean”. In: *J. Phys. Oceanogr.* 26, pp. 1165–1175.

Carton, J.A. and B.S. Giese (2008). “Reanalysis of Ocean Climate Using Simple Ocean Data Assimilation (SODA)”. In: *Mon. Wea. Rev.* 136, pp. 2999–3017.

Cassou, C., Y. Kushnir, E. Hawkins, A. Pirani, F. Kucharski, I. Kang, and N. Caltabiano (2018). “Decadal Climate Variability and Predictability: Challenges and Opportunities”. In: *Bull. Amer. Meteor. Soc.* 99, pp. 479–490.

Cayan, D.R. (1992). “Latent and Sensible Heat Flux Anomalies over the Northern Oceans: The Connection to Monthly Atmospheric Circulation”. In: *J. Climate* 5, pp. 354–369.

Cessi, P. and S. Louazel (2001). “Decadal Oceanic Response to Stochastic Wind Forcing”. In: *J. Phys. Oceanogr.* 31, pp. 3020–3029.

Cessi, P. and F. Primeau (2001). “Dissipative Selection of Low-Frequency Modes in a Reduced-Gravity Basin”. In: *J. Phys. Oceanogr.* 31, pp. 127–137.

Chang, P. (1996). “The Role of the Dynamic Ocean-Atmosphere Interactions in Tropical Seasonal Cycle”. In: *J. Atmos. Sci.* 9, pp. 2973–2985.

Chang, P., L. Ji, and H. Li (1997). “A decadal climate variation in the tropical Atlantic Ocean from thermodynamic air-sea interactions”. In: *Nature* 385.6616, pp. 516–518.

Chao, Y., M. Ghil, and J.C. McWilliams (2000). “Pacific interdecadal variability in this century’s sea surface temperatures”. In: *Geophys. Res. Lett.* 27.15, pp. 2261–2264.

Charney, J.G. and J.G. DeVore (1979). “Multiple Flow Equilibria in the Atmosphere and Blocking”. In: *J. Atmos. Sci.* 36, pp. 1205–1216.

Chen, X. and K.K. Tung (2014). “Varying planetary heat sink led to global-warming slowdown and acceleration”. In: *Science* 345.6199, pp. 897–903.

Cheng, W., M.J. McPhaden, D. Zhang, and E.J. Metzger (2007). “Recent Changes in the Pacific Subtropical Cells Inferred from an Eddy-Resolving Ocean Circulation Model”. In: *J. Phys. Oceanogr.* 37, pp. 1340–1356.

Clarke, A.J. (2010). “Analytical Theory for the Quasi-Steady and Low-Frequency Equatorial Ocean Response to Wind Forcing: The “Tilt” and “Warm Water Volume” Modes”. In: *J. Phys. Oceanogr.* 40, pp. 121–137.

Corti, S., F. Molteni, and T.N. Palmer (1999). “Signature of recent climate change in frequencies of natural atmospheric circulation regimes”. In: *Nature* 398.6730, pp. 799–802.

Cox, M.D. (1987). “Isopycnal diffusion in a z-coordinate ocean model”. In: *Ocean Model.* 74, pp. 1–5.

Dai, A. and T.M.L. Wigley (2000). “Global patterns of ENSO-induced precipitation”. In: *Geophys. Res. Lett.* 27.9, pp. 1283–1286.

Danabasoglu, G., W.G. Large, J.J. Tribbia, P.R. Gent, B.P. Briegleb, and J.C. McWilliams (2006). “Diurnal Coupling in the Tropical Oceans of CCSM3”. In: *J. Climate* 19, pp. 2347–2365.

Boisséson, E. de, M.A. Balmaseda, S. Abdalla, E. Källén, and P.A.E.M. Janssen (2014). “How robust is the recent strengthening of the Tropical Pacific trade winds?” In: *Geophys. Res. Lett.* 41, pp. 4398–4405.

Dee, D.P., S.M. Uppala, A.J. Simmons, P. Berrisford, P. Poli, S. Kobayashi, U. Andrae, M.A. Balmaseda, G. Balsamo, P. Bauer, P. Bechtold, A.C. Beljaars, L. van de Berg, J. Bidlot, N. Bormann, C. Delsol, R. Dragani, M. Fuentes, A.J. Geer, L. Haimberger, S.B. Healy, H. Hersbach, E.V. Hólm, L. Isaksen, P. Kållberg, M. Köhler, M. Matricardi, A.P. McNally, B.M. Monge-Sanz, J. Morcrette, B. Park, C. Peubey, P. de Rosnay, C. Tavolato, J. Thépaut, and F. Vitart (2011). “The ERA-Interim reanalysis: configuration and performance of the data assimilation system”. In: *Q.J.R. Meteorol. Soc.* 137, pp. 553–597.

Delworth, T.L., A.J. Broccoli, A. Rosati, R.J. Stouffer, V. Balaji, J.A. Beesley, W.F. Cooke, K.W. Dixon, J. Dunne, K.A. Dunne, J.W. Durachta, K.L. Findell, P. Ginoux, A. Gnanadesikan, C.T. Gordon, S.M. Griffies, R. Gudgel, M.J. Harrison, I.M. Held, R.S. Hemler, L.W. Horowitz, S.A. Klein, T.R. Knutson, P.J. Kushner, A.R. Langenhorst, H. Lee, S. Lin, J. Lu, S.L. Malyshev, P.C. Milly, V. Ramaswamy, J. Russell, M.D. Schwarzkopf, E. Shevliakova, J.J. Sirutis, M.J. Spelman, W.F. Stern, M. Winton, A.T. Wittenberg, B. Wyman, F. Zeng, and R. Zhang (2006). “GFDL’s CM2 Global Coupled Climate Models. Part I: Formulation and Simulation Characteristics”. In: *J. Climate* 19, pp. 643–674.

Delworth, T.L., S. Manabe, and R.J. Stouffer (1993). “Interdecadal Variations of the Thermohaline Circulation in a Coupled Ocean-Atmosphere Model”. In: *J. Climate* 6, pp. 1993–2011.

Delworth, T.L., A. Rosati, W. Anderson, A.J. Adcroft, V. Balaji, R. Benson, K. Dixon, S.M. Griffies, H. Lee, R.C. Pacanowski, G.A. Vecchi, A.T. Wittenberg, F. Zeng, and R. Zhang (2012). “Simulated Climate and Climate Change in the GFDL CM2.5 High-Resolution Coupled Climate Model”. In: *J. Climate* 25, pp. 2755–2781.

Deser, C., M.A. Alexander, and M.S. Timlin (1996). “Upper-ocean thermal variations in the North Pacific during 1970-1991”. In: *J. Climate* 9.8, pp. 1840–1855.

Deser, C. and M.L. Blackmon (1993). “Surface Climate Variations over the North Atlantic Ocean during Winter: 1900-1989”. In: *J. Climate* 6, pp. 1743–1753.

Deser, C., A.S. Phillips, and J.W. Hurrell (2004). "Pacific Interdecadal Climate Variability: Linkages between the Tropics and the North Pacific during Boreal Winter since 1900". In: *J. Climate* 17, pp. 3109–3124.

Deser, C. and A.S. Phillips (2006). "Simulation of the 1976/77 Climate Transition over the North Pacific: Sensitivity to Tropical Forcing". In: *J. Climate* 19, pp. 6170–6180.

Colin de Verdière, A. and T. Huck (1999). "Baroclinic Instability: An Oceanic Wavemaker for Interdecadal Variability". In: *J. Phys. Oceanogr.* 29, pp. 893–910.

Dijkstra, H.A. (2013). *Nonlinear climate dynamics*. Cambridge, UK: Cambridge University Press. ISBN: 9780521879170.

Di Lorenzo, E., N. Schneider, K. M. Cobb, P. J. S. Franks, K. Chhak, A. J. Miller, J. C. McWilliams, S. J. Bograd, H. Arango, E. Curchitser, T.M. Powell, and P. Rivière (2008). "North Pacific Gyre Oscillation links ocean climate and ecosystem change". In: *Geophys. Res. Lett.* 35, p. L08607.

Ding, H., R.J. Greatbatch, M. Latif, W. Park, and R. Gerdes (2013). "Hindcast of the 1976/77 and 1998/99 Climate Shifts in the Pacific". In: *J. Climate* 26, pp. 7650–7661.

Donguy, J.R., G. Eldin, A. Morlière, J.P. Rebert, and G. Meyers (1984). *A thermal interpretation of a change in equatorial western Pacific circulation*. Tech. rep. Noumea, New Caledonia.

Donner, L.J., B.L. Wyman, R.S. Hemler, L.W. Horowitz, Y. Ming, M. Zhao, J. Golaz, P. Ginoux, S. Lin, M.D. Schwarzkopf, J. Austin, G. Alaka, W.F. Cooke, T.L. Delworth, S.M. Freidenreich, C.T. Gordon, S.M. Griffies, I.M. Held, W.J. Hurlin, S.A. Klein, T.R. Knutson, A.R. Langenhorst, H. Lee, Y. Lin, B.I. Magi, S.L. Malyshev, P.C. Milly, V. Naik, M.J. Nath, R. Pincus, J.J. Ploshay, V. Ramaswamy, C.J. Seman, E. Shevliakova, J.J. Sirutis, W.F. Stern, R.J. Stouffer, R.J. Wilson, M. Winton, A.T. Wittenberg, and F. Zeng (2011). "The Dynamical Core, Physical Parameterizations, and Basic Simulation Characteristics of the Atmospheric Component AM3 of the GFDL Global Coupled Model CM3". In: *J. Climate* 24, pp. 3484–3519.

Douville, H., A. Voldoire, and O. Geoffroy (2015). "The recent global warming hiatus: What is the role of Pacific variability?" In: *Geophys. Res. Lett.* 42, pp. 880–888.

Drijfhout, S.S., A.T. Blaker, S.A. Josey, A.J.G. Nurser, B. Sinha, and M.A. Balmaseda (2014). "Surface warming hiatus caused by increased heat uptake across multiple ocean basins". In: *Geophys. Res. Lett.* 41, pp. 7868–7874.

Dunne, J.P., J.G. John, A.J. Adcroft, S.M. Griffies, R.W. Hallberg, E. Shevliakova, R.J. Stouffer, W. Cooke, K.A. Dunne, M.J. Harrison, J.P. Krasting, S.L. Malyshev, P.C. Milly, P.J. Phillipps, L.T. Sentman, B.L. Samuels, M.J. Spelman, M. Winton, A.T. Wittenberg, and N. Zadeh (2012). "GFDL's ESM2 Global Coupled Climate–Carbon Earth System Models. Part I: Physical Formulation and Baseline Simulation Characteristics". In: *J. Climate* 25, pp. 6646–6665.

Easterling, D.R. and M.F. Wehner (2009). "Is the climate warming or cooling?" In: *Geophys. Res. Lett.* 36, p. L08706.

Eckart, C. (1948). "An analysis of the stirring and mixing processes in compressible fluids". In: *J. Mar. Res.* 7.3, pp. 265–275.

Ellis, H. and S. Hales (1751). "A Letter to the Rev. Dr. Hales, F.R.S. from Captain Henry Ellis, F.R.S. Dated Jan. 7, 1750-51, at Cape Monte Africa, Ship Earl of Hallifax". In: *Philos. Trans. (1683-1775)* 47, pp. 211–216.

Enfield, D.B. and J.S. Allen (1980). "On the Structure and Dynamics of Monthly Mean Sea Level Anomalies along the Pacific Coast of North and South America". In: *J. Phys. Oceanogr.* 10, pp. 557–578.

Enfield, D.B. and D.A. Mayer (1997). "Tropical Atlantic sea surface temperature variability and its relation to El Niño-Southern Oscillation". In: *J. Geophys. Res.* 102.C1, pp. 929–945.

England, M.H. (1995). "The Age of Water and Ventilation Timescales in a Global Ocean Model". In: *J. Phys. Oceanogr.* 25, pp. 2756–2777.

England, M.H. and F. Huang (2005). "On the interannual variability of the Indonesian Throughflow and its linkage with ENSO". In: *J. Climate* 18.9, pp. 1435–1444.

England, M.H., S. McGregor, P. Spence, G.A. Meehl, A. Timmermann, ... W. Cai, and A. Santoso (2014). "Recent intensification of wind-driven circulation in the Pacific and the ongoing warming hiatus". In: *Nat. Clim. Change* 4.3, pp. 222–227.

Evans, M.N., M.A. Cane, D.P. Schrag, A. Kaplan, B.K. Linsley, R. Villalba, and G.M. Wellington (2001). "Support for tropically-driven pacific decadal variability based on paleoproxy evidence". In: *Geophys. Res. Lett.* 28, pp. 3689–3692.

Farneti, R. and G.K. Vallis (2011). "Mechanisms of interdecadal climate variability and the role of Ocean-Atmosphere coupling". In: *Clim. Dyn.* 36, pp. 289–308.

Farneti, R. (2017). "Modelling interdecadal climate variability and the role of the ocean". In: *WIREs Clim. Change* 8, e441.

Farneti, R., S. Dwivedi, F. Kucharski, F. Molteni, and G.M. Griffies (2014a). "On Pacific Subtropical Cell Variability over the Second Half of the Twentieth Century". In: *J. Climate* 27, pp. 7102–7112.

Farneti, R., F. Molteni, and F. Kucharski (2014b). "Pacific interdecadal variability driven by tropical-extratropical interactions". In: *Clim. Dyn.* 42.11-12, pp. 3337–3355.

Fedorov, A.V. and S.G. Philander (2001). "A Stability Analysis of Tropical Ocean-Atmosphere Interactions: Bridging Measurements and Theory for El Niño". In: *J. Climate* 14, pp. 3086–3101.

Ferranti, L., T.N. Palmer, F. Molteni, and E. Klinker (1990). "Tropical-Extratropical Interaction Associated with the 30-60 Day Oscillation and Its Impact on Medium and Extended Range Prediction". In: *J. Atmos. Sci.* 47, pp. 2177–2199.

Fine, R.A., J.L. Reid, and H.G. Östlund (1981a). "Circulation of Tritium in the Pacific Ocean". In: *J. Phys. Oceanogr.* 11, pp. 3–14.

Fine, R.A., W.H. Peterson, and H.G. Östlund (1981b). "The Penetration of Tritium into the Tropical Pacific". In: *J. Phys. Oceanogr.* 17, pp. 553–564.

Fischer, J., F. Schott, and L. Stramma (1996). "Currents and transports of the Great Whirl-Socotra Gyre system during the summer monsoon, August 1993". In: *J. Geophys. Res.* 101.C2, pp. 3573–3587.

Fofonoff, N.P. (1981). "The Gulf Stream". In: *Evolution of Physical Oceanography: Scientific Surveys in Honor of Henry Stommel.* Ed. by B.A. Warren and C. Wunsch. Cambridge (MA), USA: MIT Press, pp. 112–139.

Folland, C. K., D.E. Parker, A.W. Colman, and R. Washington (1999). "Large Scale Modes of Ocean Surface Temperature Since the Late Nineteenth Century". In: *Beyond El Niño: Decadal and Interdecadal Climate Variability.* Ed. by A. Navarra. Berlin, Heidelberg: Springer Berlin Heidelberg, pp. 73–102.

Folland, C.K., J.A. Renwick, M.J. Salinger, and A.B. Mullan (2002). "Relative influences of the Interdecadal Pacific Oscillation and ENSO on the South Pacific Convergence Zone". In: *Geophys. Res. Lett.* 29.13.

Fox-Kemper, B., G. Danabasoglu, R. Ferrari, S.M. Griffies, R.W. Hallberg, M.M. Holland, M.E. Maltrud, S. Peacock, and B.L. Samuels (2011). "Parameterization of mixed layer eddies. Part III: Implementation and impact in global ocean climate simulations". In: *Ocean Model.* 39, pp. 61–78.

Fox-Kemper, B., R. Ferrari, and R. Hallberg (2008). "Parameterization of Mixed Layer Eddies. Part I: Theory and Diagnosis". In: *J. Phys. Oceanogr.* 38, pp. 1145–1165.

Fox-Kemper, B. and R. Ferrari (2008). “Parameterization of Mixed Layer Eddies. Part II: Prognosis and Impact”. In: *J. Phys. Oceanogr.* 38, pp. 1166–1179.

Fraedrich, K., U. Luksch, and R. Blender (2004). “1/f model for long-time memory of the ocean surface temperature”. In: *Phys. Rev. E* 70.3, p. 037301.

Francis, R.C. and S.R. Hare (1994). “Decadal-scale regime shifts in the large marine ecosystems of the North-east Pacific: a case for historical science”. In: *Fish. Oceanogr.* 3, pp. 279–291.

Frankignoul, C. and N. Sennéchael (2007). “Observed Influence of North Pacific SST Anomalies on the Atmospheric Circulation”. In: *J. Climate* 20, pp. 592–606.

Fratantoni, D.M., W.E. Johns, T.L. Townsend, and H.E. Hurlburt (2000). “Low-Latitude Circulation and Mass Transport Pathways in a Model of the Tropical Atlantic Ocean”. In: *J. Phys. Oceanogr.* 30, pp. 1944–1966.

Freeman, E., S.D. Woodruff, S.J. Worley, S.J. Lubker, E.C. Kent, W.E. Angel, D.I. Berry, P. Brohan, R. Eastman, L. Gates, W. Gloeden, Z. Ji, J. Lawrimore, N.A. Rayner, G. Rosenhagen, and S.R. Smith (2017). “ICOADS Release 3.0: a major update to the historical marine climate record”. In: *Int. J. Climatol.* 37, pp. 2211–2232.

Fyfe, J.C., G.A. Meehl, M.H. England, M.E. Mann, B.D. Santer, G.M. Flato, E. Hawkins, N.P. Gillett, S.P. Xie, Y. Kosaka, and N.C. Swart (2016). “Making sense of the early-2000s warming slowdown”. In: *Nat. Clim. Change* 6.3, pp. 224–228.

Garreaud, R. and D.S. Battisti (1999). “Interannual (ENSO) and Interdecadal (ENSO-like) Variability in the Southern Hemisphere Tropospheric Circulation”. In: *J. Climate* 12, pp. 2113–2123.

Geisler, J.E., M.L. Blackmon, G.T. Bates, and S. Muñoz (1985). “Sensitivity of January Climate Response to the Magnitude and Position of Equatorial Pacific Sea Surface Temperature Anomalies”. In: *J. Atmos. Sci.* 42, pp. 1037–1049.

Gent, P.R. and J.C. McWilliams (1990). “Isopycnal Mixing in Ocean Circulation Models”. In: *J. Phys. Oceanogr.* 20, pp. 150–155.

Gent, P.R., J. Willebrand, T.J. McDougall, and J.C. McWilliams (1995). “Parameterizing Eddy-Induced Tracer Transports in Ocean Circulation Models”. In: *J. Phys. Oceanogr.* 25, pp. 463–474.

The GFDL Global Atmospheric Model Development Team (2004). “The New GFDL Global Atmosphere and Land Model AM2-LM2: Evaluation with Prescribed SST Simulations”. In: *J. Climate* 17.24, pp. 4641–4673.

Gnanadesikan, A., K.W. Dixon, S.M. Griffies, V. Balaji, M. Barreiro, J.A. Beesley, W.F. Cooke, T.L. Delworth, R. Gerdes, M.J. Harrison, I.M. Held, W.J. Hurlin, H. Lee, Z. Liang, G. Nong, R.C. Pacanowski, A. Rosati, J. Russell, B.L. Samuels, Q. Song, M.J. Spelman, R.J. Stouffer, C.O. Sweeney, G. Vecchi, M. Winton, A.T. Wittenberg, F. Zeng, R. Zhang, and J.P. Dunne (2006). "GFDL's CM2 Global Coupled Climate Models. Part II: The Baseline Ocean Simulation". In: *J. Climate* 19, pp. 675–697.

Godfrey, J.S., G.C. Johnson, M.J. McPhaden, G. Reverdin, and S.E. Wijffels (2001). "The tropical ocean circulation". In: *Ocean Circulation and Climate.* Ed. by G. Siedler, J. Church, and J. Goul. Vol. 77. International Geophysics. Academic Press, pp. 247–257.

Gordon, A.L., R.D. Susanto, and A. Ffield (1999). "Throughflow within Makassar Strait". In: *Geophys. Res. Lett.* 26.11, pp. 3325–3328.

Gordon, A.L. (2005). "Oceanography of the Indonesian seas and their throughflow". In: *Oceanography* 18.4, pp. 14–27.

Graffino, G., R. Farneti, F. Kucharski, and F. Molteni (2018). "The effect of wind stress anomalies and location in driving Pacific Subtropical Cells and tropical climate". In: *J. Climate, accepted.*

Graham, N.E. (1994). "Decadal-scale climate variability in the tropical and North Pacific during the 1970s and 1980s: Observations and model results". In: *Clim. Dyn.* 10.3, pp. 135–162.

Graham, N.E., T.P. Barnett, R. Wilde, M. Ponater, and S. Schubert (1994). "On the Roles of Tropical and Midlatitude SSTs in Forcing Interannual to Interdecadal Variability in the Winter Northern Hemisphere Circulation". In: *J. Climate* 7, pp. 1416–1441.

Griffies, S.M. (1998). "The Gent-McWilliams Skew Flux". In: *J. Phys. Oceanogr.* 28, pp. 831–841.

Griffies, S.M. and R.W. Hallberg (2000). "Biharmonic Friction with a Smagorinsky-Like Viscosity for Use in Large-Scale Eddy-Permitting Ocean Models". In: *Mon. Wea. Rev.* 128, pp. 2935–2946.

Griffies, S.M., M.J. Harrison, R.C. Pacanowski, and A. Rosati (2003). *A technical guide to MOM4.* Tech. rep. Princeton (NJ), USA.

Griffies, S.M. (2004). *Fundamentals of ocean climate models.* Princeton (NJ), USA: Princeton University press. ISBN: 9780691118925.

Griffies, S.M., A. Gnanadesikan, K.W. Dixon, J.P. Dunne, R. Gerdes, M.J. Harrison, A. Rosati, J.L. Russell, B.L. Samuels, M.J. Spelman, M. Winton, and R. Zhang (2005). "Formulation of an ocean model for global climate simulations". In: *Ocean Science* 1, pp. 45–79.

Griffies, S.M., M. Winton, L.J. Donner, L.W. Horowitz, S.M. Downes, R. Farneti, A. Gnanadesikan, W.J. Hurlin, H. Lee, Z. Liang, J.B. Palter, B.L. Samuels, A.T. Wittenberg, B.L. Wyman, J. Yin, and N. Zadeh (2011). "The GFDL CM3 Coupled Climate Model: Characteristics of the Ocean and Sea Ice Simulations". In: *J. Climate* 24, pp. 3520–3544.

Griffies, S.M. (2012). *Elements of the Modular Ocean Model (MOM)*. NOAA Geophysical Fluid Dynamics Laboratory. Princeton (NJ), USA.

Griffies, S.M., A. Biastoch, C. Böning, F. Bryan, G. Danabasoglu, E.P. Chassignet, ..., and W. Hazeleger (2009). "Coordinated Ocean-ice Reference Experiments (COREs)". In: *Ocean Model.* 26.1, pp. 1–46.

Griffies, S.M. (2009). *Elements of MOM4P1*. Tech. rep. Princeton (NJ), USA.

Guilderson, T.P. and D.P. Schrag (1998). "Abrupt shift in subsurface temperatures in the tropical Pacific associated with changes in El Niño". In: *Science* 281.5374, pp. 240–243.

Gu, D. and S.G. Philander (1997). "Interdecadal climate fluctuations that depend on exchanges between the tropics and extratropics". In: *Science* 275.5301, pp. 805–807.

Gutzler, D.S. (1996). "Low-Frequency Ocean-Atmosphere Variability across the Tropical Western Pacific". In: *J. Atmos. Sci.* 53, pp. 2773–2785.

Hall, M.M. and H.L. Bryden (1982). "Direct estimates and mechanisms of ocean heat transport". In: *Deep Sea. Res. Part 1 Oceanogr. Res. Pap.* 29.3, pp. 339–359.

Han, W., G.A. Meehl, and A. Hu (2006). "Interpretation of tropical thermocline cooling in the Indian and Pacific oceans during recent decades". In: *Geophys. Res. Lett.* 33, p. L23615.

Hansen, J., R. Ruedy, M. Sato, and K. Lo (2010). "Global surface temperature change". In: *Rev. Geophys.* 48, RG4004.

Hare, S.R. and N.J. Mantua (2000). "Empirical evidence for North Pacific regime shifts in 1977 and 1989". In: *Prog. Oceanogr.* 47, pp. 103–145.

Harper, S. (2000). "Thermocline ventilation and pathways of tropical-subtropical water mass exchange". In: *Tellus A: Dynamic Meteorology and Oceanography* 52.3, pp. 330–345.

Hasselmann, K. (1976). "Stochastic climate models, Part I Theory". In: *Tellus* 28.6, pp. 473–485.

Hazeleger, W., P. de Vries, and Y. Friocourt (2003). "Sources of the Equatorial Undercurrent in the Atlantic in a high-resolution ocean model". In: *J. Phys. Oceanogr.* 33, pp. 677–693.

Hazeleger, W., C. Severijns, R. Seager, and F. Molteni (2005). "Tropical Pacific–Driven Decadel Energy Transport Variability". In: *J. Climate* 18, pp. 2037–2051.

Hazeleger, W., P. de Vries, and G.J. van Oldenborgh (2001a). "Do Tropical Cells ventilate the Indo-Pacific Equatorial Thermocline?" In: *Geophys. Res. Lett.* 28.9, pp. 1763–1766.

Hazeleger, W., M. Visbeck, M. Cane, A. Karspeck, and N. Naik (2001b). "Decadal upper ocean temperature variability in the tropical Pacific". In: *J. Geophys. Res.* 160.C5, pp. 8971–8988.

Hedemann, C., T. Mauritsen, J. Jungclaus, and J. Marotzke (2017). "The subtle origins of surface-warming hiatuses". In: *Nat. Clim. Change* 7.5, pp. 336–339.

Held, I.M. (2001). "The Partitioning of the Poleward Energy Transport between the Tropical Ocean and Atmosphere". In: *J. Atmos. Sci.* 58, pp. 943–948.

— (2005). "The Gap between Simulation and Understanding in Climate Modeling". In: *Bull. Amer. Meteor. Soc.* 86, pp. 1609–1614.

Hellerman, S. and M. Rosenstein (1983). "Normal Monthly Wind Stress Over the World Ocean with Error Estimates". In: *J. Phys. Oceanogr.* 13, pp. 1093–1104.

Hoerling, M.P. and M. Ting (1994). "Organization of Extratropical Transients during El Niño". In: *J. Climate* 7, pp. 745–766.

Hong, L., L. Zhang, Z. Chen, and L. Wu (2014). "Linkage between the Pacific Decadal Oscillation and the low frequency variability of the Pacific Subtropical Cell". In: *J. Geophys. Res.: Oceans* 119, pp. 3464–3477.

Horel, J.D. and J.M. Wallace (1981). "Planetary-Scale Atmospheric Phenomena Associated with the Southern Oscillation". In: *Mon. Wea. Rev.* 109, pp. 813–829.

Hoskins, B.J., A.J. Simmons, and D.G. Andrews (1977). "Energy dispersion in a barotropic atmosphere". In: *Q.J.R. Meteorol. Soc.* 103, pp. 553–567.

Hoskins, B.J. and D.J. Karoly (1981). "The Steady Linear Response of a Spherical Atmosphere to Thermal and Orographic Forcing". In: *J. Atmos. Sci.* 38, pp. 1179–1196.

Huang, R.X. and Z. Liu (1999). "Pacific subtropical-tropical thermocline water exchange in the National Centers for Environmental Prediction ocean model". In: *J. Geophys. Res.* 104.C5, pp. 11065–11076.

Huang, R.X. and B. Qiu (1994). "Three-Dimensional Structure of the Wind-Driven Circulation in the Subtropical North Pacific". In: *J. Phys. Oceanogr.* 24, pp. 1608–1622.

— (1998). "The Structure of the Wind-Driven Circulation in the Subtropical South Pacific Ocean". In: *J. Phys. Oceanogr.* 28, pp. 1173–1186.

Huang, R.X. and S. Russell (1994). "Ventilation of the Subtropical North Pacific". In: *J. Phys. Oceanogr.* 24, pp. 2589–2605.

Huang, R.X. and Q. Wang (2001). "Interior Communication from the Subtropical to the Tropical Oceans". In: *J. Phys. Oceanogr.* 31, pp. 3538–3550.

Hurrell, J.W. (1995). "Decadal trends in the North Atlantic Oscillation: regional temperatures and precipitation". In: *Science* 269.5224, pp. 676–679.

Hüttl, S. and C. W. Böning (2006). "Mechanisms of decadal variability in the shallow subtropical-tropical circulation of the Atlantic Ocean: A model study". In: *J. Geophys. Res.* 111, p. C07011.

Ingram, W. J., C.A. Wilson, and J.F.B. Mitchell (1989). "Modeling climate change: An assessment of sea ice and surface albedo feedbacks". In: *J. Geophys. Res.* 94.D6, pp. 8609–8622.

Inui, T., A. Lazar, P. Malanotte-Rizzoli, and A. Busalacchi (2002). "Wind stress effects on subsurface pathways from the subtropical to tropical Atlantic". In: *J. Phys. Oceanogr.* 32, pp. 2257–2276.

IOC, SCOR, and IAPSO (2010). *The international thermodynamic equation of seawater - 2010: Calculation and use of thermodynamic properties*. Intergovernmental Oceanographic Commission, UNESCO. Princeton (NJ), USA.

Iwasaka, N. and M.J. Wallace (1995). "Large scale air sea interaction in the Northern Hemisphere from a view point of variations of surface heat flux by SVD analysis". In: *J. Meteor. Soc. Japan* 73.4, pp. 781–794.

Jayne, S.R. and J. Marotzke (2001). "The dynamics of ocean heat transport variability". In: *Rev. Geophys.* 39.3, pp. 385–411.

Jenkins, W.J. (1987). "3H and 3He in the Beta Triangle: Observations of Gyre Ventilation and Oxygen Utilization Rates". In: *J. Phys. Oceanogr.* 17, pp. 763–783.

— (1988). "The use of anthropogenic tritium and helium-3 to study subtropical gyre ventilation and circulation". In: *Phil. Trans. R. Soc. Lond.* 325.1583, pp. 43–61.

Jin, F.F., J.D. Neelin, and M. Ghil (1994). "El Niño on the devil's staircase: Annual subharmonic steps to chaos". In: *Science* 264.5155, pp. 70–72.

Jochum, M. and P. Malanotte-Rizzoli (2001). "Influence of the Meridional Overturning Circulation on Tropical-Subtropical Pathways". In: *J. Phys. Oceanogr.* 31, pp. 1313–1323.

Johnson, E.S. and D.S. Luther (1994). "Mean zonal momentum balance in the upper and central equatorial Pacific Ocean". In: *J. Geophys. Res.* 99.C4, pp. 7689–7705.

Johnson, G.C. and M.J. McPhaden (1999). "Interior pycnocline flow from the subtropical to the equatorial Pacific Ocean". In: *J. Phys. Oceanogr.* 29.12, pp. 3073–3089.

Johnson, G.C. (2001). "The Pacific Ocean Subtropical Cell surface limb". In: *Geophys. Res. Lett.* 28.9, pp. 1771–1774.

Johnson, G.C., B.M. Sloyan, W.S. Kessler, and K.E. McTaggart (2002). "Direct measurements of upper ocean currents and water properties across the tropical Pacific during the 1990s". In: *Prog. Oceanogr.* 52.1, pp. 31–61.

Karstensen, J. and D. Quadfasel (2002). "Formation of Southern Hemisphere thermocline waters: Water mass conversion and subduction". In: *J. Phys. Oceanogr.* 32, pp. 3020–3038.

Keith, D.W. (1995). "Meridional energy transport: uncertainty in zonal means". In: *Tellus A* 47, pp. 30–44.

Kessler, W.S., L.M. Rothstein, and D. Chen (1998). "The Annual Cycle of SST in the Eastern Tropical Pacific, Diagnosed in an Ocean GCM". In: *J. Climate* 11, pp. 777–799.

Kidston, J., A.A. Scaife, S.C. Hardiman, D.M. Mitchell, N. Butchart, M.P. Baldwin, and L.J. Gray (2015). "Stratospheric influence on tropospheric jet streams, storm tracks and surface weather". In: *Nat. Geosci.* 8.6, pp. 433–440.

Kirtman, B.P. and P.S. Schopf (1998). "Decadal Variability in ENSO Predictability and Prediction". In: *J. Climate* 11, pp. 2804–2822.

Kleeman, R. and S.B. Power (1994). "Limits to predictability in a coupled ocean-atmosphere model due to atmospheric noise". In: *Tellus A* 46, pp. 529–540.

Kleeman, R. and S. Power (2000). "Modulation of ENSO Variability on Decadal and Longer Timescales". In: *El Niño and the Southern Oscillation: Multiscale Variability and Global and Regional Impacts.* Ed. by H. Diaz and V. Markgraf. Washington D.C., USA: Cambridge University Press, pp. 411–440.

Kleeman, R., J.P. McCreary, and B.A. Klinger (1999). “A mechanism for generating ENSO decadal variability”. In: *Geophys. Res. Lett.* 26.12, pp. 1743–1746.

Klein, S.A., B.J. Soden, and N. Lau (1999). “Remote Sea Surface Temperature Variations during ENSO: Evidence for a Tropical Atmospheric Bridge”. In: *J. Climate* 12, pp. 917–932.

Klinger, B.A. and J. Marotzke (2000). “Meridional heat transport by the Subtropical Cell”. In: *J. Phys. Oceanogr.* 30.4, pp. 696–705.

Klinger, B.A., J.P. McCreary, and R. Kleeman (2002). “The Relationship between Oscillating Subtropical Wind Stress and Equatorial Temperature”. In: *J. Phys. Oceanogr.* 32, pp. 1507–1521.

Knutson, T.R. and S. Manabe (1998). “Model assessment of decadal variability and trends in the tropical Pacific Ocean”. In: *J. Climate* 11, pp. 2273–2296.

Knutti, R. and J. Sedláček (2013). “Robustness and uncertainties in the new CMIP5 climate model projections”. In: *Nat. Clim. Change* 3.4, pp. 369–373.

Kociuba, G. and S.B. Power (2015). “Inability of CMIP5 Models to Simulate Recent Strengthening of the Walker Circulation: Implications for Projections”. In: *J. Climate* 28, pp. 20–35.

Kok, C.J. and J.D. Opsteegh (1985). “Possible Causes of Anomalies in Seasonal Mean Circulation Patterns during the 1982–83 El Niño Event”. In: *J. Atmos. Sci.* 42, pp. 677–694.

Kosaka, Y. and S.P. Xie (2013). “Recent global-warming hiatus tied to equatorial Pacific surface cooling”. In: *Nature* 501, pp. 403–407.

— (2016). “The tropical Pacific as a key pacemaker of the variable rates of global warming”. In: *Nat. Geosci.* 9.9, pp. 669–673.

Kraus, E.B. and S. Levitus (1986). “Annual Heat Flux Variations across the Tropic Circles”. In: *J. Phys. Oceanogr.* 16, pp. 1479–1486.

Krishnan, R. and M. Sugi (2003). “Pacific decadal oscillation and variability of the Indian summer monsoon rainfall”. In: *Clim. Dyn.* 21, pp. 233–242.

Kröger, J., A.J. Busalacchi, J. Ballabrera-Poy, and P. Malanotte-Rizzoli (2005). “Decadal variability of shallow cells and equatorial sea surface temperature in a numerical model of the Atlantic”. In: *J. Geophys. Res.* 110, p. C12003.

Kucharski, F., F. Ikram, F. Molteni, R. Farneti, I.S. Kang, H.H. No, M.P. King, G. Giuliani, and K. Mogensen (2016). “Atlantic forcing of Pacific decadal variability”. In: *Clim. Dyn.* 46, pp. 2337–2351.

Kuhlbrodt, T., A. Griesel, M. Montoya, A. Levermann, M. Hofmann, and S. Rahmstorf (2007). “On the driving processes of the Atlantic meridional overturning circulation”. In: *Rev. Geophys.* 45, RG2001.

Kushnir, Y., W.A. Robinson, I. Bladé, N.M. Hall, S. Peng, and R. Sutton (2002). “Atmospheric GCM Response to Extratropical SST Anomalies: Synthesis and Evaluation”. In: *J. Climate* 15, pp. 2233–2256.

Lanzante, J.R. (1984). “A Rotated Eigenanalysis of the Correlation between 700 mb Heights and Sea Surface Temperatures in the Pacific and Atlantic”. In: *Mon. Wea. Rev.* 112, pp. 2270–2280.

Large, W.G., J.C. McWilliams, and S.C. Doney (1994). “Oceanic vertical mixing: A review and a model with a nonlocal boundary layer parameterization”. In: *Rev. Geophys.* 33.2, pp. 341–364.

Large, W.G. and S. Yeager (2004). *Diurnal to decadal global forcing for ocean and sea-ice models: The data sets and flux climatologies*. Tech. rep. Boulder (CO), USA.

Large, W.B. (2006). “Surface Fluxes for Practitioners of Global Ocean Data Assimilation”. In: *Ocean Weather Forecasting*. Ed. by E.P. Chassignet and J. Verron. Dordrecht: Springer Netherlands, pp. 229–270.

Large, W.G. and S.G. Yeager (2009). “The global climatology of an interannually varying air-sea flux data set”. In: *Clim. Dyn.* 33.2, pp. 341–364.

Latif, M., R. Kleeman, and C. Eckert (1998). “Greenhouse Warming, Decadal Variability, or El Niño? An Attempt to Understand the Anomalous 1990s”. In: *J. Climate* 11, pp. 602–624.

Latif, M. (2006). “On North Pacific Multidecadal Climate Variability”. In: *J. Climate* 19, pp. 2906–2915.

Latif, M. and T.P. Barnett (1994). “Causes of decadal climate variability over the North Pacific and North America”. In: *Science* 266.5185, pp. 634–637.

— (1996). “Decadal Climate Variability over the North Pacific and North America: Dynamics and Predictability”. In: *J. Climate* 9, pp. 2407–2423.

Lau, K. and T.J. Phillips (1986). “Coherent Fluctuations of Fxtratropical Geopotential Height and Tropical Convection in Intraseasonal Time Scales”. In: *J. Atmos. Sci.* 43, pp. 1164–1181.

Lau, K. and M.J. Nath (1994). “A Modeling Study of the Relative Roles of Tropical and Extratropical SST Anomalies in the Variability of the Global Atmosphere-Ocean System”. In: *J. Climate* 7, pp. 1184–1207.

— (1996). “The Role of the “Atmospheric Bridge” in Linking Tropical Pacific ENSO Events to Extratropical SST Anomalies”. In: *J. Climate* 9, pp. 2036–2057.

Lau, K. (1997). “Interactions between Global SST Anomalies and the Midlatitude Atmospheric Circulation”. In: *Bull. Amer. Meteor. Soc.* 78, pp. 21–34.

Lazar, A., R. Murtugudde, and A.J. Busalacchi (2001). “A model study of temperature anomaly propagation from the Subtropics to Tropics within the South Atlantic Thermocline”. In: *Geophys. Res. Lett.* 28, pp. 1271–1274.

Lazar, A., T. Inui, P. Malanotte-Rizzoli, A.J. Busalacchi, L. Wang, and R. Murtugudde (2002). “Seasonality of the ventilation of the tropical Atlantic thermocline in an ocean general circulaton model”. In: *J. Geophys. Res.* 107.C8, pp. 21–34.

Lee, T. and J. Marotzke (1997). “Inferring meridional mass and heat transports of the Indian Ocean by fitting a general circulation model to climatological data”. In: *J. Geophys. Res.* 102.C5, pp. 10585–10602.

Lee, T. and I. Fukumori (2003). “Interannual-to-Decadal Variations of Tropical-Subtropical Exchange in the Pacific Ocean: Boundary versus Interior Pycnocline Transports”. In: *J. Climate* 16, pp. 4022–4042.

Lee, T. (2004). “Decadal weakening of the shallow overturning circulation in the South Indian Ocean”. In: *Geophys. Res. Lett.* 31, p. L18305.

Lee, T. and M.J. McPhaden (2008). “Decadal phase change in large-scale sea level and winds in the Indo-Pacific region at the end of the 20th century”. In: *Geophys. Res. Lett.* 35, p. L01605.

Lee, S.K., W. Park, M.O. Baringer, A.L. Gordon, B. Huber, and Y. Liu (2015). “Pacific origin of the abrupt increase in Indian Ocean heat content during the warming hiatus”. In: *Nat. Geosci.* 8.6.

Lee, T. and J. Marotzke (1998). “Seasonal Cycles of Meridional Overturning and Heat Transport of the Indian Ocean”. In: *J. Phys. Oceanogr.* 28, pp. 923–943.

Lee, H.C., A. Rosati, and M.J. Spelman (2006). “Barotropic tidal mixing effects in a coupled climate model: Oceanic conditions in the northern Atlantic”. In: *Ocean Model.* 11, pp. 464–477.

Lenz, E. (1848). “Bemerkungen über die Temperatur des Weltmeers in verschiedenen Tiefen”. In: *Ann. Phys.* 149, pp. 615–626.

Levitus, S. (1987). “Meridional Ekman Heat Fluxes for the World Ocean and Individual Ocean Basins”. In: *J. Phys. Oceanogr.* 17, pp. 1484–1492.

Lewandowsky, S., J.S. Risbey, and N. Oreskes (2016). “The “Pause” in Global Warming: Turning a Routine Fluctuation into a Problem for Science”. In: *Bull. Amer. Meteor. Soc.* 97, pp. 723–733.

L'Heureux, M.L., S. Lee, and B. Lyon (2013). "Recent multidecadal strengthening of the Walker circulation across the tropical Pacific". In: *Nat. Clim. Change* 3.6, pp. 571–576.

Lindstrom, E., R. Lukas, R. Fine, E. Firing, S. Godfrey, G. Meyers, and M. Tsuchiya (1987). "The western equatorial Pacific Ocean circulation study". In: *Nature* 330.6148, pp. 533–537.

Liu, Z. (1994). "A simple model of the mass exchange between the subtropical and tropical ocean". In: *J. Phys. Oceanogr.* 24.6, pp. 1153–1165.

Liu, Z. and S.G. Philander (1995). "How Different Wind Stress Patterns Affect the Tropical-Subtropical Circulations of the Upper Ocean". In: *J. Phys. Oceanogr.* 25, pp. 449–462.

Liu, Z. (2003). "Tropical Ocean Decadal Variability and Resonance of Planetary Wave Basin Modes. Part I: Theory". In: *J. Climate* 16, pp. 1539–1550.

Liu, Z. and M.A. Alexander (2007). "Atmospheric bridge, oceanic tunnel and global climatic teleconnections". In: *Rev. Geophys.* 45, RG2005.

Liu, Z., S.G. Philander, and R.C. Pacanowski (1994). "A GCM Study of Tropical–Subtropical Upper-Ocean Water Exchange". In: *J. Phys. Oceanogr.* 24, pp. 2606–2623.

Liu, Z. and S.G.H. Philander (2001). "Tropical-extratropical oceanic exchange pathways". In: *Ocean Circulation and Climate*. Ed. by G. Siedler, J. Church, and J. Goul. Vol. 77. International Geophysics. Academic Press, pp. 247–257.

Liu, Z., L. Wu, and E. Bayler (1999). "Rossby Wave-Coastal Kelvin Wave Interaction in the Extratropics. Part I: Low-Frequency Adjustment in a Closed Basin". In: *J. Phys. Oceanogr.* 29, pp. 2382–2404.

Liu, Z., L. Wu, R. Gallimore, and R. Jacob (2002). "Search for the origins of Pacific decadal climate variability". In: *Geophys. Res. Lett.* 29.10.

Liu, Z. and S. Xie (1994). "Equatorward Propagation of Coupled Air–Sea Disturbances with Application to the Annual Cycle of the Eastern Tropical Pacific". In: *J. Atmos. Sci.* 51, pp. 3807–3822.

Liu, Z. and H. Yang (2003). "Extratropical control of tropical climate, the atmospheric bridge and oceanic tunnel". In: *Geophys. Res. Lett.* 30.5.

Lohmann, K. and M. Latif (2005). "Tropical Pacific Decadal Variability and the Subtropical-Tropical Cells". In: *J. Climate* 18, pp. 5163–5178.

Lu, P. and J.P. McCreary (1995). "Influence of the ITCZ on the Flow of Thermocline Water from the Subtropical to the Equatorial Pacific Ocean". In: *J. Phys. Oceanogr.* 25, pp. 3076–3088.

Lu, P., J.P. McCreary, and B.A. Klinger (1998). "Meridional circulation cells and the source waters of the Pacific Equatorial Undercurrent". In: *J. Phys. Oceanogr.* 28.1, pp. 62–84.

Lübbecke, J.F., C.W. Böning, and A. Biastoch (2008). "Variability in the subtropical-tropical cells and its effect on near-surface temperature of the equatorial Pacific: a model study". In: *Ocean Sci.* Pp. 73–88.

Lukas, R. and E. Firing (1984). "The geostrophic balance of the Pacific Equatorial Undercurrent". In: *Deep Sea Res. A* 31.1, pp. 61–66.

Lukas, R., E. Firing, P. Hacker, P.L. Richardson, C.A. Collins, R. Fine, and R. Gammon (1991). "Observations of the Mindanao Current during the western equatorial Pacific Ocean circulation study". In: *J. Geophys. Res.* 96.C4, pp. 7089–7104.

Luo, Y., L.M. Rothstein, and R.H. Zhang (2009). "Response of Pacific subtropical-tropical thermocline water pathways and transports to global warming". In: *Geophys. Res. Lett.* 36, p. L04601.

Luther, D.S. and E.S. Johnson (1990). "Eddy Energetics in the Upper Equatorial Pacific during the Hawaii-to-Tahiti Shuttle Experiment". In: *J. Phys. Oceanogr.* 20, pp. 913–944.

Luyten, J.R., J. Pedlosky, and H. Stommel (1983). "The ventilated thermocline". In: *J. Phys. Oceanogr.* 13, pp. 292–309.

Lyman, J.M., S.A. Good, V.V. Gouretski, M. Ishii, G.C. Johnson, M.D. Palmer, D.M. Smith, and J.K. Willis (2010). "Robust warming of the global upper ocean". In: *Nature* 465.7296, pp. 334–337.

Lysne, J., P. Chang, and B. Giese (1997). "Impact of the extratropical Pacific on equatorial variability". In: *Geophys. Res. Lett.* 24.21, pp. 2589–2592.

Ma, X., Z. Jing, P. Chang, X. Liu, R. Montuoro, R.J. Small, F.O. Bryan, R.J. Greatbatch, P. Brandt, D. Wu, X. Lin, and L. Wu (2016). "Western boundary currents regulated by interaction between ocean eddies and the atmosphere". In: *Nature* 535.7613, pp. 533–537.

Maher, N., M.H. England, A.S. Gupta, and P. Spence (2018). "Role of Pacific trade winds in driving ocean temperatures during the recent slowdown and projections under a wind trend reversal". In: *Clim. Dyn.* 51, pp. 321–336.

Malanotte-Rizzoli, P., K. Hedstrom, H. Arango, and D.B. Haidvogel (2000). "Water mass pathways between the subtropical and tropical ocean in a climatological simulation of the North Atlantic Ocean circulation". In: *Dynam. Atmos. Oceans* 32.3, pp. 331–371.

Manabe, S. and K. Bryan (1969). "Climate calculations with a combined ocean-atmosphere model". In: *J. Atmos. Sci.* 29.4, pp. 786–789.

Manabe, S., K. Bryan, and M.J. Spelman (1975). “A Global Ocean-Atmosphere Climate Model. Part I. The Atmospheric Circulation”. In: *J. Phys. Oceanogr.* 5.5, pp. 3–29.

Manabe, S. and R.J. Stouffer (1980). “Sensitivity of a global climate model to an increase of CO2 concentration in the atmosphere”. In: *J. Geophys. Res.* 85.C10, pp. 5529–5554.

Mantua, N.J., S.R. Hare, Y. Zhang, J.M. Wallace, and R.C. Francis (1997). “A Pacific Interdecadal Climate Oscillation with Impacts on Salmon Production”. In: *Bull. Amer. Meteor. Soc.* 78, pp. 1069–1079.

Marshall, J. and D.W. So (1990). “Thermal Equilibration of Planetary Waves”. In: *J. Atmos. Sci.* 47, pp. 963–978.

Marshall, J. and F. Schott (1999). “Open-ocean convection: Observations, theory, and models”. In: *Rev. Geophys.* 37, pp. 1–64.

McCreary, J.P. (1981). “A linear stratified ocean model of the equatorial undercurrent”. In: *Phil. Trans. R. Soc. Lond. A* 298.1444, pp. 603–635.

McCreary, J.P. and Z. Yu (1992). “Equatorial dynamics in a 2-1/2-layer model”. In: *Prog. Oceanogr.* 29.1, pp. 61–132.

McCreary, J.P., P.K. Kundu, and R.L. Molinari (1993). “A numerical investigation of dynamics, thermodynamics and mixed-layer processes in the Indian Ocean”. In: *Prog. Oceanogr.* 31.3, pp. 181–244.

McCreary, J.P. and P. Lu (1994). “Interaction between the subtropical and equatorial ocean circulations: The Subtropical Cell”. In: *J. Phys. Oceanogr.* 24.2, pp. 466–497.

McGowan, J.A., D.R. Cayan, and L.M. Dorman (1998). “Climate-ocean variability and ecosystem response in the Northeast Pacific”. In: *Science* 281.5374, pp. 210–217.

McGregor, S., N.J. Holbrook, and S.B. Power (2007). “Interdecadal Sea Surface Temperature Variability in the Equatorial Pacific Ocean. Part I: The Role of Off-Equatorial Wind Stresses and Oceanic Rossby Waves”. In: *J. Climate* 20, pp. 2643–2658.

— (2008). “Interdecadal Sea Surface Temperature Variability in the Equatorial Pacific Ocean. Part II: The Role of Equatorial/Off-Equatorial Wind Stresses in a Hybrid Coupled Model”. In: *J. Climate* 21, pp. 4242–4256.

McPhaden, M.J. and R.A. Fine (1981). “Continuously Stratified Models of the Steady-State Equatorial Ocean”. In: *J. Phys. Oceanogr.* 11, pp. 337–354.

— (1988). “A Dynamical Interpretation of the Tritium Maximum in the Central Equatorial Pacific”. In: *J. Phys. Oceanogr.* 18, pp. 1454–1457.

McPhaden, M.J. and D. Zhang (2002). “Slowdown of the meridional overturning circulation in the upper Pacific Ocean”. In: *Nature* 415.6872, pp. 603–608.

— (2004). “Pacific Ocean circulation rebounds”. In: *Geophys. Res. Lett.* 31.

Medhaug, I., M.B. Stolpe, E.M. Fischer, and R. Knutti (2017). “Reconciling controversies about the ‘global warming hiatus’”. In: *Nature* 545.7652, pp. 41–47.

Meehl, G.A. and H. Van Loon (1979). “The Seesaw in Winter Temperatures between Greenland and Northern Europe. Part III: Teleconnections with Lower Latitudes”. In: *Mon. Wea. Rev.* 107, pp. 1095–1106.

Meehl, G.A. and J.M. Arblaster (1998). “The Asian-Australian Monsoon and El Niño-Southern Oscillation in the NCAR Climate System Model”. In: *J. Climate* 11, pp. 1356–1385.

Meehl, G.A., G.J. Boer, C. Covey, M. Latif, and R.J. Stouffer (2000). “The coupled model intercomparison project (CMIP)”. In: *Bull. Amer. Meteor. Soc.* 81.2, pp. 313–318.

Meehl, G.A., C. Covey, B. McAvaney, M. Latif, and R. Stouffer (2005a). “Overview of the Coupled Model Intercomparison Project”. In: *Bull. Amer. Meteor. Soc.* 86, pp. 89–93.

Meehl, G.A. and A. Hu (2006). “Megadroughts in the Indian Monsoon Region and Southwest North America and a Mechanism for Associated Multidecadal Pacific Sea Surface Temperature Anomalies”. In: *J. Climate* 19, pp. 1605–1623.

Meehl, G.A., C. Covey, T. Delworth, M. Latif, B. McAvaney, J.F. Mitchell, R.J. Stouffer, and K.E. Taylor (2007). “The WCRP CMIP3 Multimodel Dataset: A New Era in Climate Change Research”. In: *Bull. Amer. Meteor. Soc.* 88, pp. 1383–1394.

Meehl, G.A., J.M. Arblaster, J.T. Fasullo, A. Hu, and K.E. Trenberth (2011). “Model-based evidence of deep-ocean heat uptake during surface-temperature hiatus periods”. In: *Nat. Clim. Change* 1.7, pp. 360–364.

Meehl, G.A., A. Hu J.M. Arblaster, J. Fasullo, and K.E. Trenberth (2013). “Externally forced and internally generated decadal climate variability associated with the Interdecadal Pacific Oscillation”. In: *J. Climate* 26.18, pp. 7298–7310.

Meehl, G.A. and H. Teng (2014). “CMIP5 multi-model hindcasts for the mid-1970s shift and early 2000s hiatus and predictions for 2016–2035”. In: *Geophys. Res. Lett.* 41, pp. 1711–1716.

Meehl, G.A., A. Hu, B.D. Santer, and S.P. Xie (2016). “Contribution of the Interdecadal Pacific Oscillation to twentieth-century global surface temperature trends”. In: *Nat. Clim. Change* 6.11, pp. 1005–1008.

— (2005b). “Variability of Upper Pacific Ocean Overturning in a Coupled Climate Model”. In: *J. Climate* 18, pp. 666–683.

Meyers, G. (1996). “Variation of Indonesian Throughflow and the El Niño Southern Oscillation”. In: *J. Geophys. Res.: Oceans* 101.C5, pp. 12255–12263.

Mikolajewicz, U. and E. Maier-Reimer (1990). “Internal secular variability in an ocean general circulation model”. In: *Clim. Dyn.* 4, pp. 145–156.

Miller, A.J., D.R. Cayan, T.P. Barnett, N.E. Graham, and J.M. Oberhuber (1994). “Interdecadal variability of the Pacific Ocean: Model response to observed heat flux and wind stress anomalies”. In: *Clim. Dyn.* 9.6, pp. 287–302.

Minobe, S. (1997). “A 50–70 year climatic oscillation over the North Pacific and North America”. In: *Geophys. Res. Lett.* 24.6, pp. 683–686.

— (1999). “Resonance in bidecadal and pentadecadal climate oscillations over the North Pacific: Role in climatic regime shifts”. In: *Geophys. Res. Lett.* 26.7, pp. 855–858.

— (2000). “Spatio-temporal structure of the pentadecadal variability over the North Pacific”. In: *Prog. Oceanogr.* 47, pp. 381–408.

— (2002). “Interannual to interdecadal changes in the Bering Sea and concurrent 1998/99 changes over the North Pacific”. In: *Prog. Oceanogr.* 55, pp. 45–64.

Mitchell, H.L. and J. Derome (1983). “Blocking-Like Solutions of the Potential Vorticity Equation: Their Stability at Equilibrium and Growth at Resonance”. In: *J. Atmos. Sci.* 40, pp. 2522–2536.

Mitchell, T.P. and J.M. Wallace (1992). “The Annual Cycle in Equatorial Convection and Sea Surface Temperature”. In: *J. Climate* 5, pp. 1140–1156.

Miyama, T., J.P. McCreary, T.G. Jensen, J. Loschnigg, S. Godfrey, and A. Ishida (2003). “Structure and dynamics of the Indian-Ocean cross-equatorial cell”. In: *Deep Sea Res. Part 2: Top. Stud. Oceanogr.* 50.12, pp. 2023–2047.

Molinari, R.L., S. Bauer, D. Snowden, G.C. Johnson, B. Bourles, Y. Gouriou, and H. Mercier (1985). “A comparison of kinematic evidence for tropical cells in the Atlantic and Pacific oceans”. In: *Interhemispheric Water Exchange in the Atlantic Ocean*. Ed. by G.J. Goni and P. Malanotte-Rizzoli. Vol. 68. Elsevier Oceanography Series. Amsterdam, Netherlands: Elsevier, pp. 269–286.

Molteni, F., S. Tibaldi, and T.N. Palmer (1990). "Regimes in the wintertime circulation over northern extratropics. I: Observational evidence". In: *Q.J.R. Meteorol. Soc.* 116, pp. 31–67.

Molteni, F., L. Ferranti, T.N. Palmer, and P. Viterbo (1993). "A Dynamical Interpretation of the Global Response to Equatorial Pacific SST Anomalies". In: *J. Climate* 6, pp. 777–795.

Molteni, F., R. Farneti, F. Kucharski, and T.N. Stockdale (2017). "Modulation of air-sea fluxes by extratropical planetary waves and its impact during the recent surface warming slowdown". In: *Geophys. Res. Lett.* 44, pp. 1494–1502.

Molteni, F., M.P. King, F. Kucharski, and D.M. Straus (2011a). "Planetary-scale variability in the northern winter and the impact of land-sea thermal contrast". In: *Clim. Dyn.* 37.1, pp. 151–170.

Molteni, F., T. Stockdale, M. Balmaseda, G. Balsamo, R. Buizza, L. Ferranti, ..., and F. Vitart (2011b). *The new ECMWF seasonal forecast system (System 4).* European Centre for Medium-Range Weather Forecasts.

Munk, W.H. (1981). "Internal waves and small-scale processes". In: *Evolution of Physical Oceanography.* Ed. by B.A. Warren and C. Wunsch. Cambridge, Mass.: MIT Press, pp. 264–291.

Murray, R.J. (1996). "Explicit generation of orthogonal grids for ocean models". In: *J. Comput. Phys.* 126, pp. 251–273.

Nakamura, H., G. Lin, and T. Yamagata (1997). "Decadal Climate Variability in the North Pacific during the Recent Decades". In: *Bull. Amer. Meteor. Soc.* 78, pp. 2215–2226.

Nakamura, H. and T. Yamagata (1999). "Recent Decadal SST Variability in the Northwestern Pacific and Associated Atmospheric Anomalies". In: *Beyond El Niño.* Ed. by A. Navarra. Berlin, Heidelberg: Springer.

Nakano, H., R. Furue, and N. Suginohara (1999). "Effect of seasonal forcing on global circulation in a World Ocean general circulation model". In: *Clim. Dyn.* 15.7, pp. 491–502.

Namias, J. (1959). "Recent seasonal interactions between north Pacific waters and the overlying atmospheric circulation". In: *J. Geophys. Res.* 64.4, pp. 631–646.

— (1969). "Seasonal interactions between the North Pacific Ocean and the atmosphere during the 1960s". In: *Mon. Wea. Rev.* 97, pp. 173–192.

Neelin, J.D. (1991). "The Slow Sea Surface Temperature Mode and the Fast-Wave Limit: Analytic Theory for Tropical Interannual Oscillations and Experiments in a Hybrid Coupled Model". In: *J. Atmos. Sci.* 48, pp. 584–606.

Neelin, J.D. and H.A. Dijkstra (1995). “Ocean-Atmosphere Interaction and the Tropical Climatology. Part I: The Dangers of Flux Correction”. In: *J. Climate* 8, pp. 1325–1342.

Newman, M., G.P. Compo, and M.A. Alexander (2003). “ENSO-Forced Variability of the Pacific Decadal Oscillation”. In: *J. Climate* 16, pp. 3853–3857.

Newman, M. (2007). “Interannual to Decadal Predictability of Tropical and North Pacific Sea Surface Temperatures”. In: *J. Climate* 20, pp. 2333–2356.

Newman, M., M.A. Alexander, T.R. Ault, K.M. Cobb, C. Deser, E. Di Lorenzo, N.J. Mantua, A.J. Miller, S. Minobe, H. Nakamura, N. Schneider, D.J. Vimont, A.S. Phillips, J.D. Scott, and C.A. Smith (2016). “The Pacific Decadal Oscillation, Revisited”. In: *J. Climate* 29, pp. 4399–4427.

Nitta, T. and S. Yamada (1989). “Recent warming of tropical sea surface temperature and its relationship to the Northern Hemisphere circulation”. In: *J. Meteor. Soc. Japan* 67.3, pp. 375–383.

Nonaka, M., S.P. Xie, and J.P. McCreary (2002). “Decadal variations in the Subtropical Cells and equatorial Pacific SST”. In: *Geophys. Res. Lett.* 29.7, pp. 201–204.

Nonaka, M., J.P. McCreary, and S.P. Xie (2006). “Influence of Midlatitude Winds on the Stratification of the Equatorial Thermocline”. In: *J. Phys. Oceanogr.* 36, pp. 222–237.

Oort, A.H., L.A. Anderson, and J.P. Peixoto (1994). “Estimates of the energy cycle of the oceans”. In: *J. Geophys. Res.* 99.C4, pp. 7665–7688.

Pacanowski, R.C. and A. Gnanadesikan (1998). “Transient Response in a Z-Level Ocean Model That Resolves Topography with Partial Cells”. In: *Mon. Wea. Rev.* 126, pp. 3248–3270.

Palmer, T.N. and S. Zhaobo (1985). “A modelling and observational study of the relationship between sea surface temperature in the North-West Atlantic and the atmospheric general circulation”. In: *Q.J.R. Meteorol. Soc.* 111, pp. 947–975.

Park, W., N. Keenlyside, M. Latif, A. Ströh, R. Redler, E. Roeckner, and G. Madec (2009). “Tropical Pacific Climate and Its Response to Global Warming in the Kiel Climate Model”. In: *J. Climate* 22, pp. 71–92.

Patzert, W.C. and G.J. McNally (1981). “Surface current variability in the tropical Pacific during 1979 and 1980 using drifting buoys”. In: *Recent progress in equatorial oceanography.* Ed. by J.P. McCreary, D.W. Moore, and J.M. Witte. Nova University. N.Y.I.T. Press, pp. 151–156.

Pedlosky, J. (1987). "An Inertial Theory of the Equatorial Undercurrent". In: *J. Phys. Oceanogr.* 17, pp. 1978–1985.

— (1988). "Entrainment and the Termination of the Equatorial Undercurrent". In: *J. Phys. Oceanogr.* 18, pp. 880–886.

Pedlosky, J. and P. Robbins (1991). "The Role of Finite Mixed-Layer Thickness in the Structure of the Ventilated Thermocline". In: *J. Phys. Oceanogr.* 21, pp. 1018–1031.

Peixoto, J.P. and A.H. Oort (1992). *Physics of climate.* New York, NY (USA): American Institute of Physics.

Peterson, W.T. and F.B. Schwing (2003). "A new climate regime in Northeast Pacific ecosystems". In: *Geophys. Res. Lett.* 30, pp. 1896–1899.

Philander, S.G.H. and R.C. Pacanowski (1986). "A model of the seasonal cycle in the tropical Atlantic Ocean". In: *J. Geophys. Res.* 91.C12, pp. 14192–14205.

Pierce, D.W., T.P. Barnett, and M. Latif (2000). "Connections between the Pacific Ocean tropics and midlatitudes on decadal timescales". In: *J. Climate* 13.6, pp. 1173–1194.

Pierce, D.W. (2001). "Distinguishing coupled ocean-atmosphere interactions from background noise in the North Pacific". In: *Prog. Oceanogr.* 49, pp. 331–352.

Power, S., T. Casey, C. Folland, A. Colman, and V. Mehta (1999a). "Interdecadal modulation of the impact of ENSO on Australia". In: *Clim. Dyn.* 15.5, pp. 319–324.

Power, S. and R. Colman (2006). "Multi-year predictability in a coupled general circulation model". In: *Clim. Dyn.* 26, pp. 247–272.

Power, S., M. Haylock, R. Colman, and X. Wang (2006). "The Predictability of Interdecadal Changes in ENSO Activity and ENSO Teleconnections". In: *J. Climate* 19, pp. 4755–4771.

Power, S., F. Tseitkin, M. Dix, R. Kleeman, R. Colman, and D. Holland (1995). "Stochastic variability at the air-sea interface on decadal timescales". In: *Geophys. Res. Lett.* 22.19, pp. 2593–2596.

Power, S., F. Tseitkin, V. Mehta, B. Lavery, S. Torok, and N. Holbrook (1999b). "Decadal climate variability in Australia during the twentieth century". In: *Int. J. Climatol.* 19, pp. 169–184.

Qasmi, S., C. Cassou, and J. Boé (2017). "Teleconnection between Atlantic Multidecadal Variability and European temperature: Diversity and evaluation of the Coupled Model Intercomparison Project phase 5 models". In: *Geophys. Res. Lett.* 44, pp. 11140–11149.

Qiu, B. and R.X. Huang (1995). “Ventilation of the North Atlantic and North Pacific: subduction versus obduction”. In: *J. Phys. Oceanogr.* 25, pp. 2374–2390.

Quay, P.D., M. Stuiver, and W.S. Broecker (1983). “Upwelling rates for the equatorial Pacific Ocean derived from the bomb 14C distribution”. In: *J. Mar. Res.* 41.4, pp. 769–792.

Rasmusson, E.M. and T.H. Carpenter (1982). “Variations in Tropical Sea Surface Temperature and Surface Wind Fields Associated with the Southern Oscillation/El Niño”. In: *Mon. Wea. Rev.* 110, pp. 354–384.

Rebert, J.P., J.R. Donguy, G. Eldin, and K. Wyrtki (1985). “Relations between sea level, thermocline depth, heat content, and dynamic height in the tropical Pacific Ocean”. In: *J. Geophys. Res.* 90.C6, pp. 11719–11725.

Redi, M.H. (1982). “Oceanic Isopycnal Mixing by Coordinate Rotation”. In: *J. Phys. Oceanogr.* 12, pp. 1154–1158.

Reynolds, R.W., N.A. Rayner, T.M. Smith, D.C. Stokes, and W. Wang (2002). “An Improved In Situ and Satellite SST Analysis for Climate”. In: *J. Climate* 15, pp. 1609–1625.

Rodgers, K.B., M.A. Cane, N.H. Naik, and D.P. Schrag (1999). “The role of the Indonesian Throughflow in equatorial Pacific thermocline ventilation”. In: *J. Geophys. Res.* 104.C9, pp. 20551–20570.

Rodgers, K.B., P. Friederichs, and M. Latif (2004). “Tropical Pacific Decadal Variability and Its Relation to Decadal Modulations of ENSO”. In: *J. Climate* 17, pp. 3761–3774.

Rumford, B. (1800). “Essay VII, the propagation of heat in fluids”. In: *Essays, Political, Economical, and Philosophical, A New Edition*. Ed. by T. Cadell Jr. and W. Davies. Vol. 2. Boston, Mass.: Manning and Loring, pp. 197–386.

Schneider, N. (2000). “A decadal spiciness mode in the Tropics”. In: *Geophys. Res. Lett.* 27.2, pp. 257–260.

Schneider, N. and B.D. Cornuelle (2005). “The Forcing of the Pacific Decadal Oscillation”. In: *J. Climate* 18, pp. 4355–4373.

Schneider, T., T. Bischoff, and G.H. Haug (2014). “Migrations and dynamics of the intertropical convergence zone”. In: *Nature* 513.7516, pp. 45–53.

Schneider, N., A.J. Millerand, M.A. Alexander, and C. Deser (1999a). “Subduction of decadal North Pacific temperature anomalies: Observations and dynamics”. In: *J. Phys. Oceanogr.* 29.5, pp. 1056–1070.

Schneider, N., S. Venzke, A.J. Miller, D.W. Pierce, T.P. Barnett, C. Deser, and M. Latif (1999b). "Pacific thermocline bridge revisited". In: *Geophys. Res. Lett.* 26.9, pp. 1329–1332.

Schoenefeldt, R. and F. A. Schott (2006). "Decadal variability of the Indian Ocean cross-equatorial exchange in SODA". In: *Geophys. Res. Lett.* 33, p. L08602.

Schopf, P.S. (1980). "The Role of Ekman flow and Planetary Waves in the Oceanic Cross-Equatorial Heat Transport". In: *J. Phys. Oceanogr.* 10, pp. 330–341.

Schott, F.A. and J.P. McCreary (2001). "The monsoon circulation of the Indian Ocean". In: *Prog. Oceanogr.* 51, pp. 1–123.

Schott, F.A., M. Dengler, and R. Schoenefeldt (2002). "The shallow overturning circulation of the Indian Ocean". In: *Phil. Trans. R. Soc. A* 363, pp. 143–149.

Schott, F.A., M. Dengler, P. Brandt, K. Affler, J. Fischer, B. Bourles, ..., and M. Rhein (2003). "The zonal currents and transports at 35 W in the tropical Atlantic". In: *Geophys. Res. Lett.* 30, p. 1349.

Schott, F.A., J.P. McCreary, and G.C. Johnson (2004). "Shallow Overturning Circulations of the Tropical-Subtropical Oceans". In: *Earth's Climate: The Ocean-Atmosphere Interaction.* Ed. by S.P. Xie C. Wang and J.A. Carton. Washington D.C., USA: American Geophysical Union.

Schott, F.A., W. Wang, and D. Stammer (2007). "Variability of Pacific Subtropical Cells in the 50-year ECCO assimilation". In: *Geophys. Res. Lett.* 34, p. L05604.

Schott, F.A., L. Stramma, W. Wang, B.S. Giese, and R. Zantopp (2008). "Pacific Subtropical Cell variability in the SODA 2.0.2/3 assimilation". In: *Geophys. Res. Lett.* 35, p. L10607.

Schott, F.A., S.P. Xie, and J.P. McCreary (2009). "Indian Ocean circulation and climate variability". In: *Rev. Geophys.* 47, RG1002.

Shaffrey, L. and R. Sutton (2006). "Bjerknes Compensation and the Decadal Variability of the Energy Transports in a Coupled Climate Model". In: *J. Climate* 19, pp. 1167–1181.

Simmons, A.J. (1982). "The forcing of stationary wave motion by tropical diabatic heating". In: *Q.J.R. Meteorol. Soc.* 108, pp. 503–534.

Simmons, H.L., S.R. Jayne, L.C.S. Laurent, and A.J. Weaver (2004). "Tidally driven mixing in a numerical model of the ocean general circulation". In: *Ocean Model.* 6, pp. 245–263.

Sloyan, B.M., G.C. Johnson, and W.S. Kessler (2003). “The Pacific Cold Tongue: A Pathway for Interhemispheric Exchange”. In: *J. Phys. Oceanogr.* 33, pp. 1027–1043.

Sobel, A.H., I.M. Held, and C.S. Bretherton (2002). “The ENSO Signal in Tropical Tropospheric Temperature”. In: *J. Climate* 15, pp. 2702–2706.

Solomon, A., J.P. McCreary, R. Kleeman, and B.A. Klinger (2003). “Interannual and Decadal Variability in an Intermediate Coupled Model of the Pacific Region”. In: *J. Climate* 16, pp. 383–405.

Solomon, A. and D. Zhang (2006). “Pacific subtropical cell variability in coupled climate model simulations of the late 19th-20th century”. In: *Ocean Model.* 15, pp. 236–249.

Song, Y., Y. Yu, and P. Lin (2014). “The hiatus and accelerated warming decades in CMIP5 simulations”. In: *Adv. Atmos. Sci.* 31.6, pp. 1316–1330.

Song, Y. and Y. Yu (2015). “Impacts of External Forcing on the Decadal Climate Variability in CMIP5 Simulations”. In: *J. Climate* 28, pp. 5389–5405.

Stacey, M.W., S. Pond, and Z.P. Nowak (1990). “Oceanic heat content variability in the tropical Pacific during the 1982-1983 El Niño”. In: *J. Geophys. Res.* 95.C12, pp. 22089–22101.

— (1995). “A Numerical Model of the Circulation in Knight Inlet, British Columbia, Canada”. In: *J. Phys. Oceanogr.* 25, pp. 1037–1062.

Stommel, H. (1960). *The Gulf Stream.* Berkeley, Calif.: Univ. of Calif. Press.

— (1979). “Determination of water mass properties of water pumped down from the Ekman layer to the geostrophic flow below”. In: *Proc. Natl. Acad. Sci. U.S.A.* 76.7, pp. 3051–3055.

Stouffer, R.J. (2004). “Time Scales of Climate Response”. In: *J. Climate* 17, pp. 209–217.

Stouffer, J.S., K.E. Taylor, and G.A. Meehl (2011). “CMIP5 long-term experimental design”. Unpublished manuscript.

Sun, D.Z. and Z. Liu (1996). “Dynamic ocean-atmosphere coupling: A thermostat for the Tropics”. In: *Science* 272.5265, pp. 1148–1150.

Sverdrup, H.U. (1947). “Wind-Driven Currents in a Baroclinic Ocean; with Application to the Equatorial Currents of the Eastern Pacific”. In: *Proc. Natl. Acad. Sci. U.S.A.* 33.11, pp. 318–326.

Talley, L.D. (1985). “Ventilation of the Subtropical North Pacific: The Shallow Salinity Minimum”. In: *J. Phys. Oceanogr.* 15, pp. 633–649.

— (2003). “Shallow, Intermediate, and Deep Overturning Components of the Global Heat Budget”. In: *J. Phys. Oceanogr.* 33, pp. 530–560.

Taylor, K.E., R.J. Stouffer, and G.A. Meehl (2009). "A summary of the CMIP5 experiment design".

— (2012). "An Overview of CMIP5 and the Experiment Design". In: *Bull. Amer. Meteor. Soc.* 93, pp. 485–498.

Timmermann, A., M. Latif, R. Voss, and A. Grötzner (1998). "Northern Hemispheric Interdecadal Variability: A Coupled Air-Sea Mode". In: *J. Climate* 11, pp. 1906–1931.

Timmermann, A. and F.F. Jin (2002). "A Nonlinear Mechanism for Decadal El Niño Amplitude Changes". In: *Geophys. Res. Lett.* 29.1.

Tourre, Y.M., Y. Kushnir, and W.B. White (1999). "Evolution of Interdecadal Variability in Sea Level Pressure, Sea Surface Temperature, and Upper Ocean Temperature over the Pacific Ocean". In: *J. Phys. Oceanogr.* 29, pp. 1528–1541.

Trenberth, K.E. (1990). "Recent observed interdecadal climate changes in the Northern Hemisphere". In: *Bull. Amer. Meteor. Soc.* 71, pp. 988–993.

Trenberth, K.E. and T.J. Hoar (1996). "The 1990–1995 El Niño-Southern Oscillation event: longest on record". In: *Geophys. Res. Lett.* 23.1, pp. 57–60.

Trenberth, K.E., G.W. Branstator, D. Karoly, A. Kumar, N.C. Lau, and C. Ropelewski (1998). "Progress during TOGA in understanding and modeling global teleconnections associated with tropical sea surface temperatures". In: *J. Geophys. Res.* 103.C7, pp. 14291–14324.

Trenberth, K.E. and J.T. Fasullo (2013). "An apparent hiatus in global warming?" In: *Earth's Future* 1, pp. 19–32.

Trenberth, K.E., J.T. Fasullo, G. Branstator, and A.S. Phillips (2014). "Seasonal aspects of the recent pause in surface warming". In: *Nat. Clim. Change* 4.10, pp. 911–916.

Trenberth, K.E. and J.M. Caron (2001). "Estimates of Meridional Atmosphere and Ocean Heat Transports". In: *J. Climate* 14, pp. 3433–3443.

Trenberth, K.E. and J.W. Hurrell (1994). "Decadal atmosphere-ocean variations in the Pacific". In: *Clim. Dyn.* 9.6, pp. 303–319.

Troup, A.J. (1965). "The 'southern oscillation'". In: *Q.J.R. Meteorol. Soc.* 91, pp. 490–506.

Tsuchiya, M. (1981). "The Origin of the Pacific Equatorial 13°C Water". In: *J. Phys. Oceanogr.* 11, pp. 794–812.

— (1986). "Thermostads and circulation in the upper layer of the Atlantic Ocean". In: *Prog. Oceanogr.* 16.4, pp. 235–267.

Tsuchiya, M., R. Lukas, R.A. Fine, E. Firing, and E. Lindstrom (1989). “Source waters of the Pacific Equatorial Undercurrent”. In: *Prog. Oceanogr.* 23.2, pp. 101–147.

Tziperman, E., L. Stone, M.A. Cane, and H. Jarosh (1994). “El Niño chaos: Overlapping of resonances between the seasonal cycle and the Pacific ocean-atmosphere oscillator”. In: *Science* 264.5155, pp. 72–74.

Vallis, G.K. (2006). *Atmospheric and oceanic fluid dynamics.* Cambridge Univ. Press.

Van Loon, H. (1979). “The Association between Latitudinal Temperature Gradient and Eddy Transport. Part I: Transport of Sensible Heat in Winter”. In: *Mon. Wea. Rev.* 107, pp. 525–534.

Van Loon, H. and D.J. Shea (1985). “The Southern Oscillation. Part IV: The Precursors South of 15°S to the Extremes of the Oscillation”. In: *Mon. Wea. Rev.* 113, pp. 2063–2074.

Van Loon, H. and J. Williams (1976). “The Connection Between Trends of Mean Temperature and Circulation at the Surface: Part I. Winter”. In: *Mon. Wea. Rev.* 104, pp. 365–380.

— (1977). “The Connection between Trends of Mean Temperature and Circulation at the Surface: Part IV. Comparison of the Surface Changes in the Northern Hemisphere with the Upper Air and with the Antarctic in Winter”. In: *Mon. Wea. Rev.* 105, pp. 636–647.

Vecchi, G.A., T. Delworth, R. Gudgel, S. Kapnick, A. Rosati, A.T. Wittenberg, F. Zeng, W. Anderson, V. Balaji, K. Dixon, L. Jia, H. Kim, L. Krishnamurthy, R. Msadek, W.F. Stern, S.D. Underwood, G. Villarini, X. Yang, and S. Zhang (2014). “On the Seasonal Forecasting of Regional Tropical Cyclone Activity”. In: *J. Climate* 27, pp. 7994–8016.

Vecchi, G.A., B.J. Soden, A.T. Wittenberg, I.M. Held, A. Leetmaa, and M.J. Harrison (2006). “Weakening of tropical Pacific atmospheric circulation due to anthropogenic forcing”. In: *Nature* 441.7089.

Vecchi, G.A. and B.J. Soden (2007). “Global Warming and the Weakening of the Tropical Circulation”. In: *J. Climate* 20, pp. 4316–4340.

Vimont, D.J., D.S. Battisti, and A.C. Hirst (2001). “Footprinting: A seasonal connection between the tropics and mid-latitudes”. In: *Geophys. Res. Lett.* 28, pp. 3923–3926.

— (2002). “Pacific Interannual and Interdecadal Equatorial Variability in a 1000-Yr Simulation of the CSIRO Coupled General Circulation Model”. In: *J. Climate* 15, pp. 160–178.

Vonder Haar, T.H. and A.H. Oort (1973). "New Estimate of Annual Poleward Energy Transport by Northern Hemisphere Oceans". In: *J. Phys. Oceanogr.* 3, pp. 169–172.

Wacongne, S. and R. Pacanowski (1996). "Seasonal Heat Transport in a Primitive Equations Model of the Tropical Indian Ocean". In: *J. Phys. Oceanogr.* 26, pp. 2666–2699.

Walker, G. (1928). "World weather". In: *Q.J.R. Meteorol. Soc.* 54, pp. 79–87.

Wallace, J.M. and D.S. Gutzler (1981). "Teleconnections in the Geopotential Height Field during the Northern Hemisphere Winter". In: *Mon. Wea. Rev.* 109, pp. 784–812.

Wallace, J.M., C. Smith, and Q. Jiang (1990). "Spatial Patterns of Atmosphere-Ocean Interaction in the Northern Winter". In: *J. Climate* 3, pp. 990–998.

Wallace, J.M., Y. Zhang, and K. Lau (1993). "Structure and Seasonality of Interannual and Interdecadal Variability of the Geopotential Height and Temperature Fields in the Northern Hemisphere Troposphere". In: *J. Climate* 6, pp. 2063–2082.

Wallace, J.M., Y. Zhang, and J.A. Renwick (1995). "Dynamic Contribution to Hemispheric Mean Temperature Trends". In: *Science* 270.5237, pp. 780–783.

Wallace, J.M., Y. Zhang, and L. Bajuk (1996). "Interpretation of Interdecadal Trends in Northern Hemisphere Surface Air Temperature". In: *J. Climate* 9, pp. 249–259.

Wang, X.L. and C.F. Ropelewski (1995). "An Assessment of ENSO-Scale Secular Variability". In: *J. Climate* 8, pp. 1584–1599.

Wang, D. and M.A. Cane (2011). "Pacific Shallow Meridional Overturning Circulation in a Warming Climate". In: *J. Climate* 24, pp. 6424–6439.

Wang, L., W. Chen, and R. Huang (2008). "Interdecadal modulation of PDO on the impact of ENSO on the East Asian winter monsoon". In: *Geophys. Res. Lett.* 35, p. L20702.

Wang, X. and R.X. Huang (2004). "Wind Energy Input to the Ekman Layer". In: *J. Phys. Oceanogr.* 34, pp. 1267–1275.

Wang, C., J. Huang, Y. He, and Y. Guan (2013). "Combined effects of the Pacific Decadal Oscillation and El Niño-Southern Oscillation on Global Land Dry-Wet Changes". In: *Sci. Rep.* 4.6651.

Wang, C. and J. Picaut (2004). "Understanding ENSO physics - A review". In: *Earth's Climate: The Ocean-Atmosphere Interaction.* Ed. by S.P. Xie C. Wang and J.A. Carton. Geophys. Monogr. Series. Washington D.C., USA: American Geophysical Union, pp. 21–48.

Warren, B.A. (1981). “Deep circulation of the world ocean”. In: *Evolution of Physical Oceanography*. Ed. by B.A. Warren and C. Wunsch. Cambridge, Mass.: MIT Press, pp. 6–41.

Watanabe, M. and T. Hibiya (2002). “Global estimates of the wind-induced energy flux to inertial motions in the surface mixed layer”. In: *Geophys. Res. Lett.* 29.8.

Watanabe, M., Y. Kamae, M. Yoshimori, A. Oka, M. Sato, M. Ishii, ..., and M. Kimoto (2013). “Strengthening of ocean heat uptake efficiency associated with the recent climate hiatus”. In: *Geophys. Res. Lett.* 40, pp. 3175–3179.

Webster, P.J. (1981). “Mechanisms Determining the Atmospheric Response to Sea Surface Temperature Anomalies”. In: *J. Atmos. Sci.* 38, pp. 554–571.

— (1982). “Seasonality in the Local and Remote Atmospheric Response to Sea Surface Temperature Anomalies”. In: *J. Atmos. Sci.* 39, pp. 41–52.

Webster, P.J., A.M. Moore, J.P. Loschnigg, and R.R. Leben (1999). “Coupled ocean-atmosphere dynamics in the Indian Ocean during 1997-98”. In: *Nature* 401, pp. 356–360.

Welander, P. (1959). “An Advective Model of the Ocean Thermocline”. In: *Tellus* 11, pp. 309–318.

Weng, W. and J.D. Neelin (1999). “Analytical Prototypes for Ocean-Atmosphere Interaction at Midlatitudes. Part II: Mechanisms for Coupled Gyre Modes”. In: *J. Climate* 12, pp. 2757–2774.

White, W.B. and T.P. Barnett (1972). “A Servomechanism in the Ocean/Atmosphere System of the Mid-Latitude North Pacific”. In: *J. Phys. Oceanogr.* 2, pp. 372–381.

Wijffels, S., E. Firing, and J. Toole (1995). “The mean structure and variability of the Mindanao Current at 8°N”. In: *J. Geophys. Res.* 100.C9, pp. 18421–18435.

Willebrand, J., S.G. Philander, and R.C. Pacanowski (1980). “The Oceanic Response to Large-Scale Atmospheric Disturbances”. In: *J. Phys. Oceanogr.* 10, pp. 411–429.

Wilson, D. and A. Leetmaa (1988). “Acoustic Doppler current profiling in the equatorial Pacific in 1984”. In: *J. Geophys. Res.* 93.C11, pp. 13947–13966.

Wong, A.P. and G.C. Johnson (2003). “South Pacific Eastern Subtropical Mode Water”. In: *J. Phys. Oceanogr.* 33, pp. 1493–1509.

Woods, J.D. (1985a). “The World Ocean Circulation Experiment”. In: *Nature* 314.6011, pp. 501–511.

— (1985b). "The physics of thermocline ventilation". In: *Coupled Ocean-Atmosphere Models*. Ed. by J.C.J. Nihoul. Vol. 40. Elsevier Oceanography Series. Amsterdam, Netherlands: Elsevier, pp. 543–590.

Wu, L., Z. Liu, C. Li, and Y. Sun (2007). "Extratropical control of recent tropical Pacific decadal climate variability: a relay teleconnection". In: *Clim. Dyn.* 28, pp. 99–112.

Wu, Z., N.E. Huang, J.M. Wallace, B.V. Smoliak, and X. Chen (2011). "On the time-varying trend in global-mean surface temperature". In: *Clim. Dyn.* 37, pp. 759–773.

Wu, L., D.E. Lee, and Z. Liu (2005). "The 1976/77 North Pacific Climate Regime Shift: The Role of Subtropical Ocean Adjustment and Coupled Ocean-Atmosphere Feedbacks". In: *J. Climate* 18, pp. 5125–5140.

Wu, L., Z. Liu, R. Gallimore, R. Jacob, D. Lee, and Y. Zhong (2003). "Pacific Decadal Variability: The Tropical Pacific Mode and the North Pacific Mode". In: *J. Climate* 16, pp. 1101–1120.

Wunsch, C. (1998). "The Work Done by the Wind on the Oceanic General Circulation". In: *J. Phys. Oceanogr.* 28, pp. 2332–2340.

— (2005). "The Total Meridional Heat Flux and Its Oceanic and Atmospheric Partition". In: *J. Climate* 18, pp. 4374–4380.

Wu, Q. and D.M. Straus (2004). "AO, COWL and Observed Climate Trends". In: *J. Climate* 17, pp. 2139–2156.

Wyrtki, K. (1975). "Fluctuations of the Dynamic Topography in the Pacific Ocean". In: *J. Phys. Oceanogr.* 5, pp. 450–459.

— (1981). "An Estimate of Equatorial Upwelling in the Pacific". In: *J. Phys. Oceanogr.* 11, pp. 1205–1214.

Wyrtki, K. and B. Kilonsky (1984). "Mean Water and Current Structure during the Hawaii-to-Tahiti Shuttle Experiment". In: *J. Phys. Oceanogr.* 14, pp. 242–254.

Xie, S.P. (2004). "The shape of continents, air-sea interaction, and the rising branch of the Hadley circulation". In: *The Hadley Circulation: Present, Past and Future*. Ed. by H.F. Diaz and R.S. Bradley. Dordrecht: Springer Netherlands, pp. 121–152.

Yang, H. and L. Wang (2008). "Estimating the nonlinear response of tropical ocean to extratropical forcing in a coupled climate model". In: *Geophys. Res. Lett.* 35, p. L15705.

Yang, C., B.S. Giese, and L. Wu (2014). "Ocean dynamics and tropical Pacific climate change in ocean reanalyses and coupled climate models". In: *J. Geophys. Res.* 119, pp. 7066–7077.

Yang, H., Y. Zhao, and Z. Liu (2015). "Understanding Bjerknes Compensation in Atmosphere and Ocean Heat Transports Using a Coupled Box Model". In: *J. Climate* 29, pp. 2145–2160.

Yang, H., Z. Liu, and Q. Zhang (2004). "Tropical Ocean Decadal Variability and Resonance of Planetary Wave Basin Modes. Part II: Numerical Study". In: *J. Climate* 17, pp. 1711–1721.

Yang, H. and Z. Liu (2005). "Tropical-extratropical climate interaction as revealed in idealized coupled climate model experiments". In: *Clim. Dyn.* 24.7-8, pp. 863–879.

Yang, H., Q. Zhang, Y. Zhong, S. Vavrus, and Z. Liu (2005). "How does extratropical warming affect ENSO?" In: *Geophys. Res. Lett.* 32, p. L01702.

Yeh, S.W. and B.P. Kirtman (2009). "Internal Atmospheric Variability and Interannual-to-Decadal ENSO Variability in a CGCM". In: *J. Climate* 22, pp. 2335–2355.

Yeh, S.W., Y. Kang, Y. Noh, and A.J. Miller (2011). "The North Pacific Climate Transitions of the Winters of 1976/77 and 1988/89". In: *J. Climate* 24, pp. 1170–1183.

Yu, L. and M.M. Rienecker (1999). "Mechanisms for the Indian Ocean warming during the 1997-98 El Niño". In: *Geophys. Res. Lett.* 26.6, pp. 735–738.

Yukimoto, S., M. Endoh, Y. Kitamura, A. Kitoh, T. Motoi, A. Noda, and T. Tokioka (1996). "Interannual and interdecadal variabilities in the Pacific in an MRI coupled GCM". In: *Clim. Dyn.* 12, pp. 667–683.

Zavala-Garay, J., A.M. Moore, C.L. Perez, and R. Kleeman (2003). "The Response of a Coupled Model of ENSO to Observed Estimates of Stochastic Forcing". In: *J. Climate* 16, pp. 2827–2842.

Zebiak, S.E. (1989). "Oceanic Heat Content Variability and El Niño Cycles". In: *J. Phys. Oceanogr.* 19, pp. 475–486.

— (1993). "Air–Sea Interaction in the Equatorial Atlantic Region". In: *J. Climate* 6, pp. 1567–1586.

Zhang, Y., J.M. Wallace, and N. Iwasaka (1996). "Is Climate Variability over the North Pacific a Linear Response to ENSO?" In: *J. Climate* 9, pp. 1468–1478.

Zhang, Y., J.M. Wallace, and D. Battisti (1997). "ENSO-like interdecadal variability: 1900-93". In: *J. Climate* 10.5, pp. 1004–1020.

Zhang, D., M.J. McPhaden, and W.E. Johns (2003). "Observational Evidence for Flow between the Subtropical and Tropical Atlantic: The Atlantic Subtropical Cells". In: *J. Phys. Oceanogr.* 33, pp. 1783–1797.

Zhang, D. and M.J. McPhaden (2006). "Decadal variability of the shallow Pacific meridional overturning circulation: Relation to tropical sea surface temperatures in observations and climate change models". In: *Ocean Model.* 15.3, pp. 250–273.

Zhang, R. and T.L. Delworth (2007). "Impact of the Atlantic Multidecadal Oscillation on North Pacific climate variability". In: *Geophys. Res. Lett.* 34, p. L23708.

Zhang, R.H., L.M. Rothstein, and A.J. Busalacchi (1998a). "Origin of upper-ocean warming and El Niño change on decadal scales in the tropical Pacific Ocean". In: *Nature* 391.6670, pp. 879–883.

Zhang, X., J. Sheng, and A. Shabbar (1998b). "Modes of Interannual and Interdecadal Variability of Pacific SST". In: *J. Climate* 11, pp. 2556–2569.

Zhang, H.M. and L.D. Talley (1998). "Heat and buoyancy budgets and mixing rates in the upper thermocline of the Indian and Global Oceans". In: *J. Phys. Oceanogr.* 28, pp. 1961–1978.

Zilberman, N.V., D.H. Roemmich, and S.T. Gille (2013). "The mean and the time variability of the shallow meridional overturning circulation in the tropical South Pacific Ocean". In: *J. Climate* 26, pp. 4069–4087.

Zuo, H., M.A. Balmaseda, and K. Mogensen (2017). "The new eddy-permitting ORAP5 ocean reanalysis: description, evaluation and uncertainties in climate signals". In: *Clim. Dyn.* 49, pp. 791–811.